OPEN ACCESS

University of BRISTOL

This electronic thesis or dissertation has been downloaded from the University of Bristol Research Portal, http://research-information.bristol.ac.uk

Author:
Tonge, Simon M

Title:
An investigation into the effect of constraint on fracture parameters

General rights
Access to the thesis is subject to the Creative Commons Attribution - NonCommercial-No Derivatives 4.0 International Public License. A copy of this may be found at https://creativecommons.org/licenses/by-nc-nd/4.0/legalcode This license sets out your rights and the restrictions that apply to your access to the thesis so it is important you read this before proceeding.

Take down policy
Some pages of this thesis may have been removed for copyright restrictions prior to having it been deposited on the University of Bristol Research Portal. However, if you have discovered material within the thesis that you consider to be unlawful e.g. breaches of copyright (either yours or that of a third party) or any other law, including but not limited to those relating to patent, trademark, confidentiality, data protection, obscenity, defamation, libel, then please contact collections-metadata@bristol.ac.uk and include the following information in your message:

•Your contact details
•Bibliographic details for the item, including a URL
•An outline nature of the complaint

Your claim will be investigated and, where appropriate, the item in question will be removed from public view as soon as possible.

AN INVESTIGATION INTO THE EFFECT OF CONSTRAINT ON FRACTURE PARAMETERS

SIMON M TONGE

A dissertation submitted to the University of Bristol in accordance with the requirements for award of Doctor of Philosophy in the Faculty of Engineering

Department of Mechanical Engineering c. 25,000 words

Abstract

Failure of a component is a safety and financial hazard in many industries, especially aerospace and nuclear. Since the beginning of the 20th century, the field of fracture mechanics has sought to understand how components fail. There have been many advances in the understanding of this area including the development of the linear elastic and elastic plastic theories of fracture mechanics. The application of fracture mechanics has been codified in the BS7910 code and R6 integrity assessment procedure, which allow a user to assess whether a flaw in a material will propagate and cause failure.

The fracture toughness of a material is a known material property which represents how resistant a material is to fracture. Numerical measures of fracture, for example the J-integral, enable the comparison of fracture toughness between materials. However, a component has a susceptibility to failure which is not only dependent on the fracture toughness of the material from which it is made. When an component cracks, at the tip of the crack a high stress region known as the plastic zone forms. In this region plastic yielding has occurred. The size of the component in question constrains this plastic zone and can partly determine the likelihood of an component failing. There are two types of constraint: In-plane constraint and out of plane constraint. In plane constraint depends on the length of uncracked solid material ahead of the crack tip. Out of plane constraint refers to the effect of the component thickness, which is its orthogonal size relative to the direction of crack propagation.

Parameters such as T-stress account for the effect of constraint on fracture. Assessment codes and procedures enable the estimation of the safety of a component by comparison to tabulated measurements of these parameters. No fracture assessment code or procedure currently accounts for the effect out of plane constraint on an component's fracture toughness. Furthermore, theories accounting for in and out of plane constraint often involve using three parameters, for example K-T-T_z. In this thesis a single parameter to quantify both in and out of plane constraint is tested, ϕ. It is compared with Q another parameter that has been suggested to quantify both types of constraint.

The first part of the project involved a tensile fracture test at a beamline which provided in-situ synchrotron X-radiation. The material used was AlTi metal matrix composite formed into a double notch tension specimen. This allowed the imaging of the plastic region, from which a novel set of computational Finite Element codes were used to calculate the K parameter, a measure of the fracture toughness. This was plotted against the ϕ and Q parameters.

Due to the limited number of experiments that were possible in the beamline only four specimens were tested which gave values of K for four different levels in the range 41.7 and 52.5 MPa√m. When plotted against φ, these results showed a limited constraint effect. For this reason, a new set of three point bending tests on Single Edge Notch Bend (SENB) specimens were performed. Nine different combinations of constraint were used by producing specimens of thickness B=5,12, 30mm and a/W=0.075,0.275,0.375. These specimens were made from Al7075 T651. This allowed both the parameters, Q and ϕ to be plotted against K. The results showed a good correlation between $\varphi \; and \; K$.

Finally, a test carried out on pipes made from Al7075 T651 enabled an industrially relevant example to be compared with the data from the SENB three-point bending test. The test was carried out using the same test setup as for the SENB specimens and K of 49.5 MPa√m and ϕ of 5.2 was

measured. This showed that in this example the data fitted with the expected trend from the previous experiment.

It can be concluded that the parameter ϕ is a potential parameter to quantify both in and out of plane constraint. This is because ϕ is sensitive to both in and out of plane constraint. Q, conversely does not combine in and out of plane constraint consistently. To enable the use of ϕ in structural integrity assessment further work would be needed, which would involve the testing of steel specimens to strengthen the evidence for this method, by proving its applicability to other materials.

Acknowledgements

I would like to acknowledge the immense and incalculable help provided by all at Solid Mechanics Research Group, Queens Building, University of Bristol. This includes Molly Probert, Harry Coules, Chris Truman, Ryan Coulthard, Megan Taylor and many others. It was a very enjoyable experience sharing Research Suite 1.10 with those who worked in this space. A shame that we did get to enjoy as much time bin the office as we would have liked to due the effect of the global pandemic.

The technical and workshop support services at University of Bristol, including Mehdi Mohktari, Steve Harding, Ricky Billingham and many more have been outstanding in the support that they provide. It is worth noting the large number of experiments which were involved in this project. This took a very large amount of time, during which then work took up a lot their space as well. So I thank them for showing such patience.

Thanks to Ahmet Cinar and Selim Barhli for allowing me to use software that they had developed and for letting me adapt this to suit my requirements. This work was an early application of these novel analysis codes and hopefully they will be used even more in future.

To everyone at National Nuclear Laboratory (NNL) especially Rajesh Patel for the hospitality at quarterly meetings. For all the advice that was given by Caroline Meek and Nick Underwood, which enabled so much of this work to be published. To Andrew Sherry as well for providing so much inspiration for this work.

Thanks most of all to the incredible Mahmoud Mostafavi, who allowed me this opportunity and took so much care over the supervision of this work, far beyond what I would have expected. He also introduced me to many of the people listed above, for this I am extremely grateful.

Lastly to Lucia MacPartlin, Brid Harper and Josephine Marsh for being so kind to me during the very strange time that we lived through in the Covid-19 pandemic of 2020 and 2021.

Author's declaration

I declare that the work in this dissertation was carried out in accordance with the requirements of the University's Regulations and Code of Practice for Research Degree Programmes and that it has not been submitted for any other academic award. Except where indicated by specific reference in the text, the work is the candidate's own work. Work done in collaboration with or with the assistance of others is indicated as such. Any views expressed are those of the author.

Signed: Simon M Tonge Date: 31/10/2022

Publications

Journal Papers

1. **Simpson, C., Tonge, S.M., Cinar, A., Reinhard, C., Marrow, T.J., & Mostafavi, M. (2018). Validating 3D two-parameter fracture mechanics for structural integrity assessments. *Procedia structural integrity, 13*, 965-970. (co-author)**
2. **Tonge, S. M., Simpson, C. A., Reinhard, C., Connolley, T., Sherry, A. H., Marrow, T. J., & Mostafavi, M. (2020). Unifying the Effects of in and out-of-plane constraint on the fracture of ductile materials. Journal of the Mechanics and Physics of Solids, 141, [103956]. https://doi.org/10.1016/j.jmps.2020.103956 (Main author)**
3. **S M Tonge , Z Chen, C Meek, M Mokhtarishirazabad, M Mostafavi (2022) Quantifying combined effects of in-plane and out-of-plane constraint in an aluminium alloy, Theoretical and applied fracture mechanics Under Review (Main author)**

Contents

1. Introduction

1.1 Fracture Mechanics

Fracture mechanics is the study of cracks. This can include how they initiate, propagate and whether a crack will eventually cause a component to fail. During a manufacturing process any component can acquire flaws. This can occur due to temperature, pressure, stress, shearing chemical effects. In the service lifetime of a component expose to different conditions depending on the environment that the component is exposed to. From components which undergo high stresses, to components which are in contact with high temperature materials, there many reasons why a crack can occur.

A. A. Griffith began the study of fracture mechanics in the early 20th century. This was motivated by experiments on glass which showed anomalously low fracture toughness of about 100MPa $m^{0.5}$. This was very low when comparing it to the theoretical value which calculated from the energy of the lattice structure. This was at least 100 times higher [1]. The difference of several orders of magnitude required explanation. This work required a series of experiments, the results of which defined linear elastic fracture mechanics. The parameters defined in Linear Elastic Fracture Mechanics (LEFM) included the stress intensity factor K and the strain energy release rate G [2]. The assumption that linear elastic fracture mechanics makes do not hold true in cases of large loads. This is because the plastic zone at the crack tip increases in size, so it is no longer comparable to the crack length. This problem led to the development of elastic plastic fracture mechanics. This was a set of relationships mostly derived empirically from experiments, to quantify crack growth in situations with a high level of non-linearity or plasticity. A new generation of scientists including James R Rice introduced more parameters. The main parameters were crack tip opening displacement (CTOD) and the J-integral which is a measure of strain energy release rate [3]. Crucially, the transition flaw size and cohesive zone models accounted for the difference between stable cracks and unstable crack growth. The development of fracture mechanics is reviewed in detail in Chapter 2.

1.2 Development of R6

In any engineering application the structural integrity of components is of vital importance. This is true regardless of the application. However, there are some situations where the failure of components would be truly disastrous. One example of this is in aerospace applications. Many components of an aircraft are critical to its safe operation and the failure of these components could lead to loss of life. The nuclear industry is another example of an application in which failure is highly consequential. In this case, structures in nuclear reactors and waste storage facilities are part of an immensely complex system of machines, designed not only to produce power, but also to prevent the release of very dangerous radioactive substances. In these cases, a high level of regulation is involved in the industry to justify the safety of all components.

Many functional components contain defects that are known and not all of these will cause failure. These defects can occur for a number of reasons, the main reasons being residual stress due to welding, secondary stresses on a component and limit load effects. To enable assessments to be standardised the R6 structural integrity assessment procedures were published in 1976, to enable UK nuclear industry professionals to make and justify decisions

relating to defects in components. There have been many updates and revisions to this since, as R6 has become the nuclear industry standard in assessing defects in components during this time [4].

Currently the Fitness for Service (FFS) assessment codes and procedures in the UK (e.g. R6 and BS7910) do not include the effects of loss of out-of-plane constraint on the fracture behaviour of components. This is because it has been long believed that thin sections with low out-of-plane constraint are more susceptible to plastic collapse than fracture. The main part of an R6 assessment is the evaluation of a component using Failure Assessment Diagram which will be discussed in Section 2. An appendix to R6 allows for the consideration of the effect of in plane constraint using correlation equations. These relate a parameter that characterises in-plane with a parameter characterising fracture toughness. Currently, the in-plane constraint parameter in the assessments are T [5] or Q [6]. The out-of-plane constraint can be quantified and included in the assessment by a separate parameter such as Tz [7]. However, it could be argued that if a unified measure of constraint is defined, the effects of both in-plane and out-of-plane constraints can be combined by a single parameter. Using a single parameter for constraint will considerably reduce the cost of experimental programmes required to quantify the effects of constraint as the in-plane and out-of-plane data can be pooled. Anderson and Dodds [8] suggested the size of the plastic zone around the crack tip as a unified measure of constraint which later developed further by Mostafavi et al. [9], and more recently by Seal and Sherry [10]. In the course of this work a parameter known as ϕ, defined as the normalised volume of the plastic zone, will be tested for sensitivity to in and out of plane constraint. The present work, supported by NNL, provides a definitive direct measurement of elastic energy and plastic work of a crack in various in-plane and out of plane constraint conditions, providing a scientific basis for the unified measure of constraint that can in due course be added to structural integrity assessment, significantly reducing the cost associated with characterising new materials for future nuclear systems.

1.3 Methodology

In this thesis, a large number of experiments were carried out. This was necessary because the nature of any work in this field involves determining when a physical component will fail. A large part of fracture also involves tabulating parameters and studying the effect of changing conditions on these parameters. It was decided that the experiments would be simulated. This had two useful outcomes: It allowed this research to determine fracture parameters that had been previously defined and ensured that the results of the experiments were reproduceable. Almost all the analytical results in this thesis have been derived from computational work and simulations and relatively few results have been taken directly from the experiments. In reality, it has been necessary to perform experiments to ensure that the simulations are representative and consistent with experimental data. This avoids the risk of the simulations giving results which are mathematically correct but unphysical. Almost all, of the simulations in this dissertation are produced using a method known as finite element analysis, which is now a familiar and standardised process in computer aided engineering. This process involves the discretization of complex geometric models into a number of shapes of known size. These are the known as finite elements (FE). A series of differential equations can be modelled over these elements, which enables the equations to be solved numerically. By modelling the experiments using FEA and proving that the model was compliant with this, numerical values of the

constraint parameters can be determined. These values can then be determined for a number of different levels of constraint.
In this work, the Q parameter is compared with ϕ, the normalised volume of the plastic zone, to enable informed decisions to be made about which of these parameters best quantifies constraint. Q was a parameter proposed by O'Dowd and Shih, which is defined as the difference between the stress field close to the crack tip and the HRR stress field[6]. This makes a useful comparison with ϕ, as Q quantifies in plane constraint and is not proven to be sensitive to out of plane constraint. This means that if fracture toughness is plotted against Q and ϕ for different levels of in and out of plane constraint, there may be a divergence between these two parameters if ϕ is correlated with fracture toughness.

1.4 Overview of work

Three experiments were performed in the course of this project:

- Experiment using X-ray diffraction and tomography to demonstrate quantification of constraint and sensitivity of the parameters to constraint. This is reported in Chapter 3. This was a tensile test with 4 specimens.
- Three-point bending test with 9 different specimens, each with a different level of constraint. This provided a range of results with repeat measurements, which showed the behaviour of each parameter at a range of levels of in and out of plane constraint.
- Three point bending test on pipe which showed the applicability of the constraint parameters to realistic specimens.

2 Literature Review

2.1 Introduction

This section begins by defining basic terminology, the fracture toughness parameters and introducing the concept of constraint. The types of constraint parameters are introduced, in-plane and out of plane and the developments of parameters that characterise both in and out of plane constraint. The motivation for the development of Fitness for Service assessments is given and an overview of how these developed, with emphasis on why the nuclear industry was a crucial part of this. The extent to which these assessments account for constraint is given and this highlights the relevance of the next sections which investigate a new fracture parameter to fulfil this requirement.

2.2 Basics of Fracture Mechanics

AA Griffith conducted a series of experiments before 1921, to explain the phenomenon that the fracture toughness of a specimen was anomalously lower than the expected value, which was then thought to be a tenth of Young's modulus. The reason for this, is because of the concentration of stress around microscopic flaws in a material which are often introduced by machining when a part is manufactured. By introducing much larger artificial flaws, in a test specimen under load Griffith proved that the fracture stress was inversely proportional to the square root of the length of the flaw introduced. This could not be explained by the existing linear elastic model of materials, so Griffith sought to explain this using an energy-based model [1].

Griffith used the first law of thermodynamics, which states that a system can only go to equilibrium from a non-equilibrium state when there is a net loss in energy. The process of forming a crack cannot violate this law, therefore a crack can only form if there is a net loss or balance of energy. Consider a plate under constant stress, with a through thickness crack of length 2a that is much smaller than the width, the thickness of the plate is B. Griffith was able to solve the energy balance equation for Π, the potential energy supplied and W_S, the energy required to create a surface. This equation was given in terms of crack area A. The work of Inglis[11] and the fact that the product of the total surface area of the crack 4aB and the energy needed to create a unit surface (surface energy γ), enabled solution of this equation. The relationships derived gave the energy release rate and the failure stress in terms of the half crack length represented by a, the half crack length.

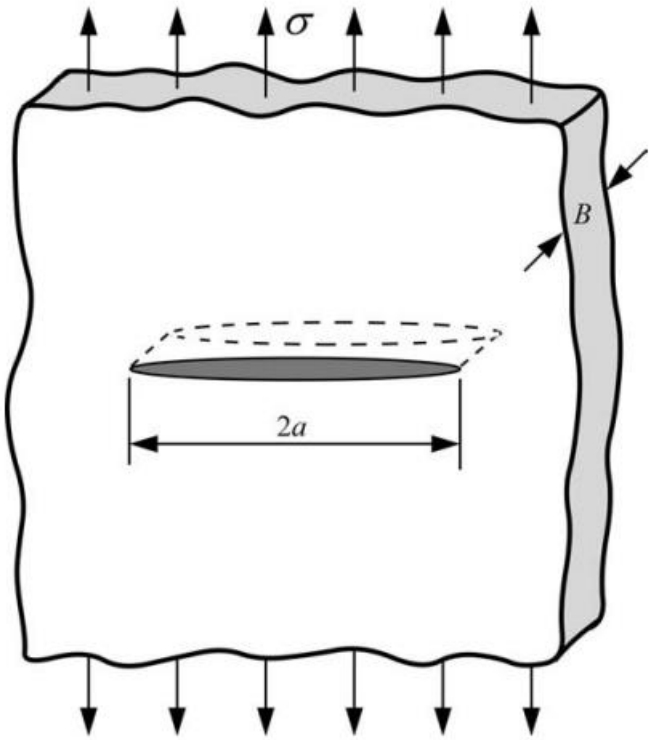

Figure 2.1: Diagram showing physical system referred to in Griffith energy equations derivation[12].

$$\frac{d\Pi}{dA} = -\frac{dW_S}{dA} \quad (2.1)$$

$$\frac{d\Pi}{dA} = -\frac{\pi\sigma a}{E} \quad (2.2)$$

$$\sigma_f = \sqrt{\frac{2E\gamma_s}{\pi a}} \quad (2.3)$$

$\frac{d\Pi}{dA}$ is the energy absorption rate for creating crack surfaces, not in terms of time but in terms of the incremental increase in crack area A. If σ is replaced with σ_f in the equation for energy rate, a criterion is found for the growth of a crack in equation (3). When the energy release rate exceeds this value, a crack will begin to grow. The work of Griffith had an impact that was developed further about 30 years later. The reason for this was that this theory did not account for the large amount of yielding that takes place around the crack tip. The theory of Griffith assumes that material behaves in a linear elastic way, as such it was unrealistic in the plastic zone around the crack tip. The Griffith energy was found to be accurate for very brittle materials, but not very accurate for ductile materials which show a higher level of plastic deformation before fracture[2].

Irwin and Orowan [13] introduced a correction to the Griffith energy release rate formula, by separating the heat energy released by plastic deformation and the elastic strain energy into two separate components. For ductile materials the plastic part is more dominant and for brittle materials the plastic part is very small.

$$\mathcal{G} = 2\gamma_s + w_s \quad (2.4)$$

They were then able to revise the formula to account for plastic work when finding the fracture criterion.

$$\sigma_f = \sqrt{\frac{\mathcal{g}E}{\pi a}} (2.5)$$

Where $\mathcal{g}$ is the energy release rate, γ_S is the surface energy, w_s is the plastic work and σ_f is critical stress at fracture[13] [14].

K was first introduced also by George Irwin in 1957 as one of the most fundamental parameters in fracture mechanics [15] [2]. For better understanding, the three modes of fracture must first be defined. Mode I is defined as the separation of the crack faces perpendicular to crack growth direction. Mode II and Mode III both involve shearing, in Mode II shearing is in a direction normal to the crack front, in Mode III shearing is in parallel with the crack front.

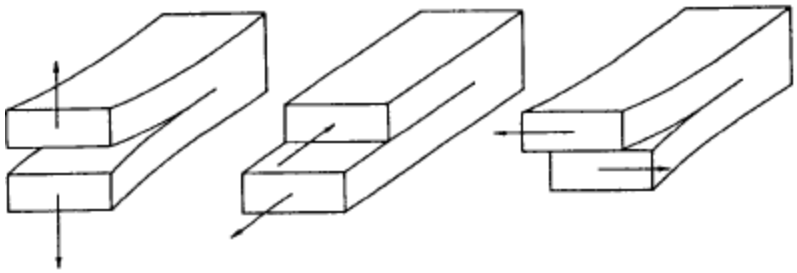

Figure 2.2: The three modes of fracture Mode I on left, Mode II in centre and Mode III on right[16]

K, known as the stress intensity factor, is an approximation of the Westergaard's solution for the stress field for the area close to the crack. The original Westergaard solution for the stress field was for the case of an infinite plate [17]. It took form of the Airy Stress functions of complex numbers [13]Irwin expressed z in Eulerian notation as shown in equation 4. This was substituted into Westergaard's expression for Z (equation 5).

$$z = a + re^{i\theta} (2.5)$$

$$Z = \frac{\sigma_\infty}{\sqrt{1-(\frac{a}{a+re^{i\theta}})^2}} (2.6) [19]$$

This allowed for the simplification using the fact that r << a in the close vicinity of the crack tip. Where r is the distance from the origin of the coordinate system, which is usually at the centre of the crack. Irwin's equations were given in terms of r and θ (equation 5).

$$\sigma_{yy} = \frac{\sigma_\infty \sqrt{\pi a}}{\sqrt{2\pi r}} (2.7) [20]$$

It can be seen, that the numerator of the fraction in equation 6 corresponds to the stress intensity factor (K). This can be used in the region at which approximately, r < a/10. For this area there is good agreement between Irwin's approximate solution and the actual stress field. The stress field equations can also be given in terms of r and θ. The inverse dependence on $r^{1/2}$ is of importance as it provides the singularity of stress at the crack mouth, r=0. The general equation for K or stress intensity factor is given, in terms of a where Y is a function of the specimen type. The stress intensity factor defines the stress state at a point near the crack tip i.e. where r is relatively small, r<<a.

$$K = Y\sigma\sqrt{\pi a} (2.8)[16]$$

Continuation of this work has also seen K be derived for the Mode II and Mode III crack opening regimes (this gives K_{II} and K_{III} respectively) and for other, more physically relevant, specimen geometries and loading regimes [21].

The use of K requires some knowledge of material properties, since it is applicable only when plasticity effects are negligible.

The stress intensity factor (K) is relevant in the case of a brittle fracture of a material. This is due to the calculation of K using the assumption that the behaviour of the material is linear elastic throughout.

The J-integral developed by Rice is a means of determining the crack driving force [22]. J is a measure of the strain energy release rate at the crack tip [23]. This is equivalent to the work done to create a unit surface area of a crack [21]. The J-integral is exclusive to elastic-plastic fracture mechanics. Experiments [24][25] have shown that it effectively characterises stress and strain fields at a crack tip in non-linear materials. In linear elastic fracture mechanics, the stress intensity factor K is used analogously [21]. It was defined as a path integral taken around a crack tip, the value of which is independent of the choice of contours [26]. To prove that the J-integral was contour independent, Rice used Greens theorem to integrate equation 1 over an area A and a path Γ. If two different paths were traversed in opposite directions, they would sum to zero.

$$J = \int_{\Gamma} W\, -\overline{T}\, \frac{du}{dx} ds \text{(2.9a)[18]}$$

$$\text{Plane stress:} K_{IC} = \sqrt{E.J_{IC}} (2.9b)$$

$$\text{Plane strain:} K_{IC} = \sqrt{\frac{E.J_{IC}}{(1-\nu)}} \text{(2.9c)}$$

W represents the strain energy density, T is a traction vector along the path of integration, u is the internal energy in the material, E is Young's modulus and v is Poisson's ratio. The equations b and c are a means of converting between J and K, for mode 1 fracture toughness, which is referred to by the subscripts. The path independence of J is a useful property This is because prior to the proposal of the J-integral, other fracture criteria were calculated by the application of numerical methods very close to the crack tip which is impractical [12]. The path of the J-integral however, can be chosen across a greater region. The J-integral is a vector with three components of which the first component is used for most purposes.

A methodology to measure the J-integral experimentally were first devised by Begley and Landes in 1971 [23]. This involved measuring the potential energy and the crack length, it was shown that the potential energy per unit crack length had a fixed relationship with J. In doing so, it allowed J to be derived, by first finding the area under a load-displacement curve at constant displacement and then plotting this against crack length [28]. It was found that a critical value of J (J_{IC}) determined the fracture toughness for an elastic-plastic material. In their original experiments Begley and Landes showed that for two different types of steel, Ni-Cr-Mo-V rotor steel and A533B pressure vessel steel, fracture occurred at J_{Ic} verifying this as the critical value [24]. Subsequent experiments supported these results and J_{IC} became an accepted parameter for fracture toughness in Mode I loading, when used in fracture assessments [29] [30]In linear elastic fracture mechanics, the fracture toughness is given equivalently by the parameter K_C.

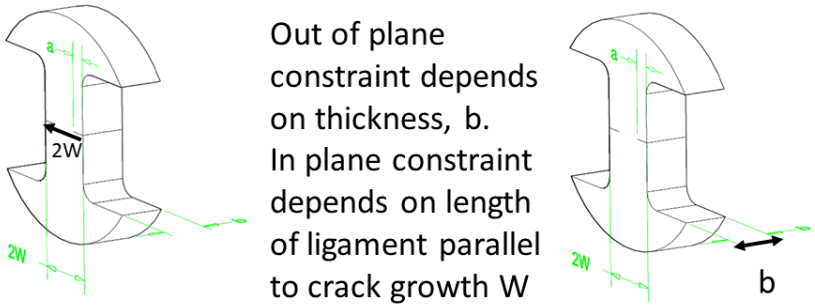

Figure 2.3: Directions of in and out of plane constraint. On left in plane constraint depends on magnitude of W, on the right out of plane constraint depends on magnitude of b.

Constraint is an effect that can be observed ahead of a crack-tip. It is defined as the resistance in an component to plastic deformation near the crack-tip. In the direction that a crack is propagating, the constraint is determined by the length of material between the crack-tip and the edge of a sample this is known as in-plane constraint [31]. The thickness of the sample is referred to as out-of-plane constraint. As such a thick sample would have high out-of-plane constraint and a thin sample would have low out-of-plane constraint. Similarly, a sample which has a long distance between the crack tip and the edge of sample would have high in-plane constraint [32]Whilst material properties, such as fracture toughness have a high impact on the behaviour, the geometry of a specimen is also important and plays a large role in fracture mechanics.

2.3 Constraint in fracture mechanics

Constraint is a very active area of research. Currently, there is no parameter that acts as an effective measure of constraint. Quantifying constraint is useful, as constraint is an important effect that should be considered in safety assessments [33]. It has been observed that there is an inherent conservatism in assessing low constraint components [34]. An overview of fracture parameters and their origins is presented below.

In-plane constraint quantifies the extent of the plastic zone around the crack tip dependent on the geometry of the sample including its crack length. Out of plane constraint, on the other hand, is associated with the change in the plastic zone size around the crack tip as a function of sample thickness. Different parameters have been used to quantify, in and out of plane constraint which are defined below.

2.4 In-plane constraint

T-stress is a higher order term that can be used for constraint in a crack opening in the Mode I regime. The origin of the term is in the Westergaard equations which were also the used in the derivation of K. These equations are for the biaxial stress field in materials with cylindrical geometries. The third component of the stress field will always be zero in Mode I cracks. Since Westergaard's equations were developed for biaxial as opposed to uniaxial loads, they always give a transverse component of the stress [35]. The term is known as the T-stress. T-stress has been observed in experiments by measuring the difference between normal strain and strain after rotation through a known angle [36]One use of T-stress developed by Coterell, is to predict crack path stability. This was determined by the sign of the T-stress, a positive value of T would mean stability and a negative value indicates that a crack would be likely to grow [37].

It has been shown, that due to the effect of the plastic region around a crack front, it is not possible to use a single parameter for fracture assessments [38]. For this reason, the T-stress found from the solutions of the Williams equations was used as in additional parameter to K in fracture assessments [39]. This is supported by the evidence of a large number of experiments, showing that the nature of the region around the crack [40]. The sign of the T-stress, as well as it's magnitude, indicates the proper properties of the plastic zone. Fracture toughness was found to increase with the increasing negative value of T-stress. A positive T-stress indicates that a crack would tend to branch. It is therefore found that the positive T values lead to high constraint, whereas negative values occur when there is a loss of constraint. T-stress is also sensitive to the loading regime; under tensile loads the T-stress will be negative, and this will switch to a low positive value for a bending load. The increase in an absolute value of T-stress would tend to make the plastic zone larger [41]. It has been possible to calculate the T-stress using both analytical and numerical methods. To enable fracture assessment to be performed using the K-T method, the T-stress for the specimen is first determined by an estimation technique. In example, Meliani et al. devised a method of evaluating T-stress in U-notch specimens. A curve with a relationship between K an T is then plotted, this known as a material failure curve. The failure point is at the intersection of this curve with the fracture driving force curve [32].

The value known as Q was defined by O'Dowd and Shih as given by equation 2 [6].

$$\boldsymbol{Q} = \frac{\boldsymbol{\sigma_{ij} - \sigma_{ij}^{HRR}}}{\boldsymbol{\sigma_0}} \textbf{(2.10)}$$ [42]

Q can be seen as the difference, at any point in the stress field, between stress and the HRR field. The purpose of Q was to quantify the triaxiality of stress in the region around a crack tip [43]. The stress triaxiality factor (h) is defined as the ratio of the hydrostatic stress to the to the von Mises stress. The parameter h that represents constraint can in itself be used as a constraint parameter [44]. However, it is Q that is used in the J-Q theory since it parameterises the strain field ahead of the crack tip.

J-Q theory was motivated by loss of constraint or increasing plasticity in the region closest to the crack [45]. This meant that two parameter methods were developed, with a parameter such as J or K quantifying the load and a second parameter, for example Q or T, providing for constraint. Prior to the development of J-Q theory either single parameter fracture mechanics, either J was used as a single parameter or J-T theory was used [34] [46]. It no longer becomes possible to account for the behaviour of the stress fields in terms of a single parameter and J-T theory begins to break down as the plastic zone increases in size it is a linear elastic parameter [47]. The stress field depends on many factors including dimensions, type of sample, material properties and where load is applied [48]. Single parameter assessments using J were found to be inaccurate for cracks growing under conditions of low constraint, the J-Q assessment method was developed [49]. In this case J is used to understand the stress field and how its magnitude varies across the entire sample, whereas Q is used to understand the stress field and stress triaxiality in the region close to the crack tip [6] [50][40]. The equation 3 is used to calculate stress in terms of a reference (HRR) field.

$$\sigma_{ij} = (\sigma_{ij})_{HRR} + Q\sigma_o\delta_{ij} \text{(2.11)}$$ [51]

This method of quantifying the stress fields, is essentially a difference between the actual stress field the HRR field at point of known distances away from a crack tip [52]. The sign of Q has a large effect of the stress field calculated using this method. It can be seen from equation 3 that when Q is negative, the actual stress field is lower than the reference stress field. When the actual stress field is greater than the reference stress field, the Q value is positive. Experiments to measure and

tabulate Q showed that it was possible to greatly increase the scope of assessments using J, by also including Q parameter [53]. Further evaluation of J-Q theory has been performed for specific samples including single edge notch bend (SENB) and compact tension (CT) specimens [54]. New formulae were proposed to optimise the calculation of Q in a situation with high plastic deformation, for bending samples [55]. The parameter Q* was developed and verified for CT and SENB specimens by Zhu et al [56], was found to accomplish this.

2.5 Out of plane constraint

T_z is the out-of-plane constraint factor. It has been defined by W Guo as shown in equation 7, in terms of different components of the stress fields[34]. The suffix notation refers to conventional cartesian co-ordinates (x,y,z) or the polar co-ordinates r,θ,z. The z-coordinate is significant as it represents the out of plane constraint.

$$T_z = \frac{\sigma_{33}}{\sigma_{11}+\sigma_{22}} \text{(2.12) [53]}$$

The motivation for using T_z is that two-parameter approaches, including the K-T and J-Q theories consider mostly the effects of in-plane constraint. To gain information about out of plane constraint finite element simulations can be used to find T_z in a range of different samples. Originally Guo used simulations of elastic plates with centre-elliptical cracks embedded. Different aspect ratios were considered, with $0.2<a/c<1$, it was found that T_z increases with increasing ϕ up 90^o where it reached a value of r/a. It was possible to calibrate these results for T_z with different aspect ratios to allow the two-parameter theory K-Tz, to be proposed to account for out of plane constraint [38]. Three parameter theories including K-T-T_z and J-Q_T-T_z have been proposed [58]. In these theories the stress fields were expressed in terms of three parameters f_{11}, f_{22} and τ_{12}. Finite Element analysis showed that f_{11} and f_{22} showed good agreement with the stress field [59]. When comparisons were made between K-T-T_z, J-Q_T-T_z and K-T and J-Q theories. It was shown that the newly proposed methods were able to account accurately for three-dimensional stress fields [60].

2.6 Unified measure of constraint

Although many of the parameters are related either in or out of plane constraint, there has also been evidence to suggest that unified constraint parameters could be used. It is possible that loci of fracture toughness could be found from a single parameter. The use of a unified constraint parameter in fracture mechanics assessments is known as one parameter fracture mechanics. It is proposed that one parameter fracture mechanics could greatly reduce the costs of such assessments.

Anderson and Dodds have proposed a method based on the area inside a stress contour [61]. An example of an equation used to plot such a contour is given in equation 8, with C being a constant, σ_1 and σ_y being the maximum principle stress and the yield stress respectively.

$$\frac{\sigma_1}{\sigma_y} = C \text{(2.13)[62]}$$

The size of area bounded by the contour determines high or low constraint.

The new parameter ϕ defined in equation 8.

$$\varphi = \frac{A_c}{A_{ssy}} \text{(2.14) [63]}$$

This represents the ratio between the plastic zone at the current load, with a reference plastic zone with small scale yielding [64]. This parameter can be used for the fracture of ductile materials. However, it is no longer applicable when large scale yielding has occurred. For this reason, the ratio A_p was proposed.

$$A_p = \frac{A_{PEEQ}}{A_{ref}} (2.15)\ [65]$$

A_{PEEQ} is the plastic strain area within the ε_p isoline and A_{ref} is the area within this line for a sample with maximal constraint. Yang et. al. have discovered that for dissimilar welded joints, the ratio between the current and reference values of J is linear [66]. This has useful feature of giving a quantifiable relationship between fracture resistance and constraint. Mostafavi et. al. also proposed an alternative to ϕ in the form of the ratio between the volumes rather than the areas of platicity. The cube root was taken of this 3-dimensional ratio of plastic zone size.

$$\varphi^p = \sqrt[3]{\frac{V_P}{V_P^{Ref}}} (2.16)[9]$$

Given that constraint can be divided into two parts, out of plane and in plane, so can the constraint parameters that are used to quantify this. There is a substantial area of research in determining the reliability and applicability of each parameter to either in plane or out of plane constraint. Analyses of three-dimensional stress fields during fracture tests on samples have identified, in many cases, whether the variable responds to in or out of plane constraint.

Studies testing the effect of in and out of plane constraint on a large number of parameters, have recently been carried out. Shlyannikov et al. showed that the plastic stress intensity factor responded to both in and out of plane constraint [67]. Recently a new unified constraint parameter, A_p, was proposed as defined in equation 10. Mu et al. carried out Finite Element (FE) simulations on a series of CT specimens within varying constraint. The aim of this was to test the sensitivity of A_p to both planes of constraint. It was found that A_p did respond to changes in both in and out plane constraint [31]. This could allow the use of A_p as a unified constraint parameter in future [68].

Seal and Sherry have recently measured constraint parameters for ductile and cleavage fracture. A and k were tabulated, and an extension to the Anderson and Dodds model with the Rice and Tracey method. This was achieved by finding the critical value for void crack growth from the Rice and Tracey model and determining the area enclosed by the Anderson and Dodds contour at this value [69].

An alternative form of the area of plasticity parameter was defined in terms of the crack tip opening displacement (CTOD). CTOD, also known as δ, is the distance between two crack faces at a point where two orthogonal lines meet when drawn from a crack tip. CTOD is a measure of loading on a crack, an alternative to J and K. It has the advantage of being easily measurable in an experiment. The A_d parameter was defined as a parameter to unify in and out of plane constraint, it is defined as a ratio of to a reference value for a specimen with a very high level of constraint.

$$A_d = \frac{\delta}{\delta_{ref}} (2.17)[70]$$

2.7 Nuclear Reactor Structure

This section introduces the structure of a nuclear reactor. The reason for unique safety culture in the nuclear industry is explained, this is significant because it led to the development of the FFS assessments part of which is being added to by this project.

The basic components of a nuclear reactor are described in this section. All reactors produce heat from the fission of the isotope U-235, which has an abundance of around 0.7% in natural uranium. Most fuels contain uranium enriched to about 3-4% U-235, but this is not always necessary. A summary equation for this reaction is shown in equation 1. A fission reaction takes place when neutrons are incident on a fissile nuclide such as U-235. For a nucleus to undergo fission the incident neutrons have energy in the order 1eV-0.1keV, which are thermal energies. Since the energy of neutrons emitted in the fission process have energy in the order of 100-200 MeV this means that neutrons need to be slowed. A substance known as the moderator is used to slow the neutrons in the reactor down to these energies. The moderators used in reactors are chosen to have a large number of light atoms, which undergo elastic collisions with the neutrons causing them to lose energy [71] [72][73].

$$^{235}_{92}U + ^{1}_{0}n \rightarrow ^{96}_{37}Rb + ^{137}_{55}Cs + ^{3}_{0}n(2.18)\ [3]]$$

Coolant is used to transfer heat produced in fission and other radioactive processes away from the fuel, produce steam to power the turbines and generate electricity. In many designs there are two types of coolant. Primary coolant is the coolant that takes heat away from the core, at the exchanger it transfers this heat to the secondary coolant to make steam to drive the turbines. It is an essential safety requirement to remove heat from the core of the reactor to prevent a large increase in temperature and an eventual meltdown. There are many designs of reactor, some of which are described below.

The Pressurised Water Reactor (PWR) is a design of reactor in which the primary coolant, light water, is kept in the liquid phase. The uranium dioxide (UO2) fuel pellets, are arranged in rods, which are held in fuel assemblies, there are 200-300 rods in fuel assembly and around 200 fuel assemblies in a reactor. The water needs to be pressurised to prevent boiling. This is achieved using a pressuriser in the primary circuit.The pressuriser consists of a large water vessel filled with water and heated to the saturation point of water for the operating pressure, usually around 618K for an operating pressure of 15MPa [73]. This is achieved with electric heaters placed under the water in the pressuriser vessel. The heaters keep the water at the required operating temperature, which is the boiling point of water for that pressure. The moderator for the reactor is the coolant water itself. Originally this design was developed for naval propulsion and was pioneered in US submarines. There are over 100 naval reactors and over 200 power reactors of this design in use worldwide [74].

An Advanced Gas Reactor (AGR) is cooled by CO_2 and fuelled by UO_2 in the form of pellets. The pellets are arranged in stainless steel tubes and the fuel enrichment is around 3%. The operating temperature is around 920K in the core. The CO_2 is circulated by gas pumps inside a gas baffle, from there it passes to the heat exchangers. It transfers heat to produce steam in the secondary coolant to power the turbines [75]

There are many other designs of reactor including Boiling Water Reactors (BWR) and Liquid Metal Fast Breeder Reactors. Currently a generation of reactors, known as Generation IV is being developed. This will give rise to new materials challenges to develop materials to withstand new and potentially harsher conditions.

The nuclear power industry has a safety responsibility due to the fundamental nuclear hazard. This is the release of radiation from a nuclear installation. Nuclear reactors have many safety features which are designed to protect against this occurrence. It is beyond the scope of this thesis describe them all, but one of these is very relevant to this research: the cooling system. This is not only important for taking away energy to make steam and drive the turbines, but also a crucial safety feature. This is because a reactor cannot immediately stop producing heat when it is shut down. There are four types of residual heat. Heat loss from the cooling high temperature of the reactor core. Heat loss from pumps, which is known as pump heat. The reactor core has many isotopes in the fuel rods which are undergoing radioactive decay, and this releases energy[155]. The neutron flux is not reduced to zero immediately and fission still occurs. The residual heat is one reason why the coolant system is important as heat from a reactor core can cause meltdown and it is not immediately possible to stop it from being released. The failure of this system is referred to as a loss of coolant accident or LOCA[156]. For this reason, the coolant systems form a key part of the safety case for a nuclear reactor. Many of the boiler tubes are made from thin section steels and fatigue and fracture of these is a matter of serious concern. The R6 code which is discussed in the next section is a part of this.

2.8 Development of R6

The nuclear industry has a unique safety culture due to the risks of releasing radiation. There is also a very substantial financial cost in taking a reactor off-grid for inspection or maintenance. In nuclear components the integrity of structures is of vital importance, since each component is part of the safe operation of the reactor. Nuclear reactors can have lifetimes of up to 40 years between being connected to the grid and the final closure of the plant. This means that given the high temperatures, pressures and in some cases radioactive environments, these components are at risk of failure, corrosion and fatigue. To decide whether a structure is still safe for use a Fitness for Service (FFS) or Fitness for Purpose (FFP) assessment is carried out. There is a significant burden on the licensee to demonstrate compliance with safety regulations to the regulator, the Office of Nuclear Regulation (ONR). Standardised methods of assessing the fitness for service (FFS) of a component that has cracks, flaws or similar defects. This can enable a safety case to be demonstrated and if permitted, the lifetime to be extended [78]

To ensure that components are being assessed in a consistent and reliable way, the Central Electricity Generating Board (CEGB) published a document known as Assessment of the integrity of structures containing defects or R6[79]. This introduced a range of techniques for assessing the integrity of a component including the Failure Assessment Diagram (FAD). The FAD is shown in Figure 2 gives an example of a FAD. On the y-axis, the value defined by K_r is the ratio of applied stress intensity factor to the fracture toughness of the material. On the x-axis, L_r is the ratio of the load on the sample in question and the load that would need to be applied to cause plastic collapse. The failure assessment line gives the boundaries of the safe region according to the assessment. This gives a conservative estimate of this region, accounting for both effects [79]R6 enables complex, mathematical fracture mechanics to be visualised in a simple diagram. As such it has become a widely used and accepted method, it also shows flexibility to different situations from basic calculations to the more rigorous Finite Element Analysis. R6 is reviewed and updated by a consortium of interested bodies this include: EDF Energy, TWI, Rolls-Royce and others [68]

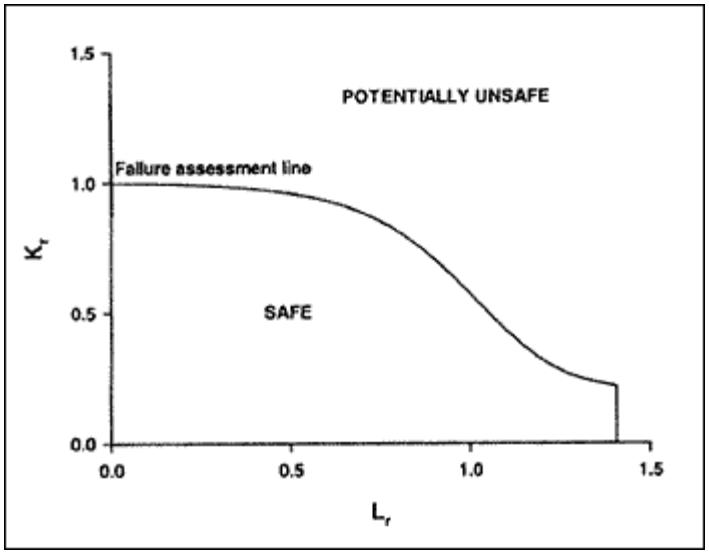

Figure 2: R6 FAD example showing failure assessment line. [81]

Many other methods for performing assessments have been developed alongside R6. These include R5, “An assessment procedure for the high temperature response of structures”. This is also a system for assessing a structure with flaws that are in the creep regime. It also includes structures that have no original flaws, but in which creep-fatigue crack initiation will occur. Many other industries and applications other than the nuclear industry also require standardised testing procedures. TWI used a method using Crack Tip Opening Displacement (CTOD) to quantify the effect of brittle fracture in welded joints. This is known as PD6493 and was essentially an alternative method of presenting the underlying fracture mechanics theory in R6. In the second edition of PD6493 it adopted the FAD method used in R6, which had previously been known as the CTOD design curve. The application of PD6493 has mainly been in welded pipelines such as those used in the offshore oil and gas industry [82] [83].

BS7910 is a fitness for service (FFS) code that was initially developed by The Welding Institute (TWI) and originally known as PD6493. It was developed for brittle materials with large amounts of plastic deformation at the crack tip. PD6493 was used extensively by offshore oil and gas industries in the UK for the assessment of pressure vessels and piping. The approach used the CTOD as a measurement of fracture toughness. In 1991, a new edition of PD6493 was published. This incorporated a FAD which brought it in to even closer alignment with R6. In 2000 the PD6493 code was renamed BS 7910, which makes it a British Standard. BS7910 and R6 are now the two most established fitness for service assessment procedures for assessing failure risk in structures containing defects, especially in the UK [105].

Whilst R6 has become an industry standard it does have the potential for improvement. R6 procedures are often considered excessively conservative. This is partly due to the upper bound values being used for variables proportional to crack driving forces, whilst the lower band values were used for variables such as the fracture toughness [82]. Also, the position of the failure assessment curve has been shown to be a long way from the points at which fracture occurs.

One means of justifying the expansion of the safe region is having a good understanding of the effect of constraint. Constraint in fracture mechanics is the effect of the physical space and geometry of sample on the stress field and the plastic zone around a crack tip. For example, a crack or defect that is long will have higher constraint than a shorter crack, since there is less space between the crack tip and the edge of the sample for the plastic zone to expand. This is known as high in-plane

constraint. A sample that is thin has a low potential for a plastic zone to expand through the thickness of the sample, therefore it could be described as having low out-of- plane constraint. Constraint in a specimen has an effect on the measured values of fracture toughness of a component.

There is another issue with the R6 approach: it does not currently incorporate effect of out-of-plane constraint in fracture toughness. It is possible that the measurement of a single constraint parameter could lead to a better understanding of defect and specimen geometry on fracture toughness and therefore lead to a reduction in the conservatism of R6 assessments.

2.9 Constraint in R6

Since it was first published in 1976, the R6 procedure has been continuously updated. These updates come out after approval by the committee which manages R6. The Failure Assessment Diagram has been a feature of R6 since the very beginning of this document. The first major update to the FAD came in 1986 [37]. This introduced the current definition of L_r as the ratio of flow stress σ_f and the 0.2% limit load stress σ_y. At this point, a new method was introduced for the failure assessment curve, the curve that defines the boundary on the FAD between the safe and unsafe regions. Instead of the original strip yielding approximation, material specific curves were created based on Ainsworth's reference stress J estimation scheme[76]. There were options for a range of different materials.

To account for more complex procedures that supplement the original FAD, the R6 procedure included appendices to be used in some circumstances that supplement the original FAD. Examples of these include mixed mode loads in 1991, local approach and finite element methods in 1998 and constraint effects in 1998. It is the constraint effects that most interests this project. In 2001 another large-scale overhaul of R6 took place. This restructured the document into 5 chapters. Chapters 1 and 2 cover the basic procedures including the FAD, Chapter 3 covers advanced procedures many of which used to be appendices, Chapter 4 covers residual stress and Chapter 5 consists of a series of worked examples which enhance the users understanding. Updates to R6 are known as amendments [85]. These amendments include an amendment by Kukla and Sherry in 2012 on constraint effects in thin sections [86].

The J-Q and K-T methods were initially adopted in the R6 constraint appendix. These are two parameter methods that account for in plane constraint only. As previously defined in this thesis, J and K are parameters which are measures of fracture toughness. Q and T are parameters which can quantify in plane constraint. In a two-parameter approach to structural integrity assessments, a relationship first has to be established between the parameters quantifying fracture toughness and constraint. These relations are specific for the material which the part is made from. R6 does this by providing the correlation equations.

$$K_{mat}^{C} = \frac{TK_{mat}}{\sigma_y}, Q \geq 0$$

$$K_{mat}^{C} = K_{mat}\{1 + \alpha(-Q)^k\} Q < 0 \text{ or}$$

$$K_{mat}^{c} = K_{mat}\left\{1 + \alpha(-\frac{T}{\sigma_y})^k\right\}/\sigma_y < 0$$

K^c_{mat} is the fracture toughness of the material when considering constraint, K_{mat} is the fracture toughness of the original R6 value, σ_y is the yield strength of the material [37].

The constants α and k are material specific. This means that they must be measured for each R6 assessed material. A series of experiments has to be performed. In these experiments, the fracture toughness is measured for specimens with different levels of in plane constraint. This means that the notches in the specimens have different depths which is usually expressed in terms of a/W. The fracture toughness, for example J or K are measured and the value of the constraint parameter Q or T is determined for each level of constraint. The values of k and α can then be obtained using a fit to the correlation equations. At least three points would be needed for such a fit, preferably more and the goodness of fit depends on the experimental data obtained. A number of experiments have been conducted which have enabled the tabulation of the fracture toughness against in plane constraint parameters T and Q [39]. These experiments are satisfactory in confirming the relationship between constraint and fracture toughness i.e., that low constraint implies high fracture toughness and high constraint implies low fracture toughness. However, this relationship is between fracture toughness and in plane constraint only. When the constraint parameters are applied to experiments involving different specimen thicknesses, that is varying out of plane constraint, no good correlation is found between T or Q and fracture toughness[87].

2.10 Application of unified constraint parameter in R6

In order to account for out of plane constraint, three parameter theories are used with one parameter each for in and out of plane constraint. These include K-T-T_z and J-Q_T-T_z theories as already referred to in the previous section “Out of Plane Constraint”. Given the time consuming and costly nature of these assessments, performing a correlation of three parameters may not be productive if used in an FFS procedure such as R6. This is exemplified by the fact that if the correlation between the parameters was to be plotted the locus of points would form a surface which would be more computationally expensive. Therefore, an alternative method is sought with a parameter that quantifies both types of constraint.

There are a number of candidates for a parameter to quantify both types of constraint that have appeared in the literature. For each candidate parameter, a large amount of tabulation work would need to be undertaken to find the correlation constants and equations for each material, before it could be accepted in a FFS code or procedure.

These are usually based on the size of the plastic region around the crack tip or the crack tip opening displacement CTOD, which is a measure of how large the plastic zone is at the crack tip. The parameter A_d and A_d^* were proposed to account for out of plane constraint by Xiao et al [88]. These are defined in the out of plane constraint section of this thesis. A large number of finite element simulations have been carried out on a wide range of materials and standard specimen types. These were mostly steels which showed ductile fracture. A wide range of specimens were used including those with semi-elliptical cracks which were used to find the m factor which connects J and CTOD on which A_d and A_d^* were based. The values of α and k were also determined for CT and SENB specimens with a many materials and constraint levels.

There has been a large body of work produced on unified constraint parameters based on plastic zone size, particularly in the 2010s. Since Dodds, Anderson and Kirk first defined A_C as the area inside the maximum stress contour, many experiments have been carried out to test parameters based on measures of plastic zone size for their sensitivity to both forms of constraint [89]. The parameter ϕ as defined as the ratio of the area A_C to the area in this zone for arbitrarily low levels of plasticity used as a reference. This parameter was found to be effective only when the yielded region was very small. Mostafavi et al, defined a variant of this known as ϕ^p in terms of the cube root of the volume

of the plastic region divided by a reference volume [68]. This parameter performed well in terms of unifying constraint but had a similar drawback to ϕ when large scale yielding occurred. In recent simulations of a large number of fracture parameter ϕ was shown to have sensitivity to in and out of plane constraint. The work of Seal and Sherry combined the Anderson-Dodds toughness scaling procedure with the Rice and Tracey model for predicting crack initiation at a critical void size. By determining the Rice and Tracey parameter the onset of fracture is predicted and the area inside the Anderson Dodds contour can be computed at this critical value. This means that the effect of constraint on fracture toughness can be estimated. This study also included tabulation of α and k at different stress contours. By finding the ratio of low constraint to high constraint it was possible to eliminate the need to know the Rice and Tracey parameters for each specific case[83].

It was decided to focus the work in this project on establishing a relationship between the ϕ parameter and fracture toughness. The reason for this is that there is a clear need to improve on the excessively conservative assessments in R6 which do not account for out of plane constraint. To account for constraint more completely a unified constraint parameter would be most convenient.

3 Credit Statement

Credit Statements for each paper

The roles of each author are clearly stated here for clarity.

Paper 1: Unifying the Effects of in and out-of-plane constraint on the fracture of ductile materials

SM Tonge: Experimental work, data analysis, simulations, image processing, writing-original draft, data curation. CA Simpson: Experimental work, writing- review and editing. C. Rheinhard: Experimental work, writing- review and editing. T. Connolley: Experimental work, writing- review and editing. A. Sherry: Methodology, writing- review and editing. T J Marrow: Funding acquisition, writing review and editing. M Mostafavi: Supervision, funding acquisition, writing review and editing.

Paper 2: Quantifying combined effects of in-plane and out-of-plane constraint in an aluminium alloy

SM Tonge: Methodology, experimental work, data analysis, simulations, writing- original draft. Z Cheng: Software development, writing- review and editing. C Meek: writing- review and editing. M Mokhtarishirazabad: Experimental work, writing review and editing. M Mostafavi: Supervision, funding acquisition, writing- review and editing.

Paper 3: Determination of constraint parameters K and ϕ from three point bending test on Al7075 pipe

SM Tonge: Experimental work, experimental design, simulations, data analysis, writing- original draft. M Mokhtarshirazabad: Experimental work. R Patel: industrial liaison. M Mostafavi: Supervision, funding acquisition.

4 Paper 1-Synchrotron experiment

This paper was listed under journal papers, it provided evidence of the sensistivity of parameters to constraint effects.

Unifying the Effects of in and out-of-plane constraint on the fracture of ductile materials

S M Tonge[1], C A Simpson[1], C Reinhard[2], T Connolley[2], AH Sherry[3], TJ Marrow[4], M Mostafavi[1,1]

a. Department of Mechanical Engineering, University of Bristol, Queens Building, University Walk, Bristol, BS8 1TR
b. Diamond Light Source Ltd, Harwell Science and Innovation Campus, Didcot, Oxfordshire OX11 0DE
c. National Nuclear Laboratory, 5th Floor, Chadwick House, Warrington Road, Birchwood Park, Warrington, WA3 6AE
d. Department of Materials Science, University of Oxford, 21 Banbury Road, Oxford OX2 6HT

Abstract

Effects of plastic constraint on the fracture of materials have been studied extensively. Often in such studies, the plastic constraint is divided into in-plane and out-of-plane directions and each treated separately. Such a separation adds considerable complexity to the engineering structural integrity assessment analyses. Despite previous suggestions for unifying the effects of constraint in a single parameter, the current engineering assessments have not been updated due to lack of direct experimental validation of such parameters. In this study, we directly measured the effects of in-plane and out-of-plane constraints, for the first time, in the form of plastic zone around the crack using advanced experimental techniques. The measurement of constraints in four specimens with different levels of in and out of plane constraints, allowed us to show and relate the interdependency of in and out of plane constraints. The tests were carried out using synchrotron X-ray tomography with in-situ loading. Attenuation contrast between the constituents of the metal matrix composite material used allowed the tomograms to be analysed using digital volume correlation which calculated the full-field displacement within the samples. The displacement fields were used via a finite element framework to calculate the energy release rate in the form of the *J*-integral along the crack fronts. The measured plastic zone sizes, dependent on the combined level of in plane and out of plane constraints, were used successfully to rank the *J*-Integral at fracture of the samples. It was therefore proved the level of plastic constraint can be quantified by using the size of the plastic zone as without separating it into two components thus simplifying the treatment of constraint in structural analyses significantly.

4.1 Background

4.1.1 Plastic constraint

Plastic constraint has been shown to considerably affect the measured toughness in metallic materials that show limited plasticity before fracture [90]. High constraint specimens such as

[1] Corresponding author
Tel: +44 (0) 117 331 5717
Email: m.mostafavi@bristol.ac.uk

compact tension and single edge notch bend, with a crack extending to almost half of the ligament with a thickness that satisfies plane strain conditions, are regraded to measure the lower bound fracture toughness [91]. This is because the loss of constraint results in an apparent increase in the fracture toughness due to the higher level of plastic work required before crack initiation [92] [93] [94]. Constraint is often divided into in-plane and out-of-plane, where in-plane is along the direction of the crack propagation and out-of-plane is perpendicular to it along the crack front. In-plane constraint is predominantly influenced by the specimen geometry and the crack length, while the major factor in out-of-plane constraint is the thickness. Despite the similarity between the physical effects of in and out-of-plane constraints, they are treated separately in engineering structural integrity assessment assessments due to lack of a unified measure of constraint [95], adding complexity to the analysis. Different parameters have been used to quantify in and out-of-plane constraint, which are briefly reviewed below.

4.1.2 In-plane constraint

The *T*-stress is a second order term of the asymptotic stress field along the crack tip independent of distance from it [5]. It has been shown that *T*-stress is a measure of in-plane constraint when the plastic zone around the crack tip is small enough for the stress field to be reliably approximated by linear elastic fracture mechanics [96]. It is argued that due to the effect of the plastic region on the stress field around a crack, it is not possible to use a single parameter for fracture assessments [7]. For this reason, *T*-stress has been used as an additional parameter to *K*, the stress intensity factor, in fracture assessments [5]. The validity of using *T*-stress as a measure of in-plane constraint is supported by the evidence of a large number of experiments, showing the variation of apparent fracture toughness as a function of *T*-stress [97] [98]. The sign of the *T*-stress as well as its magnitude indicates the size of the plastic zone which varies as the in-plane constraint changes [99]. Fracture toughness and the size of the plastic zone around the crack tip increases with increasing negative value of *T*-stress. Zero and small positive values of *T*-stress, as obtained in the standard fracture toughness specimens, are considered to minimise the size of the plastic zone around the crack tip thus resulting in the lower bound fracture toughness [100]. A more positive *T*-stress, however, can cause crack instability and branching [101]. *T*-stress is also sensitive to the loading regime; for example, in a single edge notch specimen under tensile loads the *T*-stress will be negative, while it will switch to a low positive value for a bending load. To enable fracture assessments to take the effects of constraint into account, *K* - *T* loci have been constructed empirically [102]. In order to expand the applicability of elastic *T*-stress to elastic plastic conditions, *J* - *T* loci have also been compiled (*J* is the *J*-integral, energy release rate associated with a crack in a nonlinear elastic medium) [103] [78].

While *T*-stress is a valid measure of in-plane constraint for materials with near linear elastic behaviour, *Q* is used in the case of elastic-plastic materials. It was defined by O'Dowd and Shih [6] [79] as shown in (Eq. 1).

$$\sigma_{ij} = \sigma_{ij}^{HRR} + Q\sigma_o\delta_{ij} \qquad \text{(Eq. 1)}$$

σ_{ij} is the measured/simulated stress field around the crack tip, σ_{ij}^{HRR} is the stress field as defined by Hutchinson, Rice and Rosengren [104] (HRR) for a nonlinear elastic material (e.g. Ramberg-Osgood material model) and σ_0 is the material yield stress. *Q* can be seen as the difference, at any point in the stress field, between the stress field as defined by HRR whose magnitude is quantified by the *J*-integral (*J*) and the measured/simulated stress field. It thus quantifies the deviation from the stress field in high constraint standard specimens. The

implementation of Q into the assessment codes and procedures uses the definition given in (Eq. 2.

$$Q = \left.\frac{\sigma_{yy} - \sigma_{yy}^{SSY(T=0)}}{\sigma_0}\right|_{r=\frac{2J}{\sigma_0}} \quad \text{(Eq. 2)}$$

Q is given at a radial distance $r = 2J/\sigma_0$. σ_{yy} is the opening stress (see Figure 3.1a for the coordinate system) r is the radial distance from the crack tip, and $\sigma_{yy}^{SSY(T=0)}$ the opening stress for the small scale yielding condition when T-stress is zero. When Q is negative, the stress field experienced by the material is lower than the predicted reference stress field. When the stress field is greater than the reference stress field, the Q value is positive. Therefore, similar to T-stress, negative Q shows the loss of constraint and an increase in the apparent fracture toughness while positive Q indicates high in-plane constraint resulting in the measured lower bound fracture toughness. Experiments to measure and tabulate Q showed that it was possible to greatly increase the scope of assessments using J by also including the Q parameter [80]. J - Q loci have been produced which are incorporated in the assessment procedures such as R6 [81]and BS7910 [105]. Further evaluation of J - Q theory has been performed for specific samples including single edge notch bend (SENB) and compact tension specimens and new formulae were proposed to optimise the calculation of Q in a situation with high plastic deformation for bending samples [106].

It is also argued that Q quantifies the triaxiality of stress around the crack tip [51]. The stress triaxiality factor (T_f) is the ratio of the hydrostatic stress to the von Mises stress and relationships between Q and T_f have been proposed [82]. Alternatively, T_f has also been used to quantify constraint and include it in the assessment procedures [41]. Other measures of constraints have also been proposed such as A_2 [83] which are somehow analogous to Q.

4.1.3 Out-of-plane constraint

T-stress and Q quantify in-plane constraint while T_z is the out-of-plane constraint factor [84]. It has been defined in (Eq. 3, in terms of different components of a stress field [7].

$$T_z = \frac{\sigma_{zz}}{\sigma_{xx} + \sigma_{yy}} \quad \text{(Eq. 3)}$$

It is defined for a crack plane occupying the xz plane and propagating along the x direction. The motivation for using T_z is similar to the other two-parameter approaches (e.g. K - T and J - Q), in this case taking into account the effect of out-of-plane constraint (predominantly component thickness). To gain information about out-of-plane constraint, finite element simulations can be used to find T_z in a range of different thicknesses with similar in-plane geometry. Originally, Guo used simulations of elastic plates with embedded centre-elliptical cracks and considered different aspect ratios (i.e $0.2<a/c<1$ where a is the crack depth and c is its surface length) to quantify T_z. The results were used to propose a two-parameter theory K - T_z that accounts for out-of-plane constraint [7]. To combine the effects of in and out-of-plane constraint, three parameter theories such as K - T - T_z and J - Q - T_z have been proposed [85] [86]. Comparisons were made between K - T - T_z, J – Q - T_z and K - T and J - Q theories which showed that the proposed three dimensional methods were able to account accurately for three-dimensional stress fields [68] though they are complicated and require large experimental datasets in which both in-plane and out-of-plane constraints vary.

4.1.4 Unified measure of constraint

Although many of the parameters quantifying constraint are restricted to either in or out-of-plane, there are parameters that are sensitive to both forms of constraint. It is therefore possible that a loci of fracture toughness could be found from a two-parameter fracture assessment by combining the effects of constraint regardless of its direction. For example, Dodds, Anderson and Kirk [8] proposed using the area inside a contour defined by an arbitrary constant maximum principal stress as a measure of constraint (see (Eq. 4 [106]).

$$\frac{\sigma_1}{\sigma_0} = C \qquad \text{(Eq. 4)}$$

C is an arbitrary constant, σ_1 and σ_0 are the maximum principle stress and the yield stress respectively. The size of area bounded by the contour (A_c) determines the level of constraint. High constraint results in a smaller area while low constraint yields a larger area [108]. Therefore, a dimensionless parameter φ, defined in (Eq. , is suggested as a unified measure of constraint:

$$\varphi = \frac{A_c}{A_c^{SSY}} \qquad \text{(Eq. 5)}$$

φ is the ratio between the area confined within an arbitrary isostress contour C (A_c) to the area measured when small scale yielding prevails (i.e. A_c^{SSY}) [109]. While this parameter can be used for the fracture of ductile materials which show small scale yielding, it is no longer applicable when large scale plasticity occurs. For this reason, variations of the Dodds, Anderson, Kirk method have been proposed; for example, Mostafavi and co-workers suggested φ^p [87].

$$\varphi^p = \sqrt[3]{\frac{V_P}{V_{ref}}} \qquad \text{(Eq. 6)}$$

where V_P is the volume of the plastic zone in a given component and V_{ref} is the volume of the plastic zone in a standard high constraint specimen (e.g. compact tension). While it was shown that φ^p can predict the failure of aluminium alloys in combined in and out-of-plane constraint condition [109], its application is limited to component geometries and loads in which the plastic zone size is a small proportion of the uncracked ligament, i.e. contained. Yang et al. proposed another modification to the Dodds, Anderson, Kirk method in which A_{PEEQ}, the plastic strain volume within a ε_p isoline, is normalised by A_{ref} which is the volume within the isoline for a sample with high constraint [8].

Studies testing the effect of in- and out-of-plane constraint on a large number of parameters have been carried out. Shlyannikov et al. showed that the stress intensity factor changes as both in- and out-of-plane constraints change [110]. Mu et al. carried out finite element simulations on a series of compact tension and single edge notch bend specimens with varying in and out of plane constraints; they found that φ responded to changes in both in and out-of-plane constraints well [111]. This could allow the use of A_p as a unified constraint parameter in future. Seal and Sherry have recently combined the Rice and Tracy [88] fracture criterion with the φ constraint parameter to predict the effects of fracture of ductile materials [112].

Recently different variations of Anderson – Dodds – Kirk unified measure of constraint have been considered and theoretical investigation on their validity has been performed (e.g. see [[89], [90]]). For example, a CTOD based unified measure of constraint, A_p, has been developed [113] similar to Anderson – Dodds – Kirk concept. Based on these theoretical studies, A_p – toughness loci have been built for brittle [114] and ductile [91] materials as well as weldments [115] or similarly A_d – toughness loci are built for pipes [92].

While it is shown that the normalised plastic volume near the crack tip in various forms can be used as a unified measure of constraint, potentially simplifying the methods that account for the constraint effect, they have not been included in assessment procedures yet. This is partly due to limited validation of the methods, since measuring full-field strains and the volume of plasticity around the crack tip has not been possible except on the surface of the material (e.g. using optical methods such as digital image correlation [93]). In this work, we employed advanced measurement techniques, namely X-ray tomography and Digital Volume Correlation, to make such measurements for the first time.

4.2 Experiments and Results

4.2.1 Specimens and material

The purpose of this work is to directly measure the energy release rate and the size of the plastic region developed around the crack tip upon crack initiation. The measurements will be used to validate unified measures of constraint. To this end, double edge notch tension specimens (see Figure 3.1a) were tested; the specimens had cracks with an initial length *a*, width *W* and thickness *b*. It has been shown before that for materials that show large crack tip blunting before fracture (e.g. aluminium alloys [116]), fatigue pre-cracking is not necessary. Thus, wire electro-discharge machining with a 0.1 mm wire diameter was used to introduce a sharp notch/crack in the samples. Grips were designed to attach the specimen to the test frames (see Figure 3.1b).

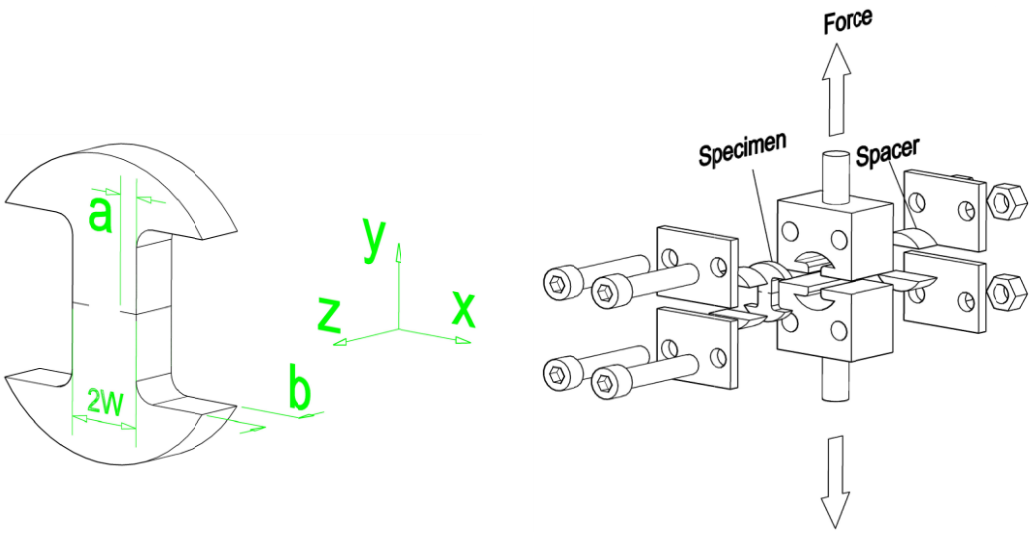

(a) ***(b)***

Figure 3.1: Test specimen (a) the fixture connecting the sample to the loading frame (b) single edge notch tension specimen

Four different samples with varying in and out-of-plane constraint levels were tested. Different thicknesses were used to vary the level of out-of-plane constraint (b = 5 and 20 mm). Different notch lengths were used (a = 0.4 and 2 mm) to provide different levels of in-plane constraint. Details of the samples can be seen in Table 1.

The applicability and quality of Digital Volume Correlation data is strongly dependent on the size and distribution of the inherent, internal speckle pattern [94]. It was therefore necessary to select a material containing microstructural features with distinct X-ray attenuation coefficients with respect to their matrix; this would provide an appropriate speckle pattern with sufficient contrast in the tomograms. To this end a metal matrix composite with an aluminium matrix and titanium particles was selected. The difference between attenuation contrast of aluminium (0.273 cm^2/g and 0.257 cm^2/g at 59.6 keV and 61.9 keV respectively) and titanium (0.742 cm^2/g and 0.664 cm^2/g at 59.6 keV and 61.9 keV respectively) was sufficient to obtain tomograms with a suitable speckle pattern (see next section for details and choice of X-ray beam energy). The mechanical response of the material, henceforth referred to AlTi, was measured according to ASTM E8 [107] using a 12.5 kN hydraulic testing frame and a round bar specimen. The load was recorded from the frame's load cell which was synchronised through a Vishay System 9000 data acquisition system with the strain measured by a rosette strain gauge. A typical stress – strain curve obtained can be seen in Figure 3.2. Since no unloading took place in the experiment (see section 4.3), a nonlinear elastic material model, namely Ramberg – Osgood, was used as defined in (Eq. 7) to describe the material properties.

$$\frac{\varepsilon}{\varepsilon_0} = \frac{\sigma}{\sigma_0} + \alpha\left(\frac{\sigma}{\sigma_0}\right)^n \qquad \text{(Eq. 7)}$$

σ_0 is yield stress, ε_0 is yield strain, n is the hardening exponent, and α is a dimensionless offset constant [27][117][118] material has a Young's modulus, E= 100.2 GPa, and n= 6, σ_0= 103 MPa, α= 2.75.

Table 3.1- details of 4 tested specimens

Name	Thickness b (mm)	Crack length a (mm)	Width $2W$ (mm)	Fracture load F_c (kN)
Short – Thin	5.0	0.4	8	4.5
Long - Thin	5.0	2.0	8	4.0
Short - Thick	20	0.4	8	14.9
Long - Thick	20	2.0	8	15.0

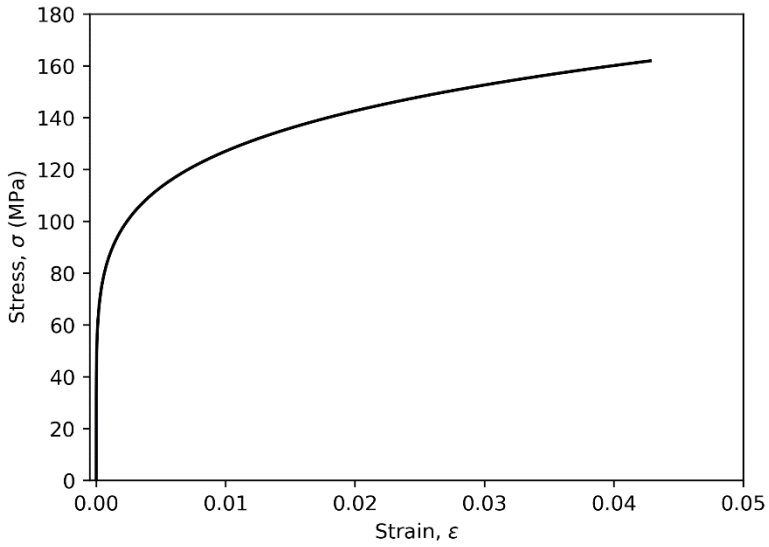

Figure 3.2: Mechanical response of AlTi

4.3 X-ray computed tomography

The experiment was carried out in Experimental Hutch 2 (EH2) of the I12 beamline at the Diamond Light Source [119] (experiments EE12606-1 and EE12606-2). A 10 kN Shimadzu electric test frame was used to load the 5 mm thick samples and a 100 kN hydraulic Instron test frame was used for the 20 mm thick specimens (these required a higher load than the capacity of the Shimadzu). A view of a fracture specimen within its grip is shown in Figure 3.3.

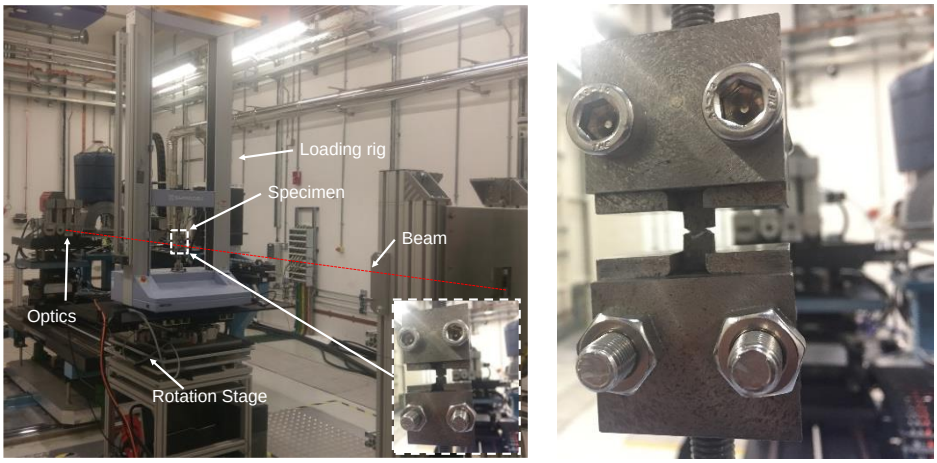

(a) (b)

Figure 3.3: Experimental setup (a) 10kN loading frame on I12's external experimental hutch tomography stage (b) view of the specimen within the fixture attached to the loading frame

Limited angle computed tomography was performed on all 4 samples (over an angular range of 145˚); this was necessary as the frames of the two-column loading rig design restricted the angles over which radiographs could be acquired. A beam energy of 59.6 keV was employed for the thick samples and 61.9 keV for the thin samples during EE12606-1 and EE12606-2 respectively. For each tomogram 2501 projections were collected using the I12 X-ray

imaging modules, utilizing a picoEdge 5.5 camera at an exposure time of 0.05 s. The projections are observed using optical modules that observe a scintillator, with a resolution that depends on the optical module. Optical module 3 was selected for the thin specimens; this module provides a X2 magnification (i.e. pixel size 3.3 μm^2) with a field of view of 8.0×7.0 mm^2. While the thin samples' full width was within the field of view, the diagonal length (9.4 mm) extended beyond this and thus the sample corners were not captured in the reconstructed tomogram. Optical module 2 was used for the thick specimens; this module has X1 magnification (pixel size 7.9 μm^2) with a field of view of 20×12 mm^2. The thick samples' diagonal lengths were also larger than the field of view thus their corners were similarly missed in the tomograms. The distance between the detector and the specimen was ~1480 mm in all cases. The distance between the specimen and the detector enhanced the phase contrast of the tomograms [120] which helps with crack detection [121].

Initial tomograms were recorded at 50 N (to settle the specimen in the grip but apply minimal load). The specimens were then loaded at 0.1 mm/min in small loading steps while real time radiograph projections were recorded. Once crack initiation was observed in the projection, a full tomogram was recorded with the specimen under load. The 3D tomograms were reconstructed using a Fourier grid reconstruction algorithm (Gridrec) [122], which is implemented in Tomopy [123] and allows for the interpolation of the missing projections (i.e. accounts for the limited angular data). The reconstruction was completed after a sequence of pre-processing steps, which included a flat-field correction, de-zinger and ring artefact removal [124] The quality of the reconstructions was high, despite the use of limited angle tomography. The focus of study was on performing Digital Volume Correlation (DVC) to track the movement of material using the internal grey scale features, which was not impaired by limited angle tomography. The reconstructed dataset was 2160 16-bit virtual *xz* slices of the specimens each measuring 2560×2000 pixels; an example series of the image slices is shown in Figure 3.4a. A representative slice before and after loading is shown in Figure 3.4b.

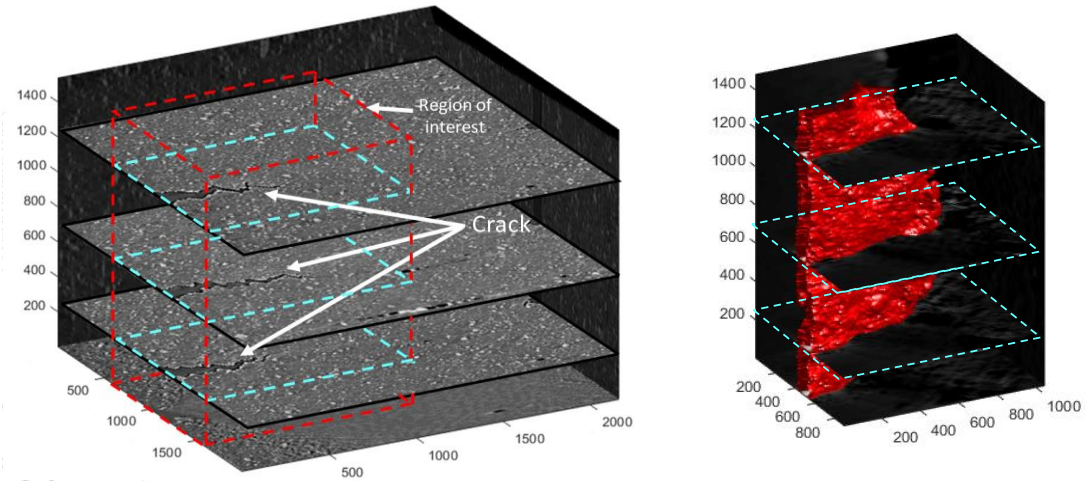

(a)

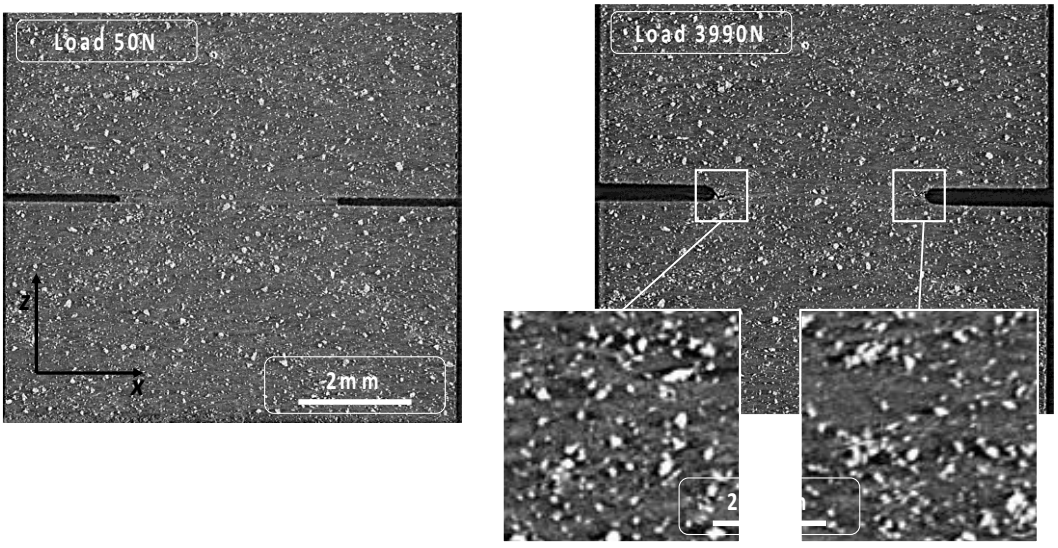

(b)

Figure 3.4: Reconstructed tomography data (a) virtual stack of xz slices of the cracked thick-long sample and the segmented crack shown in red; each voxel is 3.3µm (b) example of the xz slice before and after cracking in thin long sample at its mid-thickness

4.3.1 Digital Volume Correlation (DVC)

After the tomograms were reconstructed, each set of reference (50N applied load) and cracked volumetric tomography images for the four conditions of constraints were analysed using DVC. DVC tracks pattern of the grey scale features within the material to build 3D full-field displacement volumes [125]. The LaVision Davis 8 [126]software was used in this work, employing a cross correlation algorithm in Fourier space (direct correlation using a root mean square minimisation algorithm is available in the newer versions of the software but was not available at the time) [127]. The software divides each tomogram into smaller cubic interrogation volumes and measures their relative movement thus quantifying deformation as a displacement field. To improve the spatial resolution of the full-field displacements the software can start with large interrogation volumes, also known as subsets, which contain more features before splitting the volume into smaller volumes in subsequent passes. Overlaps between adjacent interrogation volumes can also be used to improve the spatial resolution of the displacement field, if the gradients of displacement are sufficiently small. To increase the speed of the analysis, visual inspection of the tomograms was used to identify the region of interest (i.e. the location of the crack - see Figure 3.4a) and cropping the original 2560×2160×2000 (x×y×z) image stack into smaller stacks. The thick sample with a long crack was cropped to 2200×1550×1500 and then analysed with DVC. The first pass had a subset size 64^3 voxels with an overlap of 50%. The second pass used a subset size of 32^3 voxels with an overlap of 50%. In the third pass a subset size of 16^3 voxels was used with an overlap of 80%. The thick sample with a short crack was first cropped to 2000×1550×1400, then analysed with a subset size 121^3 voxels with an overlap of 80% as the first pass. The second pass used a subset size of 64^3 voxels with an overlap of 50%. In the third pass a subset size of 32^3 voxels was used with an overlap of 50%. In the fourth pass a subset size of 16^3 and overlap of 80%. The thin sample with long notch was not well positioned relative to the beam and the initiated crack was towards the upper side of the image stack rather than its middle. In this case, the stack was be cropped to 300×1550×300 prior to a DVC analysis which started with a subset size 32^3 voxels with an overlap of 50%.

A second pass used a subset size of 16^3 voxels with an overlap of 80%. In the third pass a subset size of 8^3 voxels was used with an overlap of 80%. Finally, the thin sample with a short crack was cropped to a size of 1050×1550×900; the DVC analysis started with a first pass a subset size 256^3 voxels with an overlap of 80% was used. The second pass used a subset size of 64^3 voxels with an overlap of 80%. In the third pass a subset size of 32^3 voxels was used with an overlap of 80%. In the fourth pass a subset size of 16^3 voxels was used and an overlap of 50%.

The results of the DVC analyses were four sets of full-field displacement vectors each corresponding to an initiated crack under varying in and sets of out-of-plane constraint conditions. A previously developed code that identifies a crack in a displacement field using a volumetric phase congruency algorithm was used to segment the crack [128] [129] [130]. The code also identifies the vertical displacement on either side of the crack face and, by subtracting them from each other at every point across the crack profile, calculates the crack opening displacement along the crack face. An example of the segmented crack (the red volume) is shown in Figure 3.4a. The results of crack opening displacement calculations can be seen in Figure 3.5 for each sample. Crack opening displacement along the full thickness of the thin samples could be measured across the sample barring regions very close to the sample edge. The thick samples, however, could not be analysed through the full thickness. This was partly due to their larger diagonal length and an offset between the sample centre and the tomography rotational axis. In order to increase the evaluate the robustness of the complex methodology with which the crack opening displacement profiles were measured, profiles along *x* direction (see Figure 3.1) in mid-thickness of all samples were selected and crack opening displacements along these profiles were extracted. The opening displacements were normalised by the crack opening displacement at the tip of the notch and the distance from the notch tip was normalised by the crack length from the notch tip as measured by phase congruency code. The results can be seen in Figure 3.6.

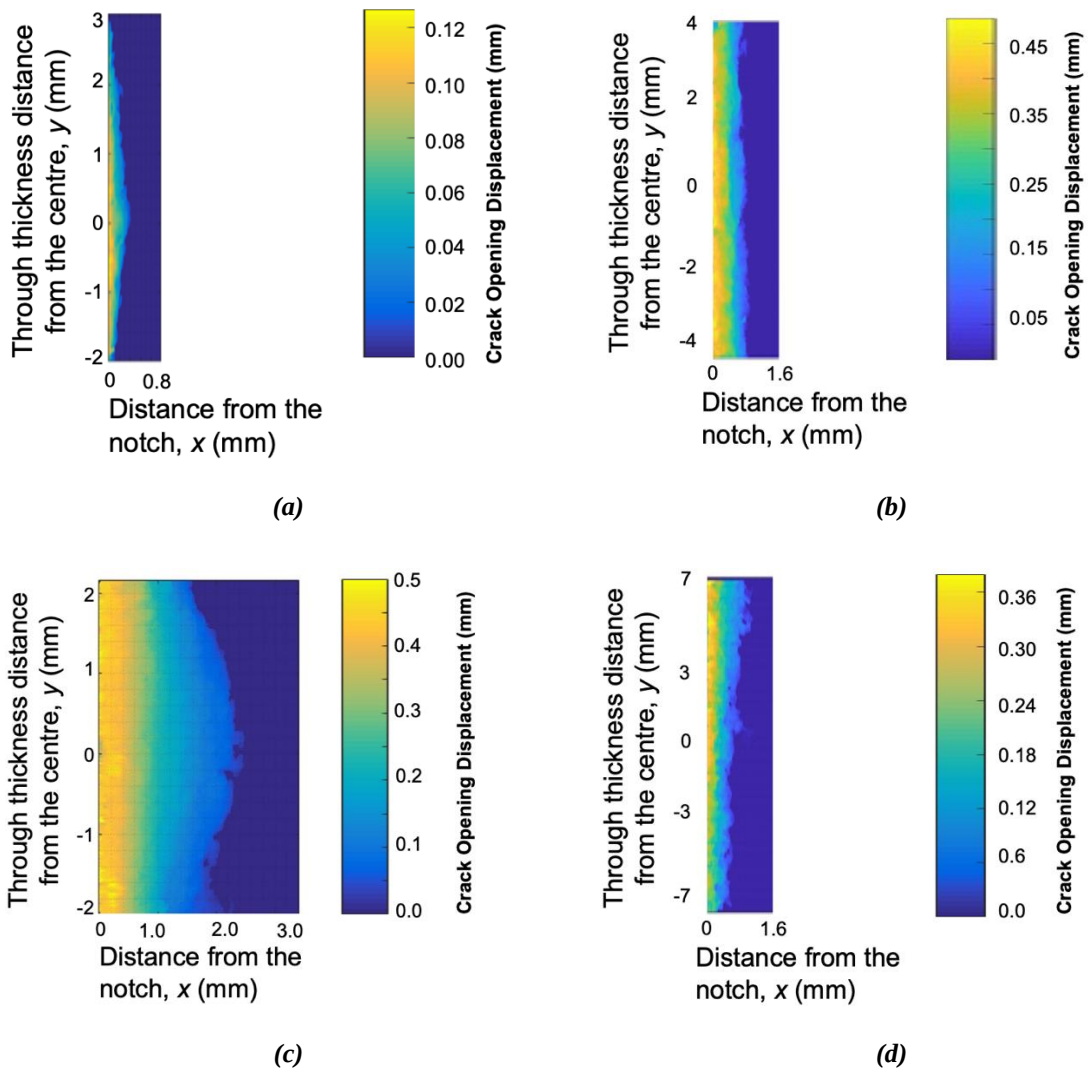

Figure 3.5: Mode I Crack opening displacement (a) thin – short (b) thick short (c) thin long (d) thick long. The crack opening displacements shown are calculated at the fracture load of each specimen, see Table 1.

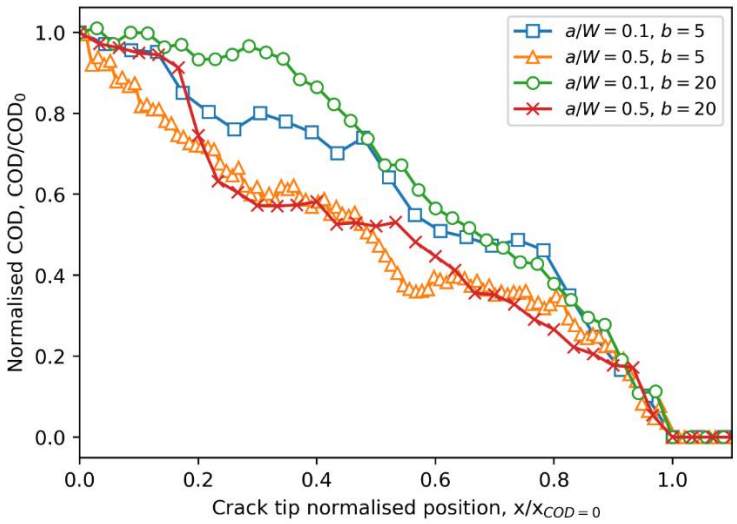

Figure 3.6: Normalised crack opening displacement profiles measured along the mid-thickness of each specimen at fracture.

4.3.2 J-integral calculation

A previously developed code [131], was used to calculate the energy release rate as a *J*-integral, from the displacement fields. The details can be found elsewhere [132]; in brief, the code creates a finite element mesh corresponding to the interrogation volumes at the final pass of the DVC analysis. It uses the geometry of the crack identified by phase congruency [133] to introduce a planar discontinuity in the mesh (i.e. two adjacent elements with nodes that are not tied together and can freely displace). It then reads the full-field displacement on every node in the model as boundary conditions. This creates an over-constrained finite element model, utilising Abaqus to calculate the strain field and the pre-defined constitutive law to calculate stress. Since the displacement field calculated by DVC near a discontinuity is not accurate [119][123], the code omits the DVC displacement field around the crack and allow the FE to solve for the displacement field in that region. Finally, it uses Abaqus' built in contour integral method to calculate the energy release rate associated with the crack. It is important to note that this analysis uses no information regarding the specimen dimensions, crack length or applied load. The current code uses two-dimensional plane strain/plane stress linear reduced integration elements (CPE4R) and imports the displacement field calculated by DVC slice by slice thus the volume of the simulation depends on the dimensions of the dataset. While this is a valid assumption for the surface (if plane stress elements are used) and middle of the specimens (if plane strain elements are used), it ignores the displacement field in the third direction (along the thickness) which could cause considerable error in the calculation of *J*-integral where plane strain or plane stress do not prevail. This point will be further discussed in the discussion section. It should be also noted that even the 20 mm thick specimens do not satisfy the ASTM E399 plane strain condition (i.e. $b>2.5(K_I/\sigma_o)^2$) as the minimum thickness dictated by the condition is above 350 mm which makes the X-ray penetration impossible.

The analysis used the material properties measured in section 5.2.1 and plane strain elements to represent the centre of the specimens. It used 20 contours around the crack tip for every virtual slice to ensure path independency of measured *J*-integrals. In all cases the values converged within the first 10 contours. The results for the *J*-integral were converted to K_J as per (Eq. 8):

$$K_J = \sqrt{\frac{JE}{1-\nu^2}} \qquad \text{(Eq. 8)}$$

Figure 3.7 shows the variation of K_J^{exp}through the normalised sample thickness. The thickness normalisation is carried out by the thickness through which *J* could be calculated x_0; that is, 5 mm and 4 mm for the thin sample with short and long cracks respectively (see Figure 3.5a and c) and 8 mm and 14 mm for the thick sample with short and long cracks respectively (see Figure 3.5b and d).

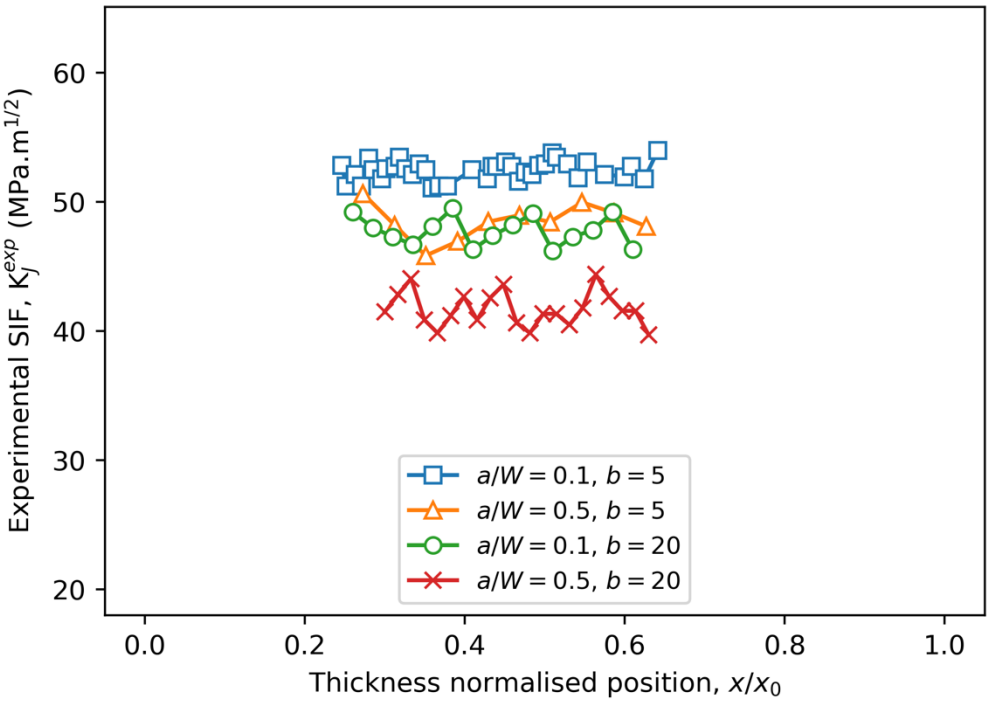

Figure 3.7: Experimentally measured stress intensity factor (SIF) plotted along the thickness of the sample by FE-DVC; typical error in K calculation estimated from the variation in K when contour independency was assumed to have been reached is 1.5 MPa.mm$^{1/2}$

4.4 Finite Element Modelling and Results

To independently validate and verify the stress intensity factors obtained in the previous section, three-dimensional finite element (3D FE) models of the experiments were created. It is important to note that in the previous section, the stress intensity factor was calculated using the displacement field measured and the measured material's constitutive law used to convert the strain to stress via DVC-FE. In the finite element analysis, on the other hand, the displacements were not used, rather the independently measured fracture force was exploited, using the material's constitutive law and specimen geometry to calculate the resultant displacements, strain field and stress field. It therefore can be argued that the two analyses are independent thus providing a robust validation route.

For the FE model, three-dimensional models of the four specimens were created using Abaqus 6.14[123]. A 3D rigid body was created using 14,830 shell discrete rigid elements representing the loading fixture (see Figure 3.1a); the sample was made of 56,320 3D deformable linear solid elements CP20R. The seeds around the crack were 0.1 mm apart and 0.5 mm for the rest of the model. The mesh seeds were biased towards the curved blunted surface, but no degenerate elements were used at the crack tip. Two planes of symmetry were used to reduce the volume of the sample to a quarter of the actual size, x and y symmetry boundary conditions were enforced at the edges of the model. Each crack was modelled by removing the boundary conditions from the nodes along the notch of the sample. The effect of reduced stress singularity at the wire electro discharge machined notch (the samples were not pre-cracked) had to be included in the model. Without it, locally, the stress fields around the crack tips are unlikely to be accurate [124]. In order to allow for the effect of the blunt notch, the model had a notch radius of 0.05 mm, which allowed for the effect of the wire EDM to be considered. The crack was defined as a symmetry plane crack with a crack tip, on the line joining the curved blunted surface to the lower symmetry plane. The crack extension direction was perpendicular to the surface of the notch [127]. The simulation

used the same Ramberg – Osgood material model, as described in section 4.3.2. The model is shown in Figure 3.8 (the contour map shows the Von-Mises stress).

The rigid body's reference point was moved in displacement control and the applied displacement was iterated until its reaction force reached the experimental load that induced failure (given in Table 1) taking into account the symmetry planes defiled. The *J*-integral was calculated by defining a history output request; for the contour integral 20 contour integrals were used, the first of which was at the crack tip to ensure contour independency. The *J*-integrals, converted into equivalent stress intensity factors K_J^{FE} were extracted from all four models along the sample thickness; they can be seen in Figure 3.9: Stress intensity factor variation along the crack front of the four samples at the onset of fracture extracted from finite element simulations.. Also extracted was the length of plastic ligament in front of the crack tip, r_p. For this purpose, it was assumed that any point in front of the crack with von-Mises stress greater than the material yield stress (103 MPa) was plastic.

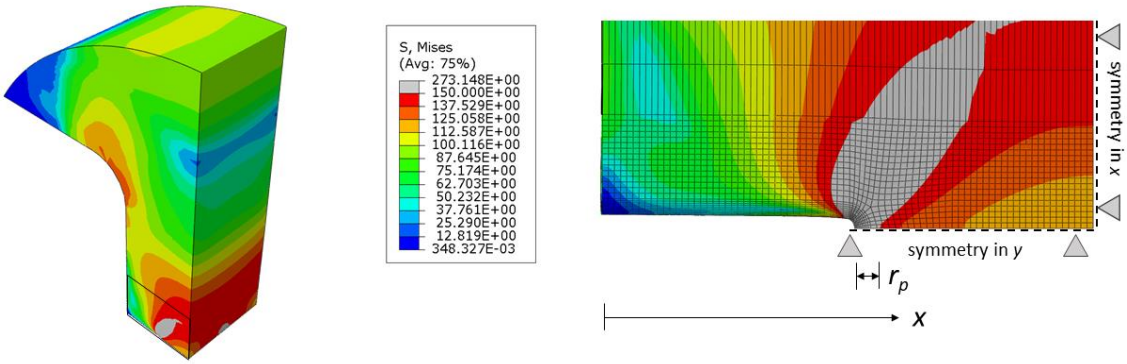

(a) ***(b)***

Figure 3.8: Finite element model of the thick sample with long crack (a) overview (b) details of the mesh at the crack tip - the grey colour shows the area in the model in which the material has deformed plastically

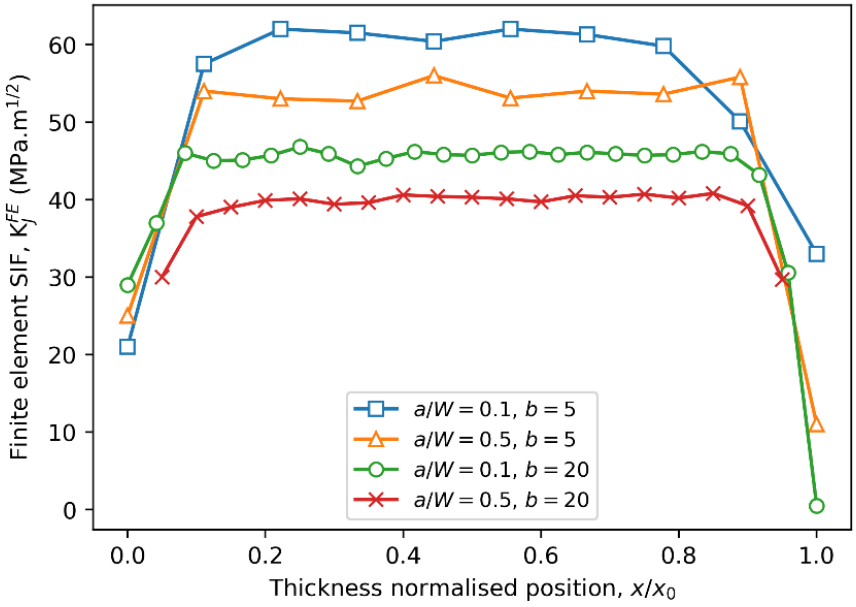

Figure 3.9: Stress intensity factor variation along the crack front of the four samples at the onset of fracture extracted from finite element simulations.

4.5 Discussion

Four specimens of a model material, an aluminium-titanium composite, with different levels of in and out-of-plane constraint were tested in this work. Tomograms of the specimens were recorded using synchrotron X-rays both before loading and at the onset of crack initiation from a sharp notch. DVC analysis of each pair of tomograms (before and after fracture) was possible due to attenuation contrast in the composite microstructure and revealed the full-field displacement field around the crack at equilibrium with the loading at the onset of fracture. Such analysis is currently not possible on more attenuating materials (e.g. uranium) and materials that do not have an inherent speckle pattern (e.g. stainless steel 316L). The displacement fields were used as an input in the finite element software, Abaqus, which calculated the corresponding strain fields at the crack. A tensile test was performed on the same material to extract its mechanical response, to which a Ramberg – Osgood constitutive law was fitted to the measured stress-strain response. The material constitutive law was used in the finite element models to enable the calculation of the stress field at the crack tip. A contour integral method, within Abaqus was then employed to calculate the through thickness *J*-integral at fracture initiation for the four levels of constraint; they are reported in Table 2. *Q* values for the four constraint conditions were calculated by subtracting the opening stress predicted by (σ_{yy}^{HRR}) for the opening stress at $x = 2J/\sigma_0$ from the model opening stress σ_{yy}^{FE} at the same location and normalising it the yield stress (σ_0); they are also reported in Table 2.

Independently, finite element models of the four specimens were created. The experimentally measured fracture loads were applied as boundary conditions to the models, using the same material constitutive law, and the through thickness *J*-integrals were calculated. The energy release rates calculated from analysis of the experiment and independent finite element simulation are compared in the form of equivalent stress intensity factor.

Table 2 – Equivalent stress intensity factor K_J (MPa.m$^{1/2}$)

Specimen	Experiment K_J^{Exp}		Finite element K_J^{FE}		
	Average	Standard deviation	Average	Standard deviation	*Q*
Thin - short	52.5	0.7	60.6	1.5	-0.67
Thin - long	48.6	1.3	54.0	1.2	-0.56
Thick - short	47.6	1.1	45.7	0.8	-1.29
Thick - long	41.7	1.3	39.9	0.7	-0.87

The experimentally extracted stress intensity factors and their variations across the thickness are reported in Table 2 along with the equivalent values extracted from the independent finite element models. In the table the values near the sample surface are discarded as the analysis was not valid in this region because the slice by slice treatment of the DVC slices assuming plane strain/plane stress condition loses the effects of out of plane displacement. It can be seen that the experimental and FE modelled average stress intensity factor in the middle of the specimen match well. However, by comparing Figure 3.7 and Figure 3.9 it is clear that

towards the edge of the sample the values and trend of stress intensity factor in the FE and experiment disagree. In the finite element model, the stress intensity factor decreases towards the surface, tending to zero at the surface as would be expected [127]. The experimental results suggest that the stress intensity factor increases towards the sample surface. There are two reasons for this discrepancy, one is that the code used to analyse the experimental data treats each virtual slice of material separately. This approach, while valid for the middle of the specimen, is not suitable for the variation of out-of-plane stress towards the surface. The solution to this issue is to develop an analysis code that creates a 3D DVC-FE model and reads the full volumetric DVC displacement in the model rather than slice by slice treatment that is used in the current version of the code. Secondly, it can be seen in Figure 3.5 that the cracks have tunnelled through the specimen and the crack front is bowed. This would tend to increase the stress intensity factor at the edges [96]; this is not modelled in the finite element simulation, which assumed a straight crack front.

Concentrating on the variation in stress intensity factor at the onset of fracture in the middle of the specimen, it can be seen that the highest value belongs to thin sample with short crack (52.5 ± 0.7 MPa.m$^{1/2}$) and lowest to the thick sample with long crack (41.7 ± 1.3 MPa.m$^{1/2}$). A comparison of equivalent stress intensity factor for the thick sample with a short crack (47.6 ± 1.1 MPa.m$^{1/2}$) or long crack (41.7 ± 1.3 MPa.m$^{1/2}$), against those in the thin samples with short crack (52.5 ± 0.7 MPa.m$^{1/2}$) or long crack (48.6 ± 1.3 MPa.m$^{1/2}$), shows the expected effect of loss of constraint i.e. thin samples have a higher toughness than thick samples and short cracks have higher toughness than samples with long cracks. The experimental values of equivalent stress intensity factor K_J^{exp} are plotted against their simulation counterpart K_J^{FE} in Figure 3.10. The figure shows the experimental and simulation value follow an acceptable one – one correlation providing confidence that the analyses are independent and are in good agreement.

Brittle fracture of materials is strongly dependent on the distribution of microstructural features such as microcracks and inclusions. As such, there is considerable variability in the toughness measured often instigating researchers to offer probabilistic distribution of toughness rather than the straightforward deterministic values. It therefore must be noted that testing 4 samples only may not provide the full picture of the toughness variability of the tested material. However, it is expected that there exists a correlation between the size of the plastic zone at the onset of fracture and the toughness measured. Therefore, it can be argued that despite the time constraints of a beamtime, which impose restrictions on the number of samples that can be fractured in-situ, the overall behaviour observed is consistent with the theoretical expectation of the variation in toughness as a function of combined in and out of plane constraint. However, the results of the current unique in-situ study must be seen in light of extensive ex-situ experimental programmes carried out previously to validate the Anderson – Dodds -Kirk unified measure of constraint.

The variation in toughness of brittle materials makes the experimental error estimation of utmost importance. There are two main outputs from the experiments, the toughness and the size of the plastic ligament, both calculated from the displacement measured by digital volume correlation analysis of the tomograms. The tomograms had of 3.3 and 7.9 micrometres voxel size for the thin and thick samples respectively. The tomograms were analysed by digital volume correlation with 16^3 and 8^3 interrogation window size for the thin and thick samples respectively. Previous investigation shows that DVC is accurate to 0.1 voxel at selected window sizes [134] resulting in an accuracy of roughly 0.3 and 0.8 micrometre in displacements measured from the thin and thick samples respectively. Considering the observable gauge length for each sample is the size of the interrogation

window, the error in measured strain is of the order of 0.005 and 0.01 which at the worst case scenario (i.e. at yield stress) translates to 20 and 30 MPa uncertainty in measured stress for thin and thick samples. It can therefore be argued that the error in measured plastic zone (accuracy of 0.3 and 0.8 for measurements between 3 and 400 micrometre) is negligible as is the error in measured toughness (accuracy of 0.2 and 0.3 measurements in 40 – 60 MPa.m$^{0.5}$). It was therefore concluded that the through thickness variation of the measured value are a good representation of the overall accuracy of the experimental measurements which are the values reported in Tables 2 and in Figures 10 -12).

Figure 3.11 shows the equivalent stress intensity factors measured and calculated as a function of *Q*. As it can be seen, the variation of apparent stress intensity factor at different levels of constraint does not form a uniform trend. If applied to a constant thickness specimens (i.e. constant out of plane constraint), the results do form a trend but *Q*, in its original form, is evidently not capable of quantifying both in and out of plane at the same time. This has been previously observed by other researchers (e.g. see [135],[136],[137]).

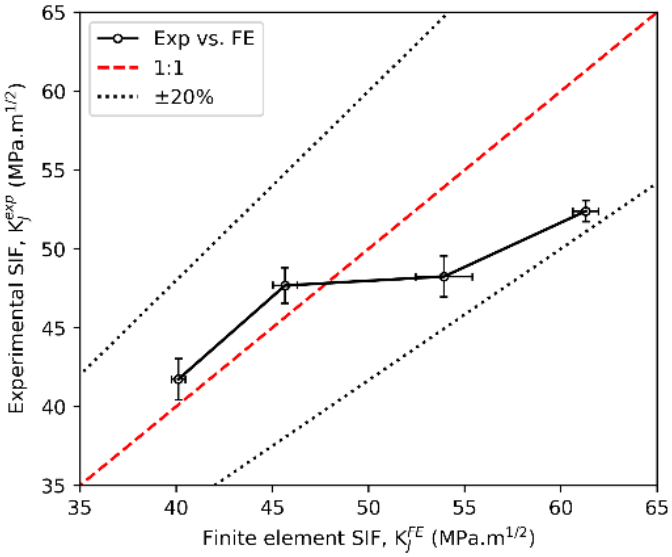

Figure 3.10: Correlation of experimentally obtained equivalent stress intensity factor and that of finite element simulation. A line highlighting a 1:1 correlation is shown, with all results falling within ±20% of this.

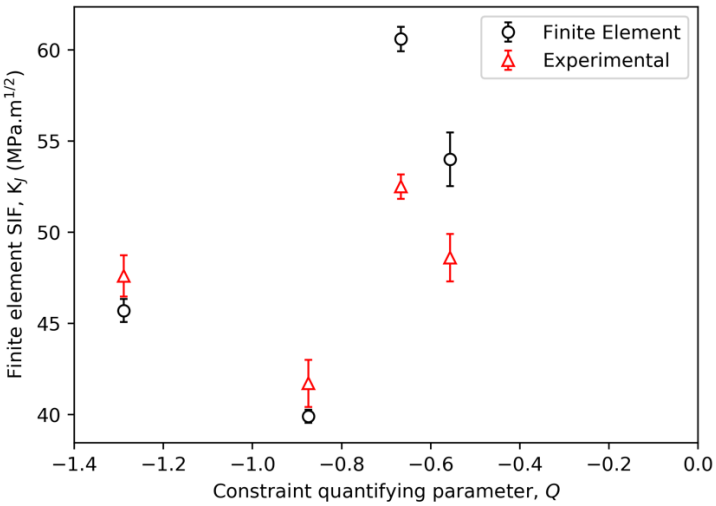

Figure 3.11: Stress intensity factor against measure of constraint Q. The error bar shows the range of values determined from experimental data and the measurement resolution (voxel size).

However, using a unified measure of constraint, it is possible to combine all the results by considering the relation between apparent stress intensity factors in the middle of sample. Figure 3.12 shows the apparent stress intensity factors measured/calculated in the middle of the specimens against a variation of Anderson, Dodds, and Kirk unified measure of constraint. In this variation, the Von Mises stress (σ_{vm}) was used instead of maximum principal stress (σ_1 - see Eq. 4) which had been originally proposed by Anderson, Dodds, and Kirk as it better represents the plastic work which is closely related to the constraint effect. This is in-line with previous work done by some of the authors (e.g. see [138]). If the arbitrary C factor in the modified Anderson. Dodds, Kirk model is considered to be one, then the unified measure of constrain would be the length of uncracked ligament which has deformed plastically is used. As noted by other researchers (e.g. see [103,125]), considering C = 1 restricts the application of such unified measure of constraint to conditions where the plastic zone size if limited within the sample. The thin specimens in this study had violated this condition as they had shown plastic deformation along the full uncracked ligament both in finite element model and in DVC. It was therefore decided to use a higher C factor (i.e. C = 1.1) to confine the area with Von-Mises stress bigger than $C\sigma_0$ within the specimen. The results are presented in Figure 3.12.

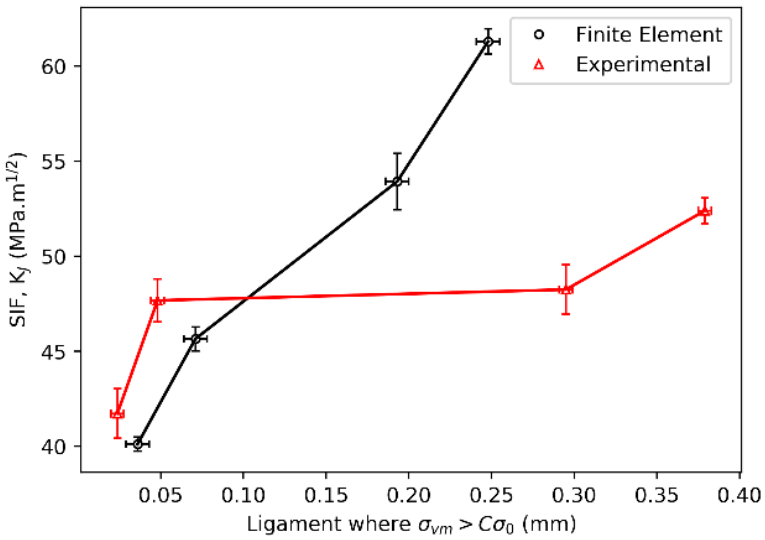

Figure 3.12: Stress intensity factor against a unified measure of constraint $C\sigma_0$ (C = 1.1). The error bar shows the range of values determined from experimental data and the measurement resolution (voxel size).

The figure shows that the apparent stress intensity factors plotted as a function of unified measure of constrain forms a uniform trend. The lowest constraint condition of thin sample with short crack show a large distance along the ligament with $\sigma_{vm} > 1.1\sigma_0$ while this distance is much smaller in the highest plastic constrain sample of thick with long crack. It appears that the FE results presented in Figure 3.12 are more in line with what is expected from the variation of toughness as a function of constraint compared to the experimental measurements. This is because the material has a low hardening exponent, expressing a near elastic – perfectly plastic behaviour. The elastic perfectly plastic behaviour results in large variation in strain as a function of small variation in stress (i.e. measured force over cross section). The large change in stress changes the finite element toughness variation considerably, exaggerating the effects of constraint and making the toughness increase as result of loss of constraint more prominent. This is not necessarily true representative of the material behaviour in service which is expected to be closer to the experimentally measured values. This is emphasising the importance of such direct measurements compared with previous theoretical studies.

Figure 3.12 suggests that using the unified measure of constraint can provide us with a relationship between combined in-plane and out-of-plane constraint level and equivalent stress intensity factor at fracture. This parameter to measure constraint can offer a methodology to include the effects of constraint in a prediction of fracture which is sensitive to both in and out-of-plane constraint. In future work we intend to use the experimentally measured displacement field to test the validity of other unified approaches, notably the Seal and Sherry method [10]. They have combined Rice and Tracey fracture model [88] with isostress contour method to produce a unified fracture criterion for a component with any thickness or crack length.

4.6 Conclusion

- Full-field volumetric displacement fields of four crack samples with four different combinations of in and out of plane constrains were measured by synchrotron X-ray tomography and digital volume correlation.

- The full-field volumetric displacement data were used in a finite element framework to calculate the through thickness energy release rate of the samples and the plastic zone sizes around the cracks at fracture.
- The plastic zone sizes at fracture were used to rank the samples constraint level regardless of their in or out of plane types. This showed, for the first time through direct measurement, that the size of plastic zone can be used as a unified measure of constraint.

Acknowledgement

SMT and MM would like to thank UK National Nuclear Laboratory for the financial support provided to carry out the work. Diamond Light Source is gratefully acknowledged the allocation of beamtime numbers EE12606-1 and EE12606-2. Drs S M Barhli and A Cinar are thanked for development of the codes that were used in the analysis of the DVC data. Professor Patrick Grant, University of Oxford is thanked for the provision of the material. We gratefully acknowledge the help and support of Dr Nghia Vo in the reconstruction of the limited angle tomography data. Mr R Patel, UK National Nuclear Laboratory and Dr A Wasylyk, Framatome, are gratefully acknowledged for their continuous and fruitful discussions.

5 Journal Paper 2

This paper gives evidence for φ being a measure of unified constraint and Q being a measure of in plane constraint, with a larger body of data.

Quantifying combined effects of in-plane and out-of-plane constraint in an aluminium alloy

S M Tonge[a,2], Z Chen[a], C Meek[b], M Mokhtarishirazabad[a], M Mostafavi[a]

e. Department of Mechanical Engineering, University of Bristol, Queens Building, University Walk, Bristol, BS8 1TR

f. National Nuclear Laboratory, 5th Floor, Chadwick House, Warrington Road, Birchwood Park, Warrington, WA3 6AE

Abstract

Fracture load of a component can depend on the geometry as well as the material properties due to the effect of constraint on the plastic region which forms around the crack tip prior to fracture. The constraint has two components: in-plane constraint, due to the size and geometry of the component, and out-of-plane constraint, mainly due to its thickness but also affected by other geometric parameters. There are currently methods to quantify both types of constraint separately as well as suggested parameters that quantify both simultaneously. However, experimental programmes that objectively compare the applicability of each are few and far between, especially on the out-of-plane constraint. In this paper we report the results of a substantial experimental programme making use of single edge notched bend (SENB) aluminium alloy specimens to study the combined effects of in-plane and out-of-plane constraint. These experiments involved testing the specimens in a three-point bending configuration with nine combinations of thickness and crack length. This allowed fracture loads to be measured then converted to stress intensity factor *K* by the use of three-dimensional finite element simulations. Common constraint parameters such as the *Q* parameter and plastic zone volume were

[2] Corresponding author
Email: simon.tonge@bristol.ac.uk

extracted from these simulations. The results showed that *K* varied between 31 and 55 MPa√m for various levels of in and out-of-plane constraint. Both the magnitude of *Q* and the plastic zone volume increase with reducing plastic constraint. We showed that both Q and plastic zone volume could be used to quantify the combined effects of in and out-of-plane constraint, however the uncertainty associated with the plastic zone volume is less than that of Q.

Highlights

- Constraint effects in fracture measured by three point bending tests.
- Al7075 single edge notched bend specimens used for brittle fracture tests.
- 9 different levels of constraint used in specimens: 3 in plane, 3 out of plane.
- Strong correlation between volume of yielded region and constraint.
- Q parameter and volume of plasticity found to be sensitive to constraint.

Keywords

Constraint, Brittle Fracture, Fracture test, Q parameter.

5.1 Background

The fracture toughness of a component has been shown to be affected not only by the standard fracture toughness of a material, but also by the resistance of the specimen to plastic yielding. One of the factors that affects resistance to plasticity is the geometry of the component which can have a significant influence on the size of the plastic region that forms around the crack prior to failure. This effect is known as plastic constraint. The constraint due to the variation in the uncracked ligament length ahead of the crack tip, or other variations in sample geometry from a standard case, is known as in-plane constraint. The constraint due to the specimen thickness is known as out-of-plane constraint. Short-cracked bending specimens have lower in-plane constraint [90] which leads to the higher measured values of the parameters quantifying fracture toughness. Specimens with high thickness have higher out-of-plane constraint [52], [92] and therefore lower measured values of fracture toughness. The plastic work done in a low constraint specimen has the effect of increasing fracture toughness. Thus, high in-plane constraint and thick (satisfying

plane strain conditions) specimens such as the Compact Tension (CT) specimen are used to measure a lower bound standard fracture toughness.

Previous experiments [90] [92] have successfully shown a correlation between constraint and fracture toughness. However, historically, in-plane and out-of-plane constraint have been treated separately in fracture assessment codes and procedures such as R6 [37] and BS7910 [139]. Nonetheless, parameters to quantify both in-plane and out-of-plane constraint have been proposed, for example by Seal and Sherry [97]. To test the reliability of parameters, sufficient fracture tests need to be performed across a range of geometries and materials. This would allow structural integrity assessment procedures to be updated using a unified measure of constraint which would improve the accuracy and efficiency of such assessments.

The stress intensity factor (*K*) at the crack tip and the strain energy release rate (*J*) are measures of fracture toughness. To account for the effects of constraint it is sometimes necessary to use two-parameter fracture assessments. In the case of in-plane constraint the second parameters often used are *Q* and *T*. The *T*-stress is the non-singular term of the Williams expansion of the crack tip stress field [98]as shown in Equation (1).

$$\sigma_{ij} = \frac{K}{\sqrt{2\pi r}} f_{ij}(\theta) + T\delta_{1i}\delta_{ij} \qquad \text{(Eq. 9)}$$

This non-singular second term describes the stress parallel to the direction of crack propagation. It includes the *T*-stress and two Kronecker deltas. In the first term of this expansion, *K* is the stress intensity factor and r and θ are the linear and angular distances from the crack tip. While negative *T* is associated with loss of in-plane constraint [140], a positive *T*-stress indicates that a crack can tend to branch [99]

Q is defined in [141]as the difference between the stress field experienced by the crack in the low constraint specimen and the stress field defined by Hutchinson Rice and Rosengren (HRR) [142] [104] . The most common form of *Q* used in fracture assessments is shown in Equation (2), where r is the distance from the crack tip to the point in the stress field at which *Q* is measured ($r = \frac{2J}{\sigma_0}$), σ_0 is yield stress, and σ_{yy} is the crack opening stress.

$$Q = \left.\frac{\sigma_{yy} - \sigma_{yy}^{HRR}}{\sigma_0}\right|_{r=\frac{2J}{\sigma_0}} \quad \text{(Eq. 10)}$$

T is only applicable to elastic conditions or small scale yielding while *Q* is more appropriate for plastic conditions. Alternatively, for simplicity, sometimes *T*-stress is used to construct a *J*-*T* loci instead of *J*-*Q* loci to define the effects of constraint on fracture.

Constraint due to specimen thickness is quantified by the parameter T_z, which is defined in Equation 3. This parameter is defined with the crack propagation being in the x-direction and the thickness of the specimen orthogonal to the direction of the crack propagation. It was originally defined by W Guo [143], who studied the fracture toughness of specimens with different thickness relative to uncracked ligament. This enabled T_z to be measured and the results to be used to quantify out-of-plane constraint in the *K*-T_z theory.

$$T_z = \frac{\sigma_{zz}}{\sigma_{xx} + \sigma_{yy}} \quad \text{(Eq. 11)}$$

σ_{xx} and σ_{yy} are stresses in the plane of the crack and σ_{zz} is the component of stress tensor perpendicular to the plane of crack propagation. T_z is not sensitive to in-plane constraint, which means that three parameter theories such as, *K*-*T*-T_z and *J*-*Q*-T_z are necessary [144] [145]. These are more complex than using two-parameter assessments, which use a single constraint parameter for both in-plane and out-of-plane. Therefore, in the interest of improving efficiency, it would be desirable if a parameter sensitive to both in-plane and out-of-plane constraint could be verified.

Other parameters that define either in or out of plane constrains have been proposed such as T11 [146], Q_{ssy}[147], A2 [148], h [147], and T33 [146]which for brevity we do not review as they have some overlap with previously defined constraint parameters.

To this end, Anderson, Dodds, and Kirk [149] proposed that the area (A_c) enclosed by a contour of constant maximum principle stress can be used to define constraint. The area enclosed by the contour defined in Equation 4, is taken to have yielded. The contour was defined in Equation (4),

$$\sigma_1 = C\sigma_0 \quad \text{(Eq. 4)}$$

$$A_c = \sum_{i=1}^{i=e} a_i \quad \text{(Eq. 5)}$$

C is an arbitrary constant, σ_1 is the maximum principal stress and σ_0 is the yield stress. The area (2D) or volume (3D) inside the contour (A_c) is the measure of constraint found by summing individual areas of finite elements. In Equation 5 these individual elements each have area given by a_i and the number of elements enclosed by the contour is e. The finite elements included in the summation are the set of elements enclosed within the contour defined in Equation 4.

High constraint results in low fracture toughness and a small contour size, while low constraint gives high fracture toughness and a larger area [116]. As an alternative, a dimensionless parameter φ, defined in Equation (5), was postulated as a unified measure of constraint:

$$\varphi = \frac{A_c}{A_c^{SSY}} \quad \text{(Eq. 6)}$$

where φ is the ratio between the size of the area enclosed by the arbitrary isostress contour C (A_c) to the area enclosed by the same contour in a sample with a standard constraint condition (i.e. A_c^{SSY}) [150].

Parameters based on the size of the yielded region have been shown to be applicable in the fracture of ductile materials with low plasticity yet it is not reliable in cases where large scale plasticity occurs [8]The Dodds, Anderson, Kirk method has been modified to account for in-plane as well as out-of-plane constraint. For example, Mostafavi et al. suggested φ^p [138].

$$\varphi^p = \sqrt[3]{\frac{V_P}{V_P^{Ref}}} \quad \text{(Eq. 7)}$$

where V_P is the plastic zone volume for the specimen and V_P^{Ref} is the volume of the plastic zone in a standard high constraint specimen (e.g. compact tension).

When this parameter was tested, it was shown that it could predict the failure of aluminium alloys and showed sensitivity to both in-plane and out-of-plane constraint [151]. However, its application is limited to component geometries and loads in which the volume occupied by the plastic zone is contained within a relatively small part of the uncracked ligament. To widen the applicability of this parameter to conditions where plastic volume is uncontained, another parameter A_{PEEQ} has been proposed [152]. A_{PEEQ} gives another form of the Anderson, Dodds, Kirk method, in which the plastic strain volume is bounded by the plastic strain, ε_p, isoline. The area of plasticity for a case with high constraint, A_{Ref}, is used to normalise the value in a similar way that V_P^{Ref} is used in Equation 6 [154].

This is an active area of research. For example Seal and Sherry [57] have recently combined the Rice and Tracy [83] fracture criterion with the φ constraint parameter to predict the effects of fracture of ductile materials. Tonge et al. [155] have performed experimental work complemented by finite element simulations to assess the validity of the contour method. These tests have shown that there is a clear dependence of fracture toughness parameters such as K and J on the level of constraint of a sample but have not directly attempted to validate the accuracy of unified measures of constraint experimentally. This is important as the industry direction of travel is towards reducing conservatism which can be achieved through more realistic analyses with fewer simplifications. As such, combining the two measures of constraint which in the past were defined for simplicity of application by hand calculations can offer an advance in engineering practice.

The present work offers a combined experimental and numerical study. The experiments described in this paper test the effect of varying constraint, in and out of plane, on the range of values of the fracture parameters. They are complemented by detailed finite element simulations to assess the validity of the most frequently used measures of constraint.

5.2 Experiments and Results

5.2.1 Specimens

Three-point bending tests were carried out using the ASTM 399 standard [30]. The material used was Al7075 T651 [155], a grade of Aluminium prone to brittle fracture. The nine different specimen geometries and the codes used to identify them are

shown in Table 1; a diagram of the specimens is shown in ***Figure 4.13***. The specimen geometries were designed to give three different levels of in-plane constraint, corresponding to notch lengths: a/W = 0.075, 0.275, 0.375. For each different notch length there were three different thicknesses, (b = 5, 12, 30 mm) and therefore three different levels of out-of-plane constraint for each notch length. This gave nine specimen types, each with a unique combination of in-plane and out-of-plane constraint. The specimen with b = 30 and a/W = 0.375 is a standard specimen with high level of constraint while the specimens with a/W<0.375 have low in-plane constraint and the specimens with b < 30 have low out-of-plane constraint. The samples with combined low in and out of plane constraint could have maintained the same span and width or could have been scaled. The former was chosen to avoid confusion with studies that focus on size effect (e.g. see [156]).

Side grooves, as depicted by Figure 4.13, were used to ensure fracture direction along the electro-discharge machining (EDM) notch. The depth of the side grooves is 10% of the specimen thickness, this means that for b = 30side grooves with 3mm depth are used. For B=12mm side grooves are 1.2mm in depth. The span length, S, is four times specimen width. In this case this is 160mm.

The experiment was repeated for each specimen geometry. Cracks were introduced in the specimen using a 0.1 mm wire EDM, as previous experiments on a comparable aluminium alloy, similar specimen type, and temperature showed no statistical difference between fracture toughness measured by EDM notched and fatigue pre-cracked specimens due to crack blunting before fracture [108] (see appendix B). Thin samples (b = 5 mm) were equipped with anti-buckling plates. The experiments were carried out at room temperature between 18 and 22^{O}C.

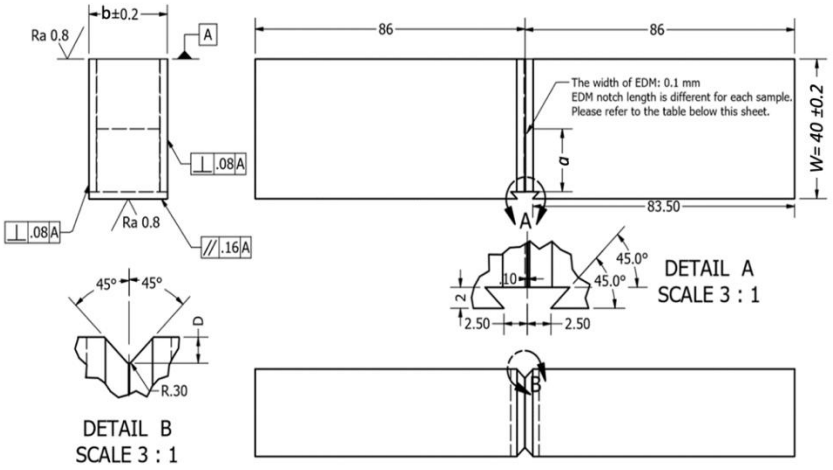

Figure 4.13 – Schematic of the specimen geometry

Table 4.1 – details of the specimens

Sample Code	b (thickness, mm)	a (initial crack length, mm)	a/W	Failure Loads/kN
5S	5	3	0.075	14.7,14.8,16.9,18.8
5M	5	11	0.275	7.7,7.8,8.1,8.4
5L	5	15	0.375	5.4, 5.6, 5.7, 5.9
12S	12	3	0.075	32.7,33.1
12M	12	11	0.275	13.9,14.8,19,19.3
12L	12	15	0.375	11.2,13.4,14.4
30S	30	3	0.075	64
30M	30	11	0.275	37.9,40.7,43.5
30L	30	15	0.375	29.4,33.6

5.2.2 Test set-up

Figure 4.14 shows the test setup. The load in the three-point bending tests was applied by a servo hydraulic, Schenk 75 kN testing rig, equipped with a load cell of the same capacity. The load was applied in displacement control with a linear ramp rate of 0.5 mm/minute until the specimen failed by sudden fracture.

To validate the finite element models (see next section) used to convert fracture loads to fracture toughness, crack mouth opening displacement (CMOD) was measured directly at the crack tip using an Epsilon clip gauge. The clip gauge was calibrated using a barrel micrometre prior to the experiment. The Epsilon clip gauge (model 3541-005M-120M-LT) had a travel range of 12 mm which was found sufficient for all experiments including the lowest constraint ones.

The integral knife edges of the sample, with gauge length 5 mm, were used for mounting the gauge. The gauge was connected to the controller so that the load, measured by the tensile frame's load cell, and the CMOD, measured by the clip gauge, could be synchronised. The width of specimen W = 40 mm and the distance between rollers where load was applied S = 120 mm.

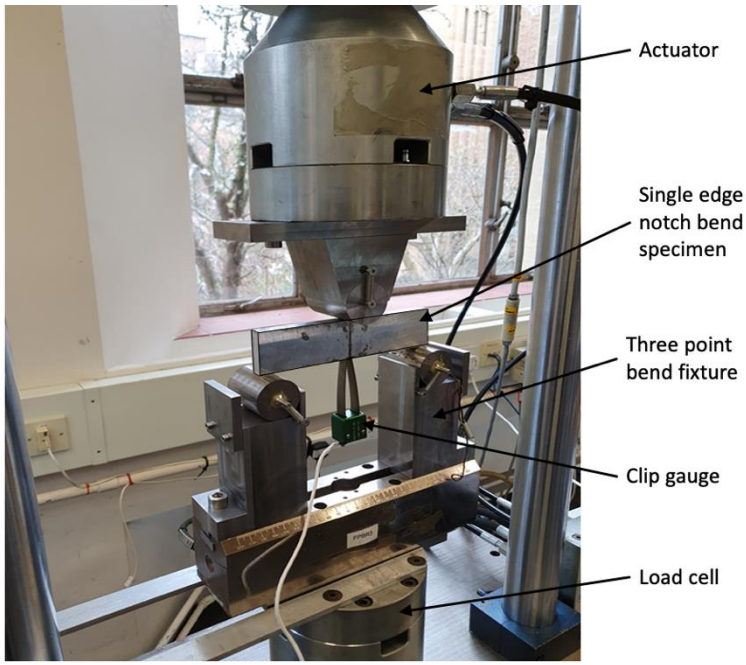

Figure 4.14 – Experimental setup and specimens

5.3 Finite Element Modelling

Finite element (FE) models were created to calculate the *J*-integral and determine the plastic zone size ahead of the crack tip as well as *Q*. Compliance of the model in its elastic regime (crack mouth displacement divided by load) was calculated and compared with that measured by the experiments to ensure that the model is directly comparable with the physical experiments.

Abaqus 6.14 [123] was used to run a script that created the nine specimens with each individual geometry. Between 14,500 and 64,312 elements were used in a 3D configuration which modelled the nine specimen geometries. The model was reduced to a quarter of its original size by using the plane of symmetry along the direction of crack propagation. Symmetry boundary conditions were used to define the planes of symmetry. ***Figure 4.15*** shows an example of the FE model. The crack tip was modelled by concentrated mesh. Biased mesh was used so that larger elements near the free surfaces are defined to accurately represent the asymptotic stress field. The crack was defined as a symmetry half-crack model with nodes along the crack tip through the thickness of the specimen. The mesh seeds around the crack tip were 0.05 mm apart and 0.5 mm for the region of the model away from the crack. 20-node brick solid elements with reduced integration points were used throughout the model.

Rollers, which in the experiments were made of toughened steel, were defined as rigid bodies. Hard, frictionless contact was defined between the rollers and the specimens. Reference points were defined for the rollers whose movement defines the movement of the whole rigid roller. The outer roller was fixed at its reference point and load was applied to the reference point of the lower roller. The model was loaded in displacement control by pushing the upper roller in the specimen until the same fracture load as the specimen in the physical experiment was achieved.

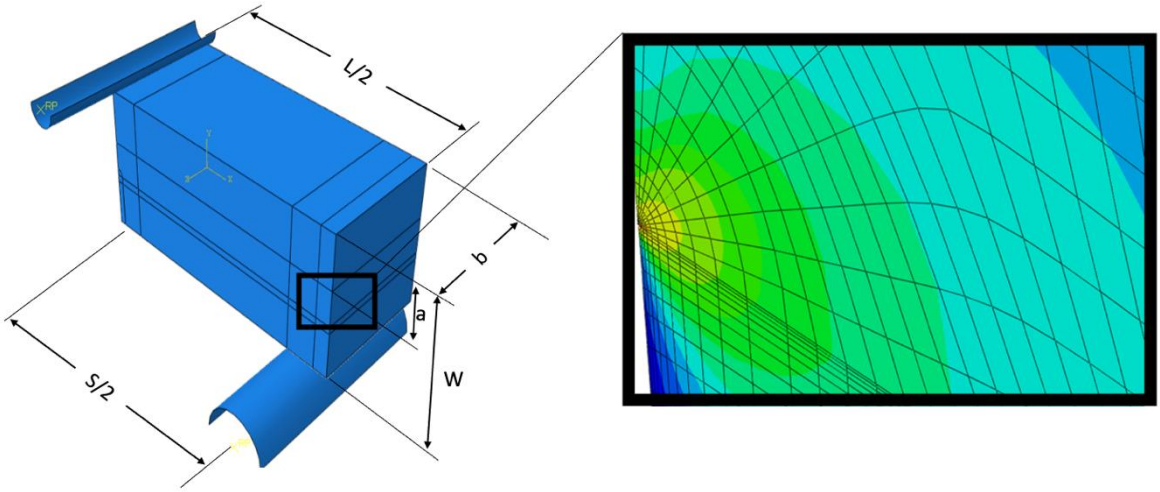

Figure 4.15 – Example of finite element model of the fracture tests showing the general overview of the quarter model and close up of the crack tip mesh in an inset

The specimens' material properties were described by a Johnson-Cook model:

$$\bar{\sigma} = A + B(\bar{\varepsilon})^n \quad \text{(Eq. 12)}$$

where $\bar{\sigma}$ is plastic stress and $\bar{\varepsilon}$ is plastic strain. The elastic properties were E = 71.7 GPa and Poisson's ratio v = 0.33. The Johnson-Cook parameters were A = 450 MPa, B = 488 MPa and n = 0.3498 as identified previously for this material [155].

The effect of blunting on the notch was modelled by considering the radius of the EDM wire, which was 0.05 mm, as the radius of the blunted notch. This was necessary because the measurement of the stress field at the crack tip was taken as a measure of the size of the plastic zone so a high level of accuracy in this part of the specimen was required.

The previous work [157] indicated that the side-grooves have a local effect in the simulations thus will marginally change the calculation of Q, which is performed in the middle of the sample thickness (please see below). The plastic zone at the surface is the most affected parameter in this simplification which will be minimised by summing up the whole plastic volume of each specimen. Therefore, for simplicity the side-grooves were not simulated in FE models.

To calculate Q, [157] , the opening stress for the high constraint specimen (i.e. sample with a/W = 0.375 and 30 mm thickness) was used as a reference; there was only less than 5% difference between this value and that calculated by HRR. The opening stress at $\frac{r\sigma_0}{J} = 2$, that is r = 0.05 mm, was measured for each case and averaged over repeats. The difference between the opening stress of each case and that of the reference was calculated and normalised by the yield stress, giving a value of Q for each sample geometry.

Abaqus' in-built contour integral method was utilised to calculate J-integral. To ensure the contour independency of the calculated J values, 20 contours were used which, after a rise, reached a plateau. As is common practice, only the maximum J-integral observed in the middle of the specimen was extracted from the simulations to represent the toughness of each specimen [8]. The results shown in the graphs were evaluated at the centre of the specimen with respect to thickness, which is the point of maximum stress concentration.

We have calculated Q in the middle of each specimen, where fracture initiation is expected to happen. While the distribution of Q (similar to J) could be extracted along the crack front, such analysis is more suitable for cases where there is ambiguity in where along the crack front the growth initiates [158]. In our case, the crack front is straight thus as previous studies on comparable materials shown, the crack is expected to initiate growth at its mid-thickness point [159]. We therefore reported the J and Q values at mid-thickness point.

A code in Python 2.7 was developed to segment the elements using the equivalent von-Mises stress calculated as an average over their integration points. If the average von-Mises stress is more than the yield stress of the material, the element was assumed to have yielded. The code adds the volume of the segmented elements thus returning the volume of plasticity formed around the crack prior to fracture, V_p. Care was taken so that any plasticity at the rollers (beyond the plastic hinge) was not added to the plastic zone volume formed around the crack tip.

5.4 Results and discussion

5.4.1 Load-CMOD curves

Each specimen was loaded until final fracture load was observed. The load-crack mouth opening displacements, constructed by the measurements from the load cell and the clip gauge, for each thickness, are depicted in Figure 4.16. Limited nonlinearity is observed before the final fracture, indicative of the abrupt brittle failure of the material. As expected, specimens with lower *a*/*W* had the higher compliance. Compliance was determined by finding CMOD in the FE model at the failure loads for each specimen. At 40kN load, CMOD for specimen 30S was 0.4mm. At 50kN load, CMOD for specimen 30M was 0.3mm.

It can be seen from the experimental results in Table 1, that the loads ranged between 5.4 kN (for sample 5L) and 64 kN (for sample 30S). The range of these loads is narrow between each experiment with the same specimen geometry as can be seen in Figure 4.16.

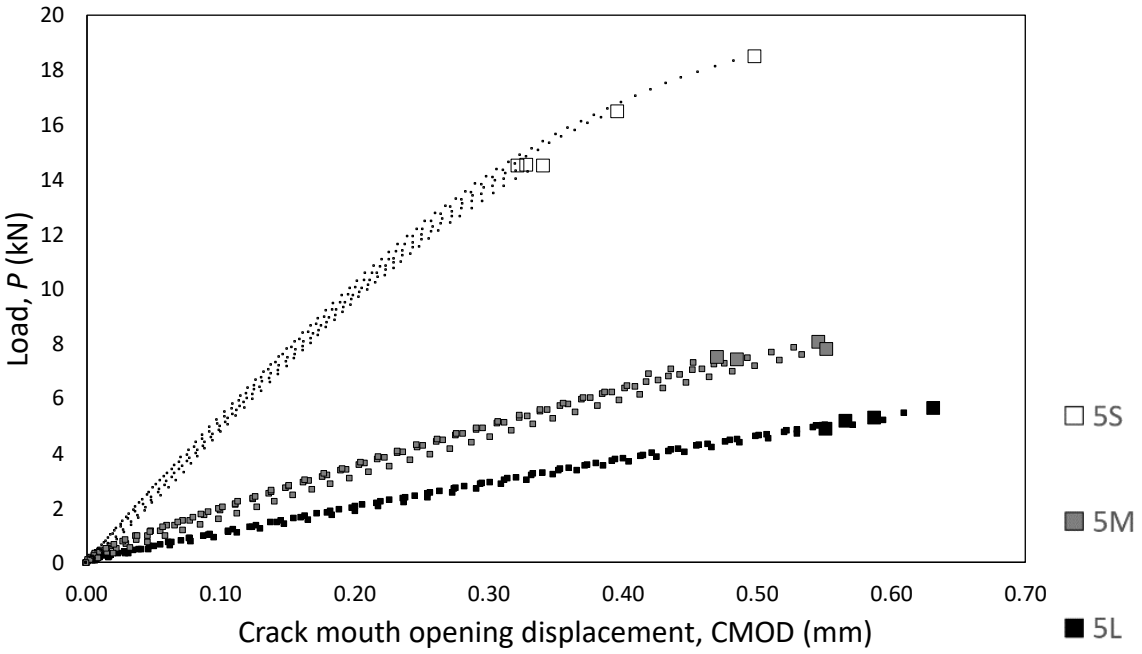
Load, P (kN)
Crack mouth opening displacement, CMOD (mm)
5S
5M
5L

(a)

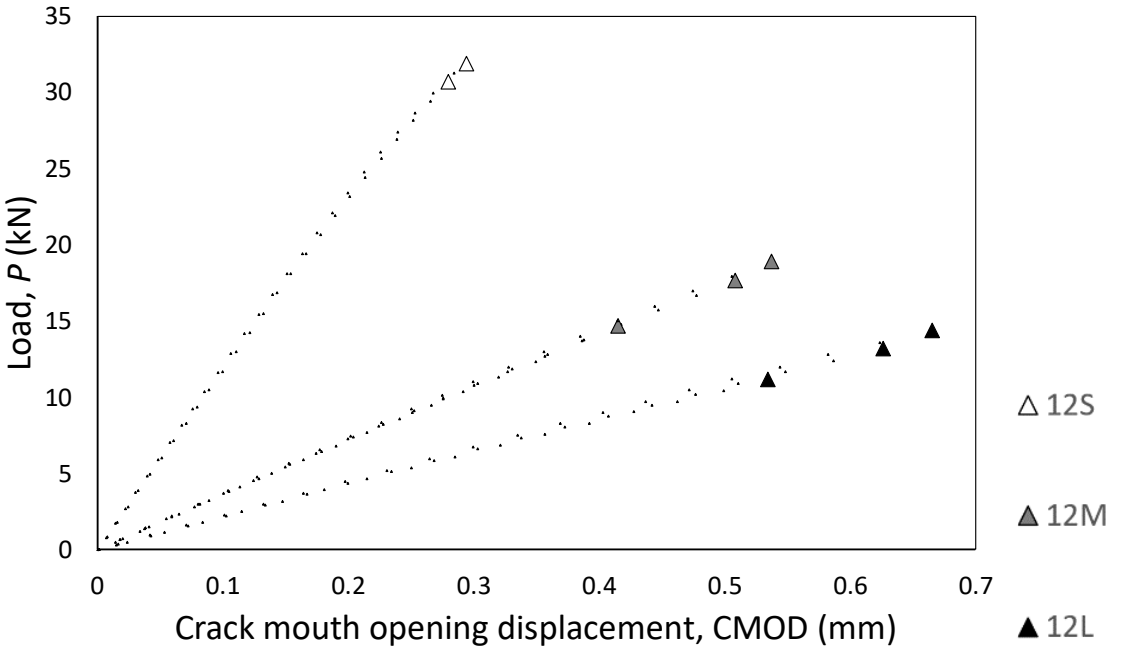
Load, P (kN)
Crack mouth opening displacement, CMOD (mm)
12S
12M
12L

(b)

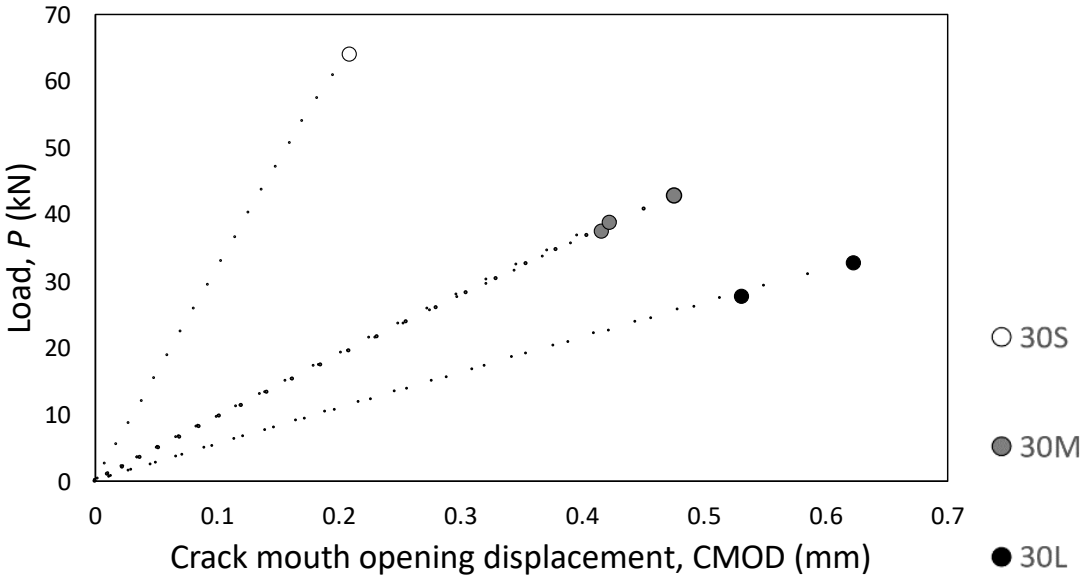

(c)

Figure 4.16 – Load-crack mouth opening displacements for each experiment. (a) thin samples (b = 5 mm) (b) mid-thick samples (b = 12 mm) (c) thick samples (b = 20 mm) - Note that, for clarity, the fracture points are depicted with a much bigger symbol.

5.5 Fractography

Light microscopy images were taken using blue light with 0.05 mm/pixel. The images for each specimen are shown in Figure 4.17. Although the magnification was not sufficient to identify the finer details of the fracture process (e.g. initiation site), they provided ample evidence of ductile fracture throughout the tests. The specimens with the shortest initial crack length (a/W =0.075) with b = 5 and b =12 showed fracture surfaces that were rougher than other samples.

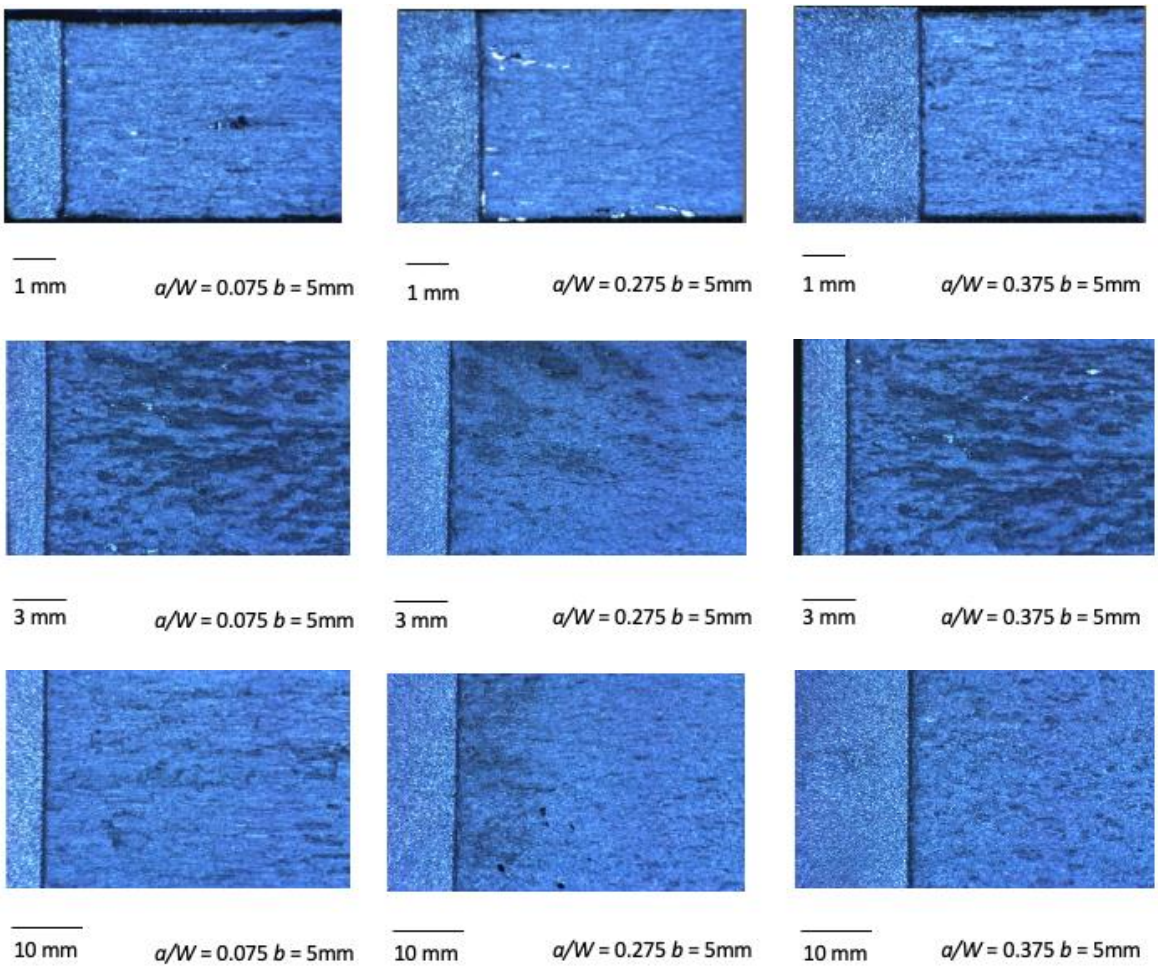

Figure 4.17 - A light microscopy image of the crack surface is shown in blue light

To give higher resolution images of the fracture surface, an electron microscope was used. The either ends of constraint level were examined with x200 magnification; that is standard specimen with maximum constraint (b=30mm, a/W=0.375) and the specimen with minimum level of constraint (b=5mm, a/W= 0.075). The high resolution images are shown in Figure 4.18. The images focused just in front of the EDM notched region to capture behaviour ta crack initiation. A clear contrast is seen between the high constraint and low constraint fracture surfaces similar that observed by the optical microscopy. A more regular pattern of flat surfaces, akin to cleavage planes, is seen in the higher constraint specimens. In contrast, rough, elongated voids with more random flat surface orientations are seen in specimens with lower constraint. This is indicative of tensile type fracture in the high constraint sample and shear type fracture in ow constraint sample. To evaluate other samples, electron microscopy of the surface of all samples were taken at 1000x which are shown in Figure 4.19. Although not a clear cut, it can be argued that the samples

with rough surfaces in optical microscopy (i.e. all but samples with shortest cracks) show tensile type fracture and the samples with smooth optical samples (i.e. samples with shortest cracks) are more of shear type fracture.

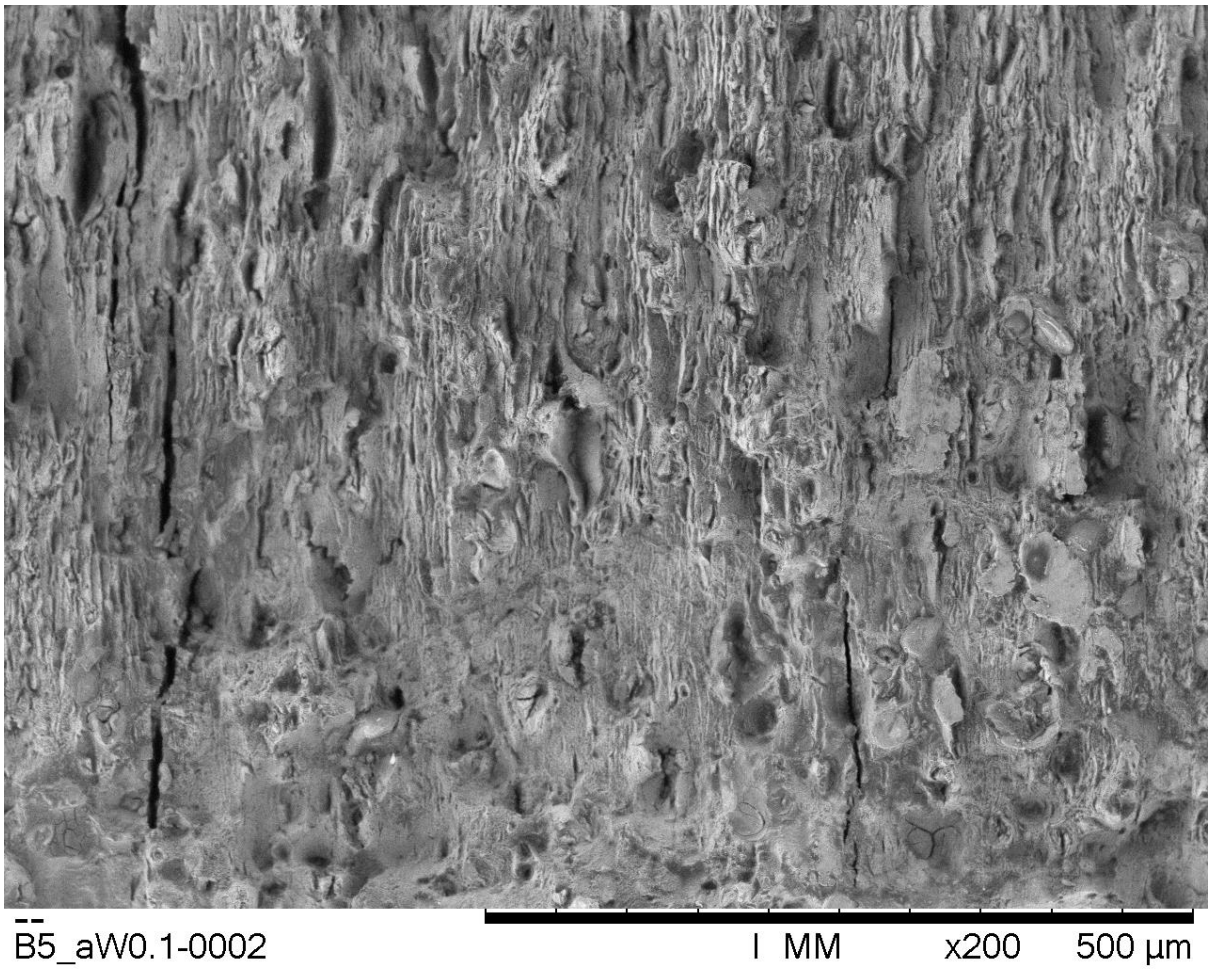

(a)

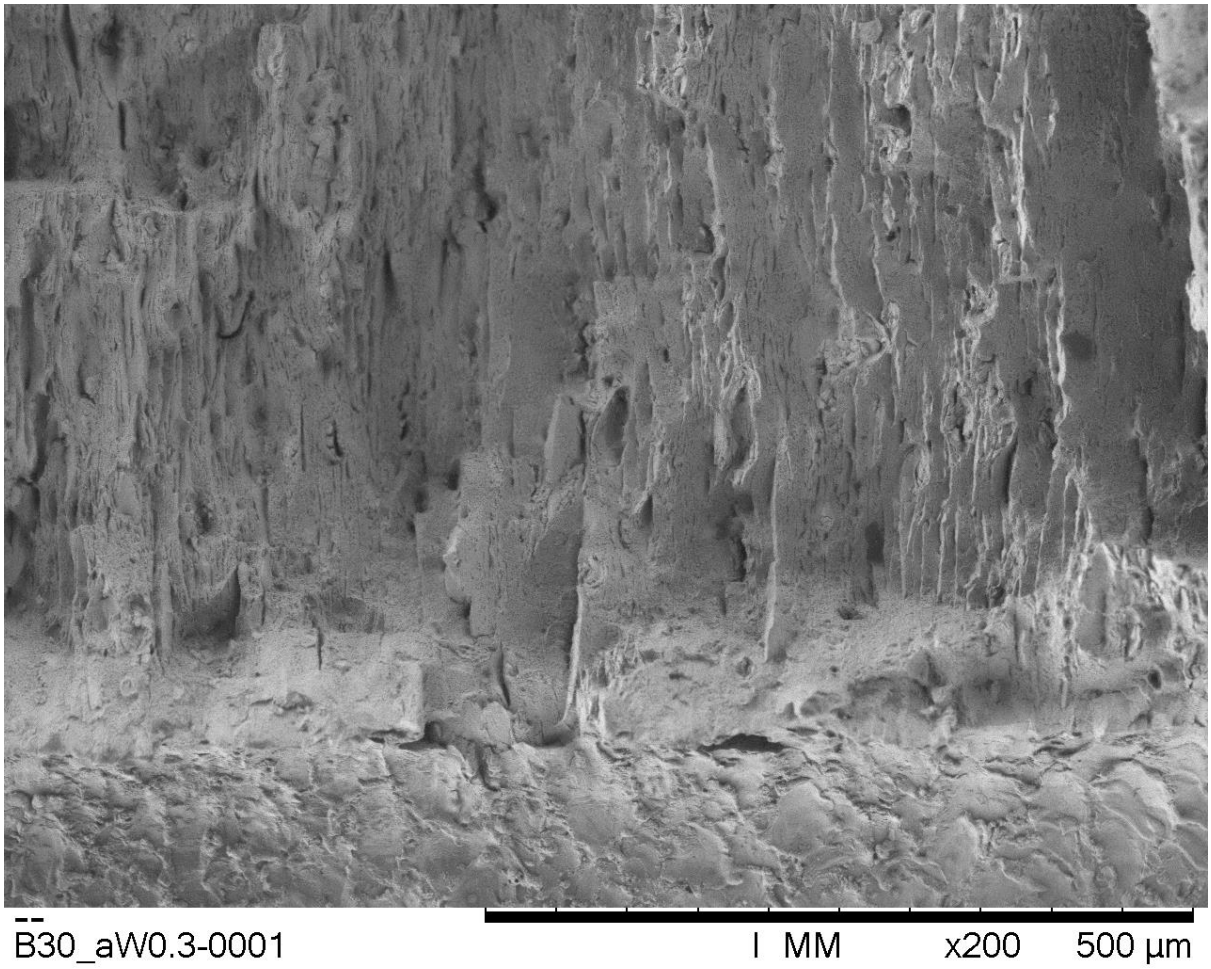

(b)

Figure 4.18 - 200x Magnification scanning electron microscopy image of (a) a/W=0.075, B=5mm, taken at centre of specimen (b) a/W=0.375, B=30mm, taken at centre of specimen.

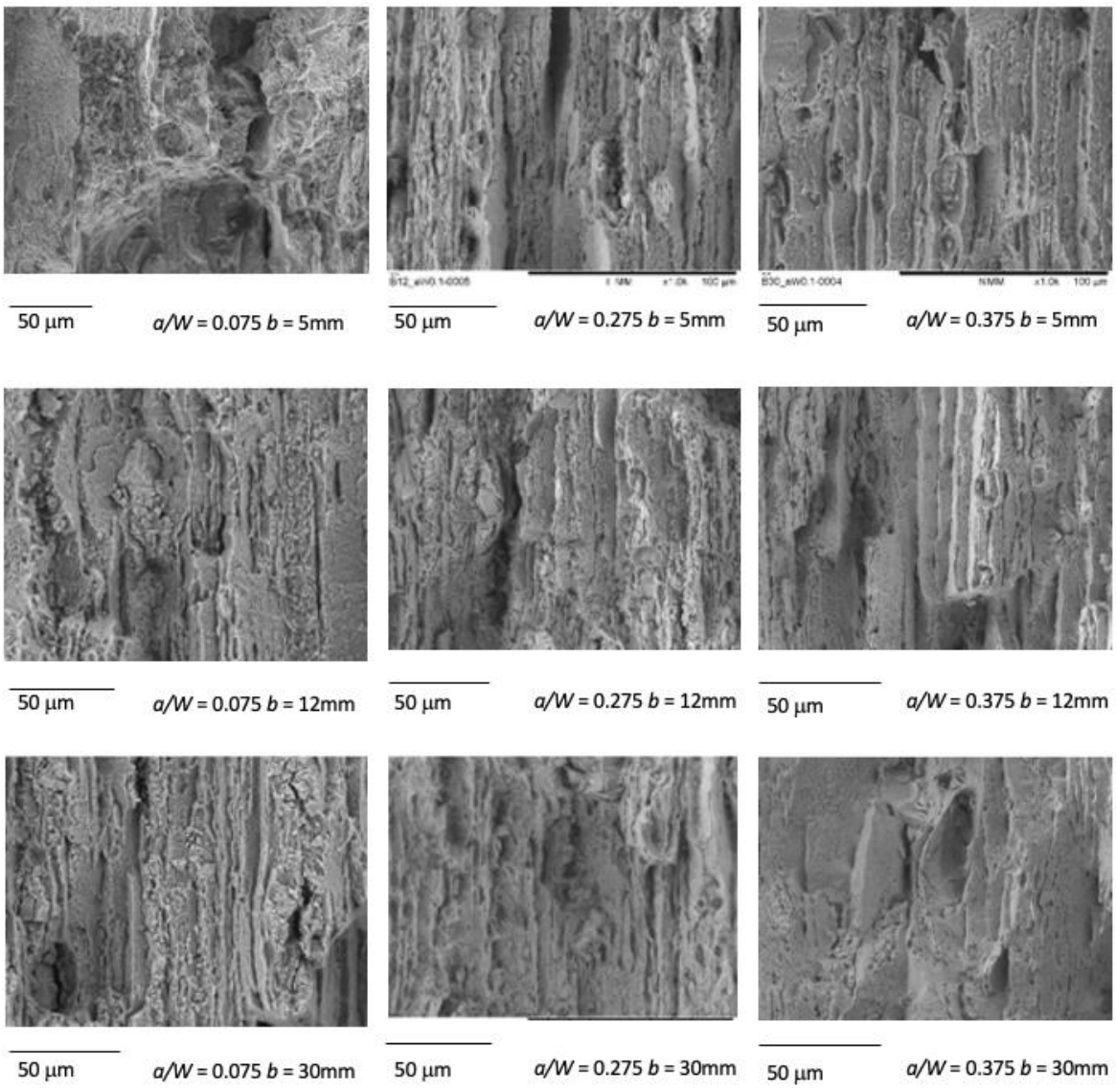

Figure 4.19-1000x Magnification sample image of each specimen geometry

5.6 Finite element results

In Figure 4.20, examples of the plastic zone for each sample, as calculated by finite element can be seen. The plastic zone is shaded grey. This is taken as the region with nodes having Von Mises stress exceeding the yield stress for Al7075. It can be seen that when the constraint is low and fracture toughness is higher, there is a greater volume of plasticity. This is consistent with the expected trend due to the constraint effect

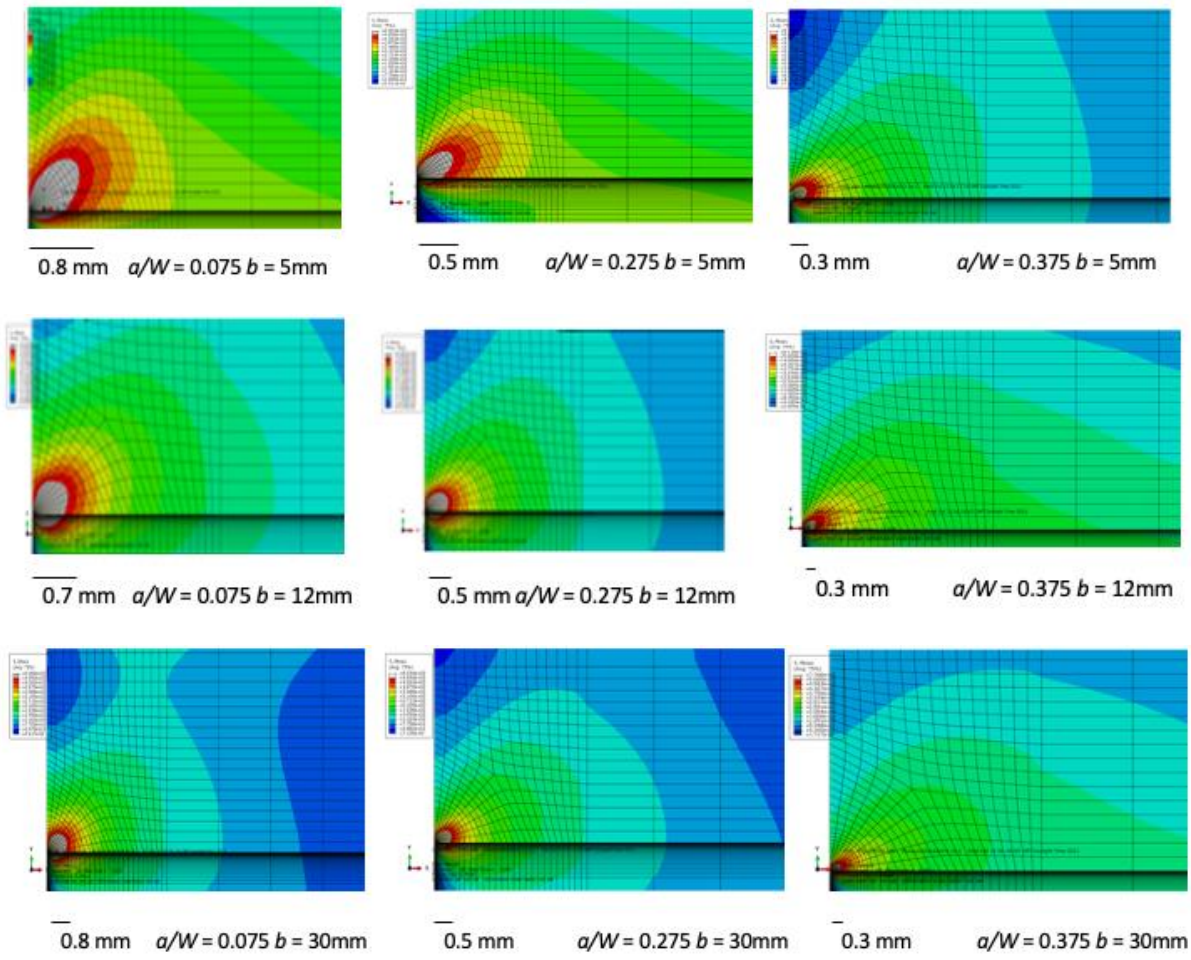

Figure 4.20- Plastic zone at fracture. For each sample geometry at a median level of load, an image of the plastic region derived from FE simulations which is shown in grey. The images are slice of the middle-thickness of the specimen. The scale bar indicates the radius of the plastic zone in the mid-section.

Figure 4.21 depicts the variation of the fracture toughness as a function of *Q* while Figure 4.22 is the fracture toughness as a function volume of plasticity per unit thickness. The fracture toughness values were calculated using finite element simulations as for the non-standard specimens there is no Widley accepted standard equation to convert fracture load to toughness. Interaction integral [160] incorporated in Abaqus was used over 25 contours to ensure path independency of energy release rate. The value at the centre of the sample thickness was chosen and

converted to toughness (*Kc*) using linear elastic equation (that is $K_c = \sqrt{JE/(1-\nu^2)}$ as is customary. *Q* is determined by extracting σ_{yy} from FE for each specimen at fracture load at $\sigma_0 r/J = 2$ and using Eq. 2 to find the normalised difference between opening stress at fracture of each specimen with that of the high constrain condition. In this work we used the opening stress of high constrain sample (*a*/*W* = 0.375 and *b* = 30 mm) as the value for high constraint condition. This was calculated to be 3% less than the value calculated by HRR [161].

Figure 4.21 shows that as *Q* becomes more negative (the loss of constraint), the higher the fracture toughness. Similarly, it can be seen in Figure 4.22 that as the constraint is lost, the volume of plasticity increases with increase in its fracture toughness. However, it can be seen in Figure 4.21 that there is no trend in *K* plot against *Q* when the thickness changes. No meaningful relationship between *K* and the *Q* parameter can be derived from the data in this experiment when all the thicknesses and crack lengths are combined. However, the biggest outliers belong to the shortest cracks (*a*/*W* = 0.075) in thin samples (*b* = 5 mm and *b*= 12 mm). This is consistent with the change in the fracture surface as observed in Figure 4.17 and Figure 4.18. It can be argued that as the constraint is reduced, the dominant mode of fracture from tensile, where the hydrostatic stress is governing factor, changes to shear, in which the shear stress is more prominent in driving the crack. Another indication of such a change is seen in Figure 4 where in *a*/*W* = 0.075 with *b* = 5 mm and *b*= 12 mm more nonlinearity is observed in Load-CMOD before final fracture indicative of higher plasticity (i.e. shear). Thus, as the fracture mechanism has changed in *a*/*W* = 0.075 with *b* = 5 mm and *b*= 12 mm, the fracture data of these specimens cannot be pooled together with the rest of the data.

In the case of the φ parameter, there is a clear relationship that can be seen when this parameter is plotted against *K*, especially if *a*/*W* = 0.075 with *b*= 5 mm and *b*= 12 mm are excluded. It can be seen in Figure 6 that φ and *K* have a strong positive correlation. It is therefore possible to use the plastic volume to combine the effects of in and out-of-plane constraint and form a unified measure which can predict the effects of one on the other.

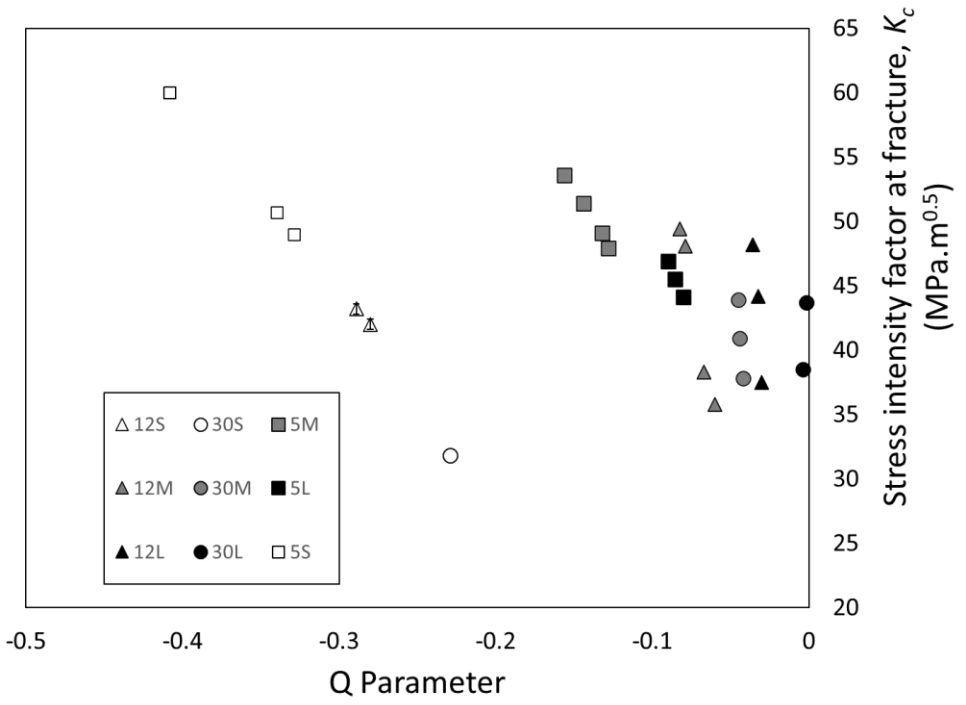

Figure 4.21 – Fracture toughness as a function of Q

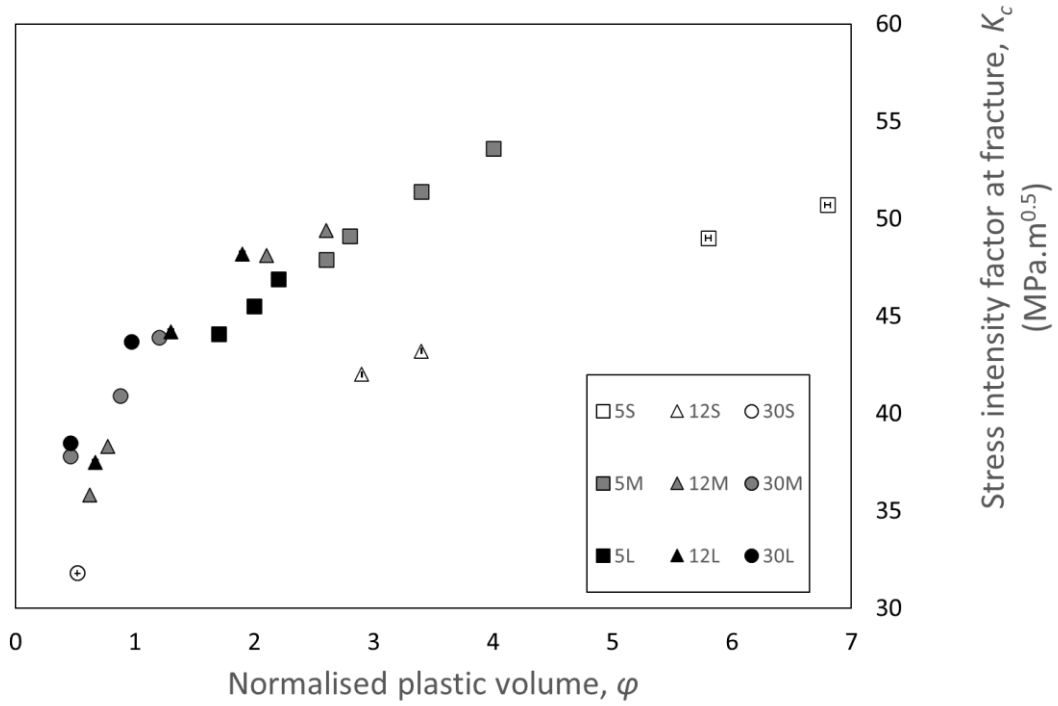

Figure 4.22 – Fracture toughness as a function of volume of plasticity

5.7 Conclusion

A series of three-point bending tests were carried out for specimens with nine different combinations of constraint. There were three levels of in-plane constraint (a/W = 0.075, 0.275, 0.375) and three levels of out of plane constraint (b = 5 mm, 12 mm, 30 mm). The narrow range of loads in the experiment and the abrupt nature of the specimen failure, show that the fracture of Al7075 T651 is generally very brittle although in the case of a/W = 0.075 with b = 5 mm, 12 mm evidence of shear type fracture was observed. This means that there is a contained region of plasticity ahead of the crack tip as can be seen in data from the FE results.

Fracture toughness represented by the stress intensity factor was plotted against the two parameters Q and φ. Q is a widely used parameter which quantifies the deviation of opening stress from the high constraint condition, while φ offers a normalised plastic zone size around the crack tip at fracture initiation. φ may be a useful parameter to quantify in-plane and out-of-plane constraint, as φ offers a more consistent trend when the in and out-of-plane constraint data were combined. Q is a parameter defined for quantifying in plane constraint and although its application to out of plane constraint has not been fully investigated, this study may suggest that it is not uniformly quantifying in and out of plane constraint simultaneously.

Acknowledgement

The financial support, provided by EPSRC through NNL, is gracefully acknowledged. ST thanks the laboratory technicians and workshop staff at the University of Bristol's Heavy Structures facilities. MM acknowledges the support of Royal Academy of Engineering support through a Research Chair.

[1]

6 Conference Paper

A paper to be presented at a conference showing a more industrially relevant application of constraint. It has not yet been submitted to a conference.

Determination of constraint parameters K and ϕ from three point bending test on Al7075 pipe

S.M. Tonge[1], M. Mohktari, R. Patel, M. Mostafavi

Queen's Building, University Walk, Clifton, Bristol, BS8 1TR

[1] st16173@bristol.ac.uk

Abstract A series of unique non-standard three-point bending tests were performed on a series of 5 pipes of known diameter. The dimensions of the pipes represent a realistic situation applicable to the nuclear industry namely a thin walled pressure vessel tube in an AGR. The material used had previously been used in a series of experiments on SENB specimens in three-point bending tests. The results of these experiments show the applicability of the constraint parameters Q and A_p. Finite Element simulations were carried out on this setup which allowed the stress intensity factor K, a measure of fracture toughness. Q and A, which are measures of the constraint of the plastic region at the crack tip by the geometry of material are also determined. The value of K was measured to be 49.5 and the value of ϕ was 5.2. This meant that in comparison with standardised experiments on SENB specimens, the results from tests with pipes showed a good comparison with experimental data.

6.1 Background

Methods such as R6 [4] enable a user to evaluate a defect in a body to determine whether a crack in an component is likely to propagate. The resistance of a component to failure will be determined by is fracture toughness, which is a material property, and the size of the component. The dependence of fracture toughness on specimen geometry is known as the constraint of the plastic region. The plastic region is a volume of yielded material that forms ahead of the crack tip. The constraint is divided into two parts: in-plane constraint and out of plane constraint. Out of plane constraint refers to the effect of the specimen thickness, whereas in plane constraint accounts for the effect of the uncracked ligament length in front of the crack tip. Out of plane constraint can be quantified by Q and other parameters [6], in plane constraint can be quantified by Tz [7]. However, there is no parameter in use that yet quantifies both in and out of plane constraint. The parameter ϕ [52], has been shown to be a candidate due its sensitivity to both forms of constraint in three-point bending tests on standardised specimens. ϕ will be tested in this experiment using a pipe specimen, which is more applicable to industrial use than previous tests.

6.2 Introduction

Three-point bending tests were performed on pipes manufactured from the aluminium alloy Al707-

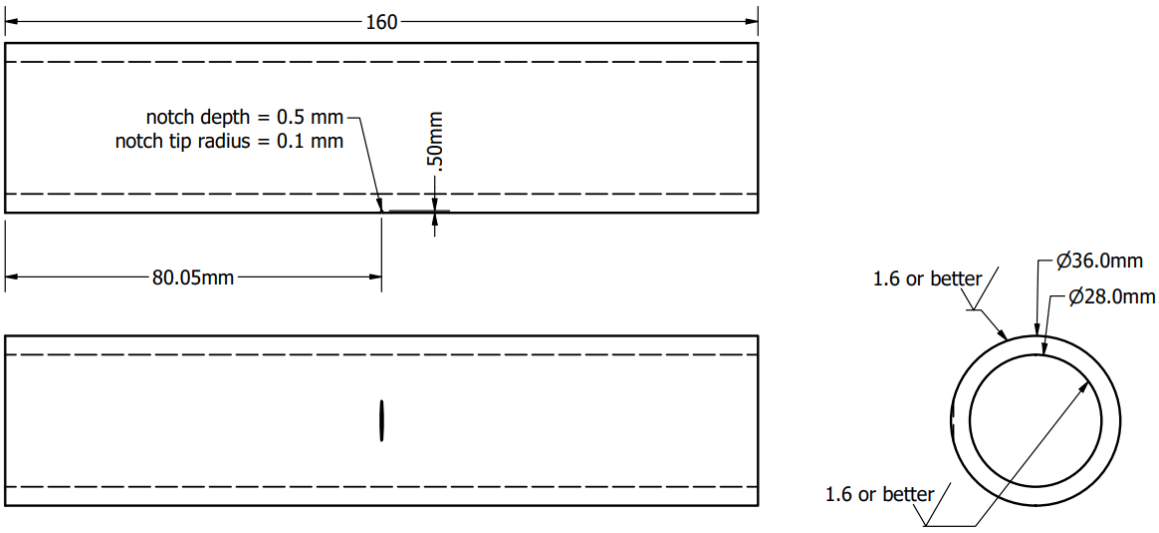

Fig. 5.1: Diagram of Sample showing dimensions.

T651. This material was chosen due to its use in previous experiments which enables comparability with previously measured values of fracture parameters K and ϕ.

The pipes had an outer diameter of 36mm and an inner diameter of 28mm. These dimensions were chosen for applicability to nuclear industry applications and are shown in Fig. 1. The pipes were laser cut from a 500x1000x30mm aluminium plate. To ensure that the specimens were homogenous, the direction that the pipes were cut was along the same of the axis of the plate. This plate had first been cut into rectangular sections which were at a uniform angle to the original plate. This alloy was chosen for the purpose of comparison with previous work. By determining the value of the preciously tested parameters in these novel experiments, using industrially relevant components, it is possible to verify the applicability of the previous experiments on a more realistic specimen. This allows the extension of the verification of these constraint quantifying parameters to a different, more relevant sample. Which could enable safety procedures to be updated to include this. From the data obtained, it is then possible to provide evidence on the behaviour of the parameter in a different level of constraint.

6.3 Experimental Method

Experiments carried out on a cylindrical specimen using sample dimensions shown in Fig. 1. Novel, bespoke pipes with dimensions given in Fig. 1 were used. These represent a coolant pipe with realistic dimensions representing a boiler tube in a nuclear reactor. The material used was Al7075-T651. This had the following elastic material properties: E = 71.7 GPa and Poisson's ratio, ν = 0.33. The pipes had a notch made on the outside by EDM machining which was 1.5mm deep. The initial notch had been 0.5mm, but it was decided to increase to 1.5mm this during the experiment to increase the constraint effect.

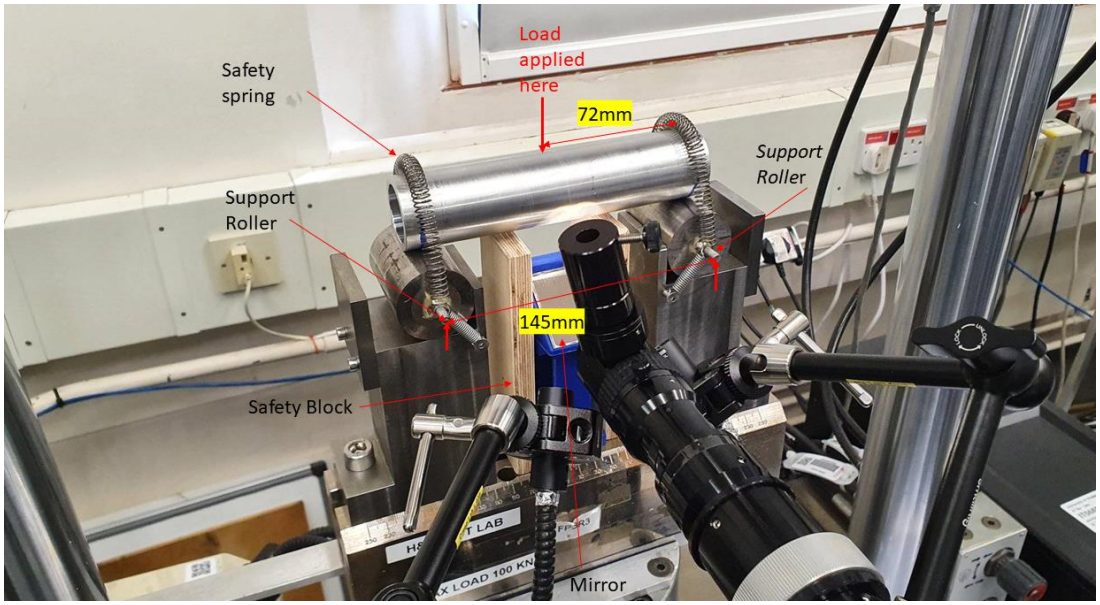

Fig. 5.2 Experimental setup for the three point bending test.

In the construction of the experimental setup, a novel experimental rig has been equipped to carry out novel three-point bending tests on specimens without a flat base. This example was cylindrical and had a tangential point of contact with the rollers. The dimensions were 72mm between the rollers and the centre on each side and the distance between the two supports was 145mm. The experimental setup is shown in Fig. 3. The load was applied using a Schenk 75kN servo-hydraulic test machine. Despite this being a bespoke test, the standards of ASTM E399 [95] were not followed as this was a unique specimen. The distance between the rollers was the same as for the three point bend test described in Chapter 4, which was kept as standard despite the other aspects of the test being bespoke. Springs were added to increases the capability of the equipment to withstand slipping. To validate the finite element models (see next section) used to convert fracture loads to fracture toughness, crack mouth opening displacement (CMOD) was measured directly on the surface of the specimen, using an Epsilon clip gauge. The clip gauge had been calibrated using a barrel micrometre at regular intervals during the experiment. The Epsilon clip gauge was used(model 3541-005M-120M-LT) which had a travel range of 12 mm .

To facilitate the growth of a crack in a consistent, repeatable way; fatigue pre-cracking was performed. The load range was from 0.8 to 8kN and the frequency of the sinusoidal loading was 7Hz. This was chosen due to the restricted loads to ensure the stability and safe operation of the machine. After fatigue pre-cracking, 3-5mm of crack growth was visible either side of the crack tip. The crack growth was diagonal through the cross section of the cylinder as shown in Fig. 4. After fatigue pre-cracking the specimen, which now had a through crack, was placed under linearly increasing load until failure. This load was applied in displacement control at 0.1 mm/s until 2mm of displacement had been applied or failure occurred. Fig. 5 shows the load vs displacement curves for the growth of a crack to failure by linear loading in displacement control. The failure loads are shown together with the displacement that produced this load in both FE and experiment. Compliance of the model in its elastic regime (crack mouth displacement divided by load) was calculated and compared with that measured by the experiments to ensure that the model is directly comparable with the physical experiments.

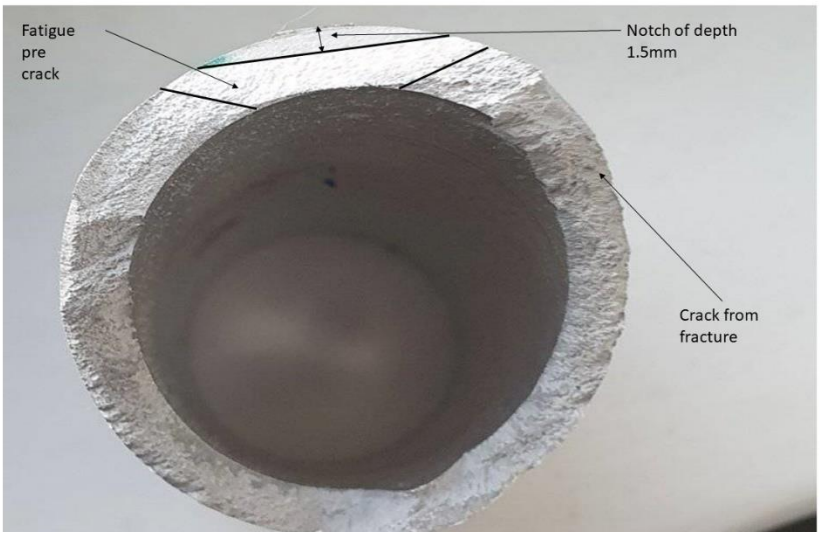

Fig 5.3: Diagram of Sample showing crack formation.

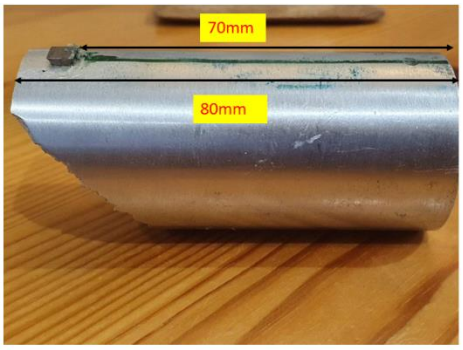

Fig. 5.4: Diagram of showing dimensions how clip gauge was attached to the specimen using a block .

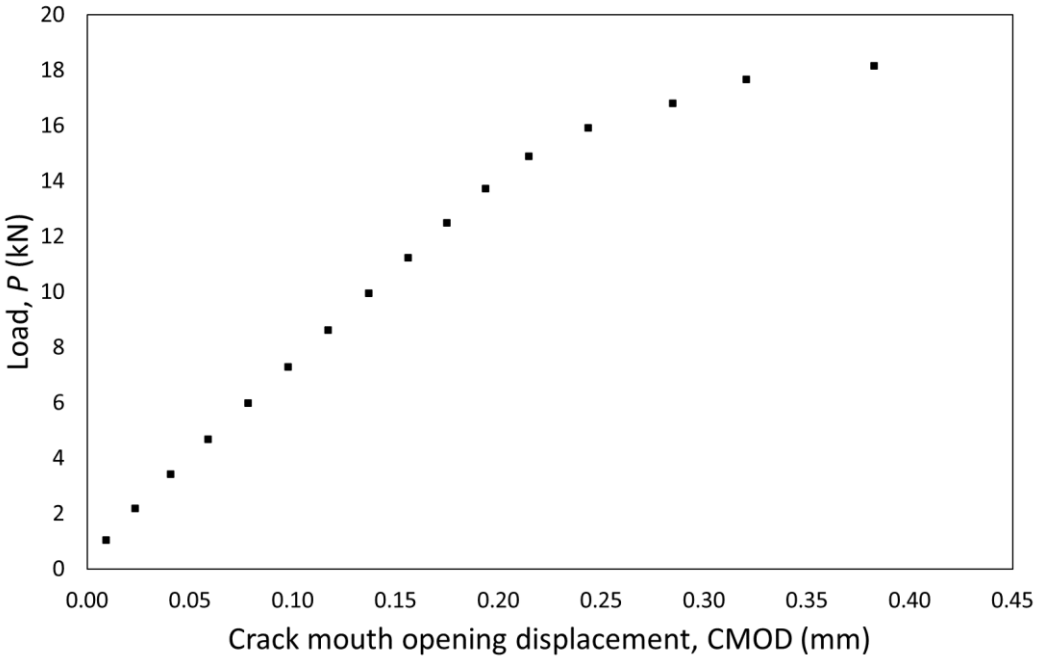

Fig. 5.5: Diagram of Sample showing dimensions.

6.4 Finite Element Analysis

To obtain the value of the stress intensity factor K, a series of Finite Element (FE) simulations were performed.

Abaqus 6.14 [33] was used to run a python script that defined the pipe specimens with fatigue pre-crack built into the geometry. This meant that the only the linear, displacement loading stage was simulated. Around 12,000 3D elements were used. A quarter of the original specimen was modelled, defined by two planes of symmetry, one which was parallel to the crack and another which was perpendicular to the direction of crack propagation. The planes of symmetry were defined by symmetry boundary conditions. The layout of the simulation is shown diagrammatically in Fig. 6. Rigid bodies were created to define the solid roller, which were defined as being in frictionless contact with the pipe. The rollers were representing the points that which load was applied in displacement control. The lower roller was fixed by applying boundary conditions its reference point and displacement was applied at the reference point of the roller above the notch. The simulated pipe was loaded in displacement control by applying displacement at the same rate as in the physical test, that is 0.1mm/s, until an equal failure load as the pipe in the physical experiment was achieved. The material was applied to the model using a Johnson-Cook model that was given material properties a Johnson-Cook model:

$$\overline{\sigma} = \mathrm{A} + \mathrm{B}(\overline{\varepsilon})^{\mathrm{n}} \qquad \text{(Eq. 1)}$$

where $\overline{\sigma}$ is plastic stress and $\overline{\varepsilon}$ is plastic strain. The elastic properties were E = 71.7 GPa and Poisson's ratio v = 0.33. The Johnson-Cook parameters were A = 450 MPa, B = 488 MPa and n = 0.3498 as identified previously for this material [155].

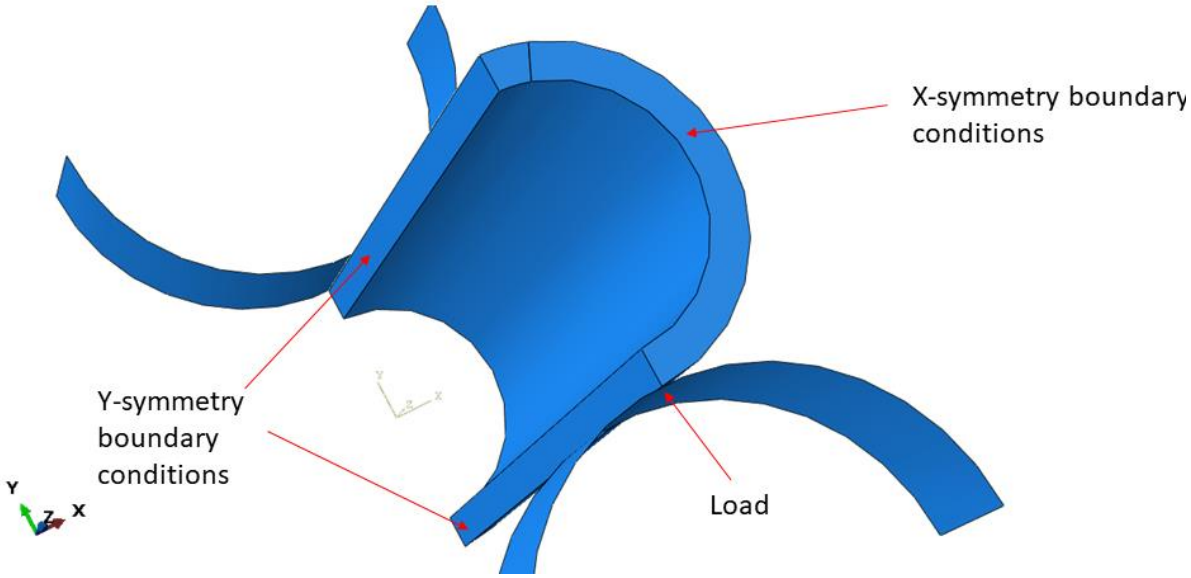

Fig. 5.6: Diagram of Sample showing dimensions.

Three dimensional hex elements were used to form a structured mesh in the model shown in Fig. 7. In the partition around the crack tip a sweep technique was used, with the mesh density being increased by a factor of four in the region of interest. The crack was defined by the removal of symmetry boundary conditions on the crack face and also as a contour integral with 12 contours to be evaluated.

We could see with reference to Fig. 5 that the FE model was compliant with the data, with a reaction

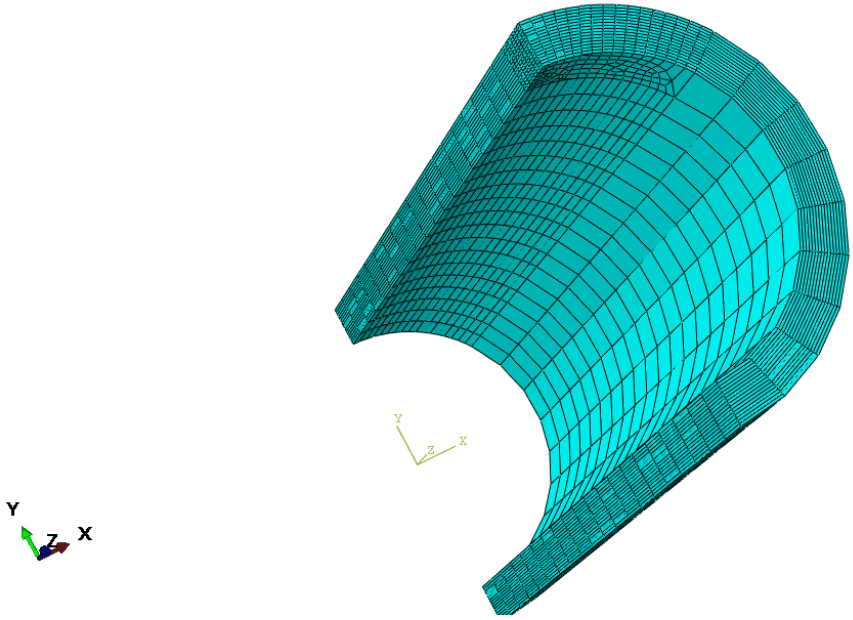

Fig. 5.7: Finite Element Mesh on 1/4 pipe simulation

force at the point of 20kN to 2 significant figures. This means that there is some confidence that the results are realistic picture of the experiment.

Results

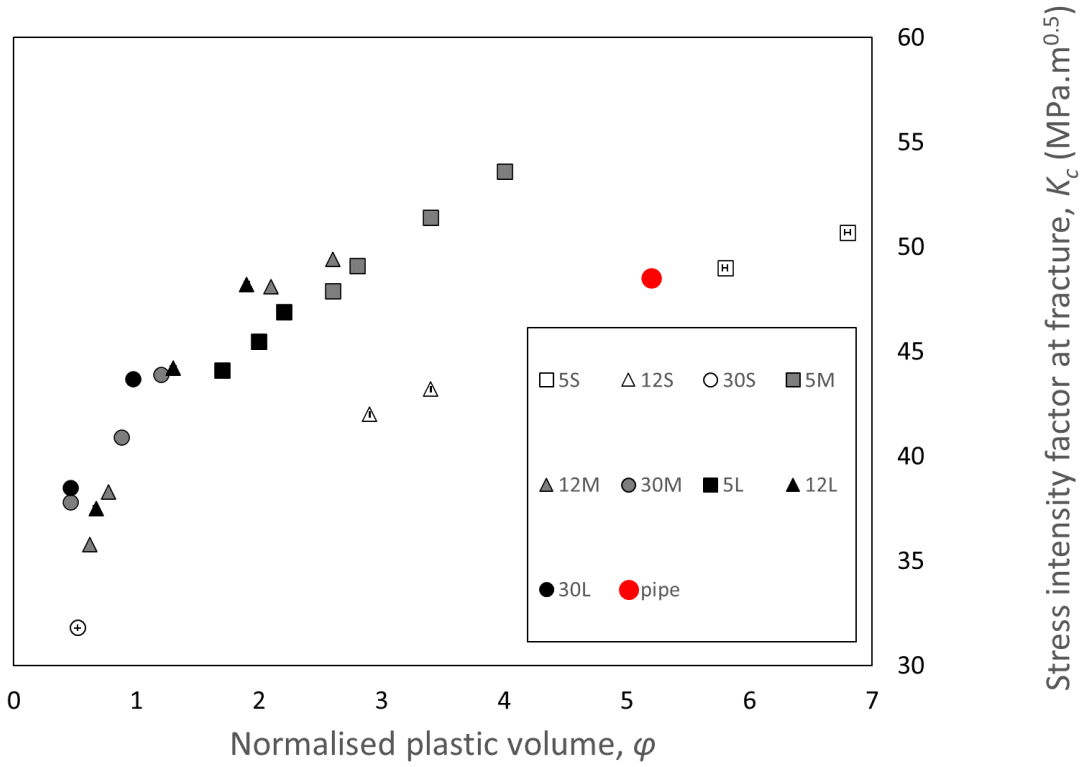

Fig 5.8 Graph showing the fracture parameters determined for pipe test compared with the results of the previous standardised experiments.

It can be seen from graph in Fig. 8 that the results for the stress intensity factor and ϕ are comparable to the results previous experiments. This means that this result supports the idea that ϕ could be a useful parameter for quantifying in and out of plane constraint.

6.5 Conclusion

This work shows that the parameter ϕ can be used to unify constraint for fracture assessments of components. The results of this experiment are broadly in line with what would be expected to be consistent with previous standardised tests in Chapter 4. However, these results should be viewed with caution as more work is needed to be able to have a full picture of the trend in constraint for these specimens.

- More different levels of constraint would need to be tested e.g. different pipe thicknesses.
- Currently these tests have used only one material, which was Al7075 T651. This material had two specific fracture mechanisms which were apparent from the fractography results. The tests would need to be carried out on a more ductile material such as stainless steel to ensure that this method produces consistent results with different materials.
- A number of different specimen types would need to be used to prove applicability to all different specimens.

7 Thesis Conclusion

Fitness for Service (FFS) procedures are used for assessing the integrity of components containing cracks or flaws. The needs of the nuclear power industry were the catalyst for the development of R6 which was first published in 1976. The procedures are continuously updated to reflect advances in the field of fracture mechanics, research is ongoing into new methods that can enhance the R6, BS7910 and other procedures.

FFS assessment procedures currently can consist of the following parts:

- The early chapters often show the user the basic methods of assessment. This includes the Failure Assessment Diagram (FAD). The FAD is a visual representation of the current knowledge of failure from the theory of fracture mechanics. It consists of a region bounded by two axes. On the vertical axis is the ratio of the stress intensity factor K at the applied stress to the material fracture toughness. On the horizontal axis is the ratio of the applied load to the tensile strength.
- There are chapters covering more advanced procedures, including the effect of constraint on fracture toughness which is the part of the procedure that is considered by the work in this thesis.
- A series of worked examples of fracture assessments are normally provided.

Although the FFS procedures have been widely used in the nuclear power industry for structural integrity assessments there are still aspects of this which could be improved. The FFS assessment procedures have long been considered unrealistically conservative. One of the reasons for this is that they don't completely account for the effect of constraint on fracture toughness. In FFS procedures, the current method of accounting for the constraint effect, is to use the J-Q and K-T methods which are incorporated into the constraint sections of current FFS procedures. This involves the use of the correlation equations which relate the fracture toughness parameter to an in-plane constraint parameter. A series of three, material specific relationships are used in current FFS procedures that relate K, which represents fracture toughness and the constraint parameters Q and T. The correlation coefficients need to be determined for each material to be able to perform an assessment, which is time consuming and expensive. Another problem with this is that the parameters currently considered in FFS assessments are thought to be sensitive to in plane constraint only. Therefore, they do not account for the effect of out of plane constraint. To correct for this, approaches using a third parameter to account for out of plane constraint have been proposed. These include K-T-T_z and J-Q_T-T_z. The major drawback of these theories is that the locus of points found in the correlation of the fracture toughness and constraint parameters would be a three-dimensional space. This would be even more computationally expensive than the current method used to account for constraint in FFS assessments.

A number of constraint parameters have been proposed that are sensitive to both in and out of plane constraint. During this work the unified constraint parameters including A_p, A_d and ϕ were reviewed. These parameters were thought to have potential for incorporation in fracture assessment procedures. This would have the benefit of more accurately considering out of plane constraint which is not effectively quantified by any parameter in current FFS assessments. For this to be realised, sufficient evidence of their effectiveness and reliability in quantifying constraint would need to be gathered. It was decided to perform a series of experiments which would provide evidence of the correlation between ϕ and fracture toughness. Previously, the ϕ parameter had only been tested by Finite Element simulations, in which it had shown sensitivity to both in and out of plane constraint. If ϕ was shown to be a single parameter which quantifies both types of constraint, a

calibration between ϕ and a fracture toughness parameter such as K could be derived. This could then be included in assessments including the R6 procedures, with the potential to improve accuracy whilst reducing the complexity of accounting for constraint in these assessments.

In the course of the experiments in this thesis, the ϕ parameter, the in-plane constraint parameter Q and K_J which is a measure of fracture toughness were tested. The inclusion of Q in these tests allowed for a comparison between an in-plane constraint parameter currently used in FFS assessments and a parameter that has been proposed for the purpose of unifying in and out of plane constraint. This involved a series of fracture tests with a range of different specimen types. In the first instance, a series of four non-standard specimens were fractured in tensile tests. These were carried out in a synchrotron X-ray source, which allowed X-ray tomography and diffraction to be performed. The novel analysis methods enabled the determination of the parameters directly from experimental methods. This was successful in showing that ϕ was sensitive to in and out of plane constraint for the first time by experimental means. However, it was not possible to show that K_J and ϕ were correlated due to the limited number of tests which could be performed under such conditions. The numerical values of the parameters measured in these experiments were verified by Finite Element simulations.

Using standard SENB specimens, three-point bending tests were performed on specimens with nine different levels of constraint. These tests were used with compliant Finite Element models to determine the values of K_J, ϕ and Q. From the results of the experiments and simulations, it was possible to see that ϕ was more sensitive to both types of constraint than Q, which is consistent with expectations of Q as an in-plane constraint parameter. ϕ provided a better correlation with fracture toughness than Q when considering all the constraint levels that were tested. This shows that it is possible to account for both in and out of plane constraint effects on fracture toughness with a single parameter. The measurements of ϕ would suggest that it is a candidate for use in accounting for constraint in a procedure such as R6. This is further supported by the measurement of ϕ for a pipe specimen which was more similar to a typical component undergoing assessment than a standard test specimen. The measurement of ϕ and K_J in this experiment was consistent with values of these parameters previously measured for standardised test specimens. This represents a considerable step towards to the acceptance of a parameter that unifies in and out plane constraint.

To extend this work a number of future investigations could carried out.

1. A correlation relationship would need to be derived between the parameter ϕ and a parameter representing fracture toughness such as J or K. This would be similar to the correlation equations in the constraint sections of FFS procedures.
2. The tests in this work were performed using two different alloys of Aluminium. Al7075 shows particularly brittle fracture. It may be necessary to perform similar experiments on another material with a more ductile fracture mechanism to show that this parameter is still applicable. It could be useful to use a heat-treated steel to simulate the effect of aging of a material.
3. More tests are needed on realistic components such as the pipe considered in Paper 3. Considering that FFS procedures are used extensively by the UK nuclear industry, tests based on realistic dimensions should be considered.

This work was carried out with the author of this thesis as the lead author of three papers. The contribution of the other authors is noted in the credit statement. The lead author's contribution to the publications involved taking part in all experiments either the main investigator or as part of a team in the case of the synchrotron experiment. Dr M Mohktari is acknowledged for providing

training on the three-point bend test rig, which had been developed for a previous experiment, as well as access to other laboratory equipment. Data analysis was performed by the lead author, the software for this analysis had in some cases been developed by previous researchers and where this is the case it is referenced. Simulations were carried out by the author, in the case of the SENB specimens the code for generating the simulation was provided by another author, Z Cheng who is credited with this. All data analysis was performed by the author, Dr A Cinar and Dr S Barhli are especially acknowledged for providing codes which the author used for analysing data from the synchrotron experiment. All three papers were written by the author and sent to co-authors for editing.

Bibliography

[1] Griffith Alan Arnold 1921VI. The phenomena of rupture and flow in solidsPhilosophical Transactions of the Royal Society of London. Series A, Containing Papers of a Mathematical or Physical Character221163–198

[2] Irwin G (1957), Analysis of stresses and strains near the end of a crack traversing a plate, Journal of Applied Mechanics 24, 361–364.

[3] Rice, J. R. (1968), "A path independent integral and the approximate analysis of strain concentration by notches and cracks" (PDF), Journal of Applied Mechanics, 35 (2): 379–386,

[4] Dowling, A.R. & Sharples, J. & Budden, P.J.. (2000). An overview of R6 revision 4. 423. 33-37.

[5] Williams, M.L.: On the stress distribution at the base of a stationary crack. J. Appl. Mech. 24, 109–114 (1957) n.d.

[6] O'Dowd NP, Shih CF. Family of crack-tip fields characterized by a triaxiality parameter-I. Structure of fields. J Mech Phys Solids 1991.

[7] Zhao J, Guo W, She C, Meng B. Three dimensional K-Tzstress fields around the embedded center elliptical crack front in elastic plates. Acta Mech Sin Xuebao 2006.

[8] .. Dodds RH, Anderson TL, Kirk MT. A framework to correlate a/W ratio effects on elastic plastic fracture toughness. Int J Fract 1991; 48:1–22.

[9] Mostafavi, M., Pavier, M. J. and Smith, D. J. (2009) Unified Measure of Constraint, ESIA10: Manchester, UK n.d.

[10] Seal CK, Sherry AH. Predicting the effect of constraint on cleavage and ductile fracture toughness using area contour toughness scaling. Eng Fract Mech 2017; 186:347–67

[11] C.E. Inglis, "Stresses in a plate due to the presence of cracks and sharp corners," Trans. Inst. Nav. Archit. London 55, 1913, pp. 219-230.

[12] Anderson TL. Fracture Mechanics: Fundamentals and Applications. vol. 58.,2012

[13] Orowan, E., 1949.*Fracture and strength of solids*. Reports on Progress in Physics XII, 185–232.

[14] Margolin, Len. (1984). A generalized Griffith criterion for crack propagation. ENGINEERING FRACTURE MECHANICS. 19. 539. 10.1016/0013-7944(84)90010-9.

[15] E. E. Lewis, Fundamentals of Nuclear Reactor Physics. 2008.

[16] Wang, C. H. "Introduction to Fracture Mechanics," DSTO Aeronautical and Maritime Research Laboratory, DSTO-GD-0103, 1996.

[17] K. S. Krane and D. Halliday, Introductory Nuclear Physics. 1987.

[18] World Nuclear Association, “Nuclear Power Reactors,” 2018. [Online]. Available: http://www.world-nuclear.org/information-library/nuclear-fuel-cycle/nuclear-powerreactors/nuclear-power-reactors.aspx. [Accessed: 12-Jan-2019].

[19] J. R. Lamarsh, “Introduction to Nuclear Reactor Theory,” Interactions, 2005.

[20]] “Radioactive Waste Management,” World Nuclear Association. [Online]. Available: http://www.world-nuclear.org/information-library/nuclear-fuel-cycle/nuclearwastes/radioactive-waste-management.aspx. [Accessed: 05-Mar-2017].

[21] E. Nonbel, “Description of the Advanced Gas Cooled Type of Gas Cooled Reactor (AGR),” 1996.

[22] G. C. Sih, P. C. Paris, and G. R. Irwin, “On cracks in rectilinearly anisotropic bodies,” Int. J. Fract. Mech., 1965.

[23] Irwin, G.R., ‘Analysis of Stresses and Strains Near the End of a Crack Traversing a Plate,’ Journal of Applied Mechanics, Vol. 24, pp. 361-364, 1957.” ,

[24] Westergaard, H.M., ‘Bearing Pressures and Cracks,’ Journal of Applied Mechanics, Vol. 6, pp. A49-53, 1939.”

[25] “Fracture Mechanics Lecture notes - course 4A780 Concept version Dr. P.J.G. Schreurs Eindhoven University of Technology Department of Mechanical Engineering Materials Technology September 6, 2012.”

[26] Bob McGinty, “Stress Intensity Factor, Fracture Mechanics,” 2018. [Online]. Available: http://www.fracturemechanics.org/.

[27] 2012., Anderson TL. Fracture Mechanics: Fundamentals and Applications. vol. 58.

[28] J. R. Rice, “A Path Independent Integral and the Approximate Analysis of Strain Concentration by Notches and Cracks,” J. Appl. Mech., 1968.

[29] Hadj Meliani, M., Azari, Z., Pluvinage, G., Matvienko, Yu.G., The Effective T-stress Estimation and Crack Paths Emanating from U-notches, Engng Fracture Mechanics, Vol 77, Issue 11, July : 1682-1692, (2010). (PDF)

[30] J. W. Hutchinson, “Singular behaviour at the end of a tensile crack in a hardening material,” J.

Mech. Phys. Solids, 1968.

[31] Betegón C, Hancock JW. Two-Parameter Characterization of Elastic-Plastic Crack-Tip Fields. J Appl Mech 1991.

[32] K. Kishimoto, S. Aoki, and M. Sakata, “On the path independent integral- ∫,” Eng. Fract.

Mech., 1980.

[33] S. Suresh, “Elastic-Plastic Fracture Mechanics Lecture Notes,” MIT. 2005

[34] R. F. Lee and J. A. Donovan (1987) J-Integral and Crack Opening Displacement as Crack

Initiation Criteria in Natural Rubber in Pure Shear and Tensile Specimens. Rubber Chemistry

and Technology: September 1987, Vol. 60, No. 4, pp. 674-688.”

[35] J. Begley and J. Landes, “The J integral as a fracture criterion,” 1972.

26

[36] Cravero S, Ruggieri C. Structural integrity analysis of axially cracked pipelines using conventional and constraint-modified failure assessment diagrams. Int J Press Vessel Pip 2006.

[37] Assessment of the integrity of structures containing defects’, R6 Rev. 4, British Energy Generation Ltd/BEG(UK)L, 2001. n.d.

[38] J. D. Landes and J. A. Begley, “Test Results from J-Integral Studies: An Attempt to Establish a

JIC Testing Procedure,” Fract. Anal. ASTM STP 560, 1974.

[39] M. Y. Mu, G. Z. Wang, S. T. Tu, and F. Z. Xuan, “Three-dimensional analyses of in-plane and

out-of-plane crack-tip constraint characterization for fracture specimens,” Fatigue Fract. Eng.

Mater. Struct., 2016.

[40] “Brocks, W. and Schmitt, W. (1993) Second Parameter in J–R Curves: Constraint or Triaxiality

in: Proceedings of the 1993 Conference on Constraint Effects in Fracture: Theory and

Applications, ASTM: Dallas (USA).No Title.”

[41] M. Mostafavi, “Improving the Accuracy of Fracture Assessments,” University of Bristol, 2009

[42] N. O. Larrosa and R. A. Ainsworth, “Ductile fracture modelling and J-Q fracture mechanics: A

constraint based fracture assessment approach,” Frat. ed Integrita Strutt., 2016.

[43] Omar, Bouledroua & Mohammed, hadj meliani & Guy, Pluvinage. (2016). A review of T stress calculation methods in fracture mechanics computation. Nature Technologie.”

[44] Hadj Meliani, M., Azari, Z., Pluvinage, G., Matvienko, Yu.G., The Effective T-stress Estimation

and Crack Paths Emanating from U-notches, Engng Fracture Mechanics, Vol 77, Issue 11, July :

1682-1692, (2010). (

[45] B. Cotterell and J. R. Rice, “Slightly curved or kinked cracks,” Int. J. Fract., 1980.

[46] J., Zhao, W., Guo, Three-parameter K-T-Tz characterization of the crack-tip fields in compact-tension-shear specimens. Engineering Fracture Mechanics 92 (2012) 72–88. n.d.

[47] “Williams,M.L.: On the stress distribution at the base of a stationary crack. J. Appl. Mech. 24,

109–114 (1957).”

[48] “Close S. Melin The influence of the T-stress on the directional stability of cracks Int J Fract,

114 (3) (2002), pp. 259-265.”

[49] M. Gupta, R. C. Alderliesten, and R. Benedictus, “A review of T-stress and its effects in

fracture mechanics,” Engineering Fracture Mechanics. 2015.

[50] N. P. O’dowd, “Applications of two parameter approaches in elastic-plastic fracture

mechanics,” Eng. Fract. Mech., 1995.

[51] Henry BS, Luxmoore a. R. The stress triaxiality constraint and the Q-value as a ductile fracture parameter. Eng Fract Mech 1997.

[52] Constraint and toughness parameterised by T. C. E. Hancock, J. W., Reuter, W. G. and Parks, D. M., K.-

[53] Y.J. Chao, P.S. Lam, L. Zhang,

Effect of constraint on fracture controlled by stress or strain,

Theoretical and Applied Fracture Mechanics,

Volume 30, Issue 1,

1998,

Pages 75-86,

ISSN 0167-8442,

https://doi.org/10.1016/S0167-8442(98)00043-3.

[54] C. Betegón and J. W. Hancock, “Two-Parameter Characterization of Elastic-Plastic Crack-Tip

27

Fields,” J. Appl. Mech., 1991.

[55] M. Kirk and A. Bakker, Editors, Constraint Effects in Fracture – Theory and Applications:

second Volume, ASTM STP 1244, American Society for Testing and Materials, West

Conshohocken, 1994.”

[56] Rice JR, Tracey DM. On the ductile enlargement of voids in triaxial stress fields. J Mech Phys Solids 1969; 17:201–17.

[57] N. P. O’dowd, “Applications of two parameter approaches in elastic-plastic fracture

mechanics,” Eng. Fract. Mech., 1995.

[58] Zhu X.K., Joyce J.A. Review of fracture toughness (G, K, J, CTOD, CTOA) testing and

standardization. Eng. Fract. Mech. 2012;85:1–46. doi: 10.1016/j.engfracmech.2012.02.001.”

[59] S. Kumar, I. A. Khan, V. Bhasin, and R. K. Singh, “Characterization of crack tip stresses in

plane-strain fracture specimens having weld center crack,” Int. J. Solids Struct., 2014.

[60] G. Pluvinage, J. Capelle, and M. Hadj Méliani, “A review of fracture toughness transferability

with constraint and stress gradient,” Fatigue and Fracture of Engineering Materials and

Structures. 2014.

[61] S. Cravero and C. Ruggieri, “Structural integrity analysis of axially cracked pipelines using

conventional and constraint-modified failure assessment diagrams,” Int. J. Press. Vessel. Pip.,

2006.

[62] Jin H.J., Wu S.J. Effect of plasticity constraint on structural integrity assessment of pressure

vessel welds. Int. J. Pressure Vessels Pip. 2015;134:72–81. doi: 10.1016/j.ijpvp.2015.09.001.”

[63] Wang YH, Wang GZ, Tu ST, Xuan FZ. Ductile fracture prediction based on J-integral and unified constraint parameters for cracked pipes. Eng Fract Mech 2019; 215:1–15.

[64] Zhu X.K., Leis B.N. Bending modified J-Q theory and crack tip constraint quantification. Int. J.

Fract. 2006;141:115–134. doi: 10.1007/s10704-006-0068-5."

[65] B. Zhang and W. Guo, "Three-dimensional stress state around quarter-elliptical corner cracks

in elastic plates subjected to uniform tension loading," Eng. Fract. Mech., 2007.

[66] 2008, Bay BK. Methods and applications of digital volume correlation. J Strain Anal Eng Des; 43:745–60.

[67] ASTM E8. ASTM International, ASTM E8 Standard Test Methods for Tension Testing of Metallic Materials 2015.

[68] J., Zhao, W., Guo, C., She. The in-plane and out-of-plane stress constraint factors and K-T-Tz description of stress field near the border of a semi-elliptical surface crack. International Journal of Fatigue 29 (2007) 435–443. n.d.

[69] Wolfenden, A., Anderson, T. L. and Dodds, R. H. (1991) Specimen size requirements for

fracture toughness testing in the transition region. J. Test. Eval., 19, 123–134.

[70] J.Y. Xu, G.Z. Wang, F.Z. Xuan, S.T. Tu,

Unified constraint parameter based on crack-tip opening displacement,

Engineering Fracture Mechanics,

Volume 200,

2018,

Pages 175-188,

ISSN 0013-7944,

[71]] I I. Milne, R. A. Ainsworth, A. R. Dowling, and A. T. Stewart, "Background to and validation of

CEGB report R/H/R6-Revision 3," Int. J. Press. Vessel. Pip., 1988.

[72] British Energy, "Assessment of the integrity of Structures Containing Defects Revision 4,"

2001.

[73] Dowd BA, Campbell GH, Marr RB, Nagarkar V V, Tipnis S V, Axe L, et al. Developments in

synchrotron x-ray computed microtomography at the National Synchrotron Light Source. Proc.SPIE, vol. 3772, 1999.

[74] TWI, “The Future of Fracture Assessment.” [Online]. Available: https://www.twi global.com/technical-knowledge/published-papers/the-future-of-fracture-assessment. [Accessed: 20-Jan-2018].

[75] R. A. Ainsworth and D. G. Hooton, “R6 and R5 procedures: The way forward,” Int. J. Press. Vessel. Pip., 2008.

[76] Lewis, E.E.. (2008). Fundamentals of Nuclear Reactor Physics. 10.1016/B978-0-12-370631-7.X0001-0.

[77] Batur, Maryna & Alkan, Reha. (2023). What can we learn from past nuclear accidents? A comparative assessment of emergency response to accidents at the Three Mile Island, Chernobyl, and Fukushima Nuclear Power Plants. 3. 23-36.

[78] Dodds, R. H., Anderson, T. L. and Kirk, M. T. (1991) A framework to correlate a/W ratio effects on elastic plastic fracture toughness. Int. J. Fract., 48, 1–22.”

[79] “Mostafavi, M., Pavier, M. J. and Smith, D. J. (2009) Unified Measure of Constraint, ESIA10: Manchester, UK.”

[80] M. Mostafavi, D. J. Smith, and M. J. Pavier, “Reduction of measured toughness due to out-of plane constraint in ductile fracture of aluminium alloy specimens,” Fatigue Fract. Eng. Mater.

[81] Mostafavi, M., Smith, D., & Pavier, M.J. (2011). A micromechanical fracture criterion accounting for in-plane and out-of-plane constraint. Computational Materials Science, 50, 2759-2770.

[82] V. N. Shlyannikov, N. V. Boychenko, A. V. Tumanov, and A. Fernández-Canteli, “The elastic and plastic constraint parameters for three-dimensional problems,” Eng. Fract. Mech., 2014.

[83] C. K. Seal and A. H. Sherry, “Predicting the effect of constraint on cleavage and ductile fracture toughness using area contour toughness scaling,” Eng. Fract. Mech., 2017.

[84] Ainsworth, R. A. (1984). “The assessment of defects in strain hardening material”, Engng Frac. Mech., 19, 633-642.

[85] Ainsworth, R. A., Bannister, A. C. and Zerbst, U. (2001). “An overview of the European flaw assessment procedure SINTAP and its validation”, Int. J. Pres. Ves. Piping, 77, 869-876.

[86] Kulka, R. S. and Sherry, A. H. (2012), “Fracture toughness evaluation in C(T) specimens with reduced out-of-plane constraint”, Proc. ASME PVP Conference, Paper PVP2012-78751, July, Toronto

[87] M.Y. Mu, G.Z. Wang, F.Z. Xuan, S.T. Tu,Unified correlation of in-plane and out-of-plane constraints with cleavage fracture toughness,Theoretical and Applied Fracture Mechanics,Volume 80, Part B, 2015,Pages 121-132,

ISSN 0167-8442,

[88] J.Y. Xiao, G.Z. Wang, J.X. Zhao, S.T. Tu, F.Z. Xuan,A general correlation between ductile fracture toughness and unified constraint parameter for different materials,Engineering Fracture Mechanics,Volume 285,2023,109296,ISSN 0013-7944,

[89] Dodds, R.H., Anderson, T.L. and Kirk, M.T. (1991). A framework to correlate *a/W* ratio effects on elastic-plastic fracture toughness *(Jc)*. *International Journal of Fracture* **48**, 1–22.

[90] Cotterell B, Li QF, Zhang DZ, Mai YW. On the effect of plastic constraint on ductile tearing in a structural steel. Eng Fract Mech 1985.

[91] Henry BS, Luxmoore a. R. The stress triaxiality constraint and the Q-value as a ductile fracture parameter. Eng Fract Mech 1997.

[92] Brocks W, Schmitt W. The Second Parameter in J-R Curves: Constraint or Triaxiality ? In: Kirk M, Bakker A, editors. Constraint Eff. Fract. Theory Appl. Second Vol., West Conshohocken, PA: ASTM International; 1995, p. 209–31.

[93] hu XK, Chao YJ. Constraint effects on crack-tip fields in elastic-perfectly plastic materials. J Mech Phys Solids 2001; 49:363–99.

[94] Yuan H, Brocks W. Quantification of constraint effects in elastic-plastic crack front fields. J Mech Phys Solids 1998; 46:219–41.

[95] J., Zhao, W., Guo, C. S. The in-plane and out-of-plane stress constraint factors and K-T-Tz description of stress field near the border of a semi-elliptical surface crack. International Journal of Fatigue 29 (2007) 435–443. n.d

[96] Omar, Bouledroua & Mohammed, hadj meliani & Guy, Pluvinage. (2016). A review of T-stress calculation methods in fracture mechanics computation. Nature Technologie. n.d.

[97] Hancock J, Reuter W, Parks D. Constraint and toughness parameterized by T. ASTM STP 1171 Constraint Eff. Fract., 1993, p. 21–40.

[98] Larsson SG, Carlsson AJ. Influence of non-singular stress terms and specimen geometry on small-scale yielding at crack tips in elastic-plastic

[99] nt J Fract, 114 (3) (2002), pp. 259-265Close SM. The influence of the T-stress on the directional stability of cracks. Int J Fract 2002; 114:259–65.

[100] Gupta M, Alderliesten RC, Benedictus R. A review of T-stress and its effects in fracture mechanics. Eng Fract Mech 2015.

[101] Ayatollahi MR, Pavier MJ, Smith DJ. Mode I cracks subjected to large T-stresses. Int J Fract 2002; 117:159–74.

[102] Hadj Meliani, M., Azari, Z., Pluvinage, G., Matvienko, Yu.G., The Effective T-stress Estimation and Crack Paths Emanating from U-notches, Engng Fracture Mechanics, Vol 77, Issue 11, July : 1682-1692, (2010). (PDF)

[103] Larrosa NO, Ainsworth RA. Ductile fracture modelling and J-Q fracture mechanics: A constraint based fracture assessment approach. Frat Ed Integrita Strutt 2016.

[104] Rice JR, Rosengren GF. Plane strain deformation near a crack tip in a power-law hardening material. Journal of the Mechanics and Physics of Solids 1968; doi:10.1016/0022-5096(68)90013-6., 16:1–12.

[105] BS 7910: “Guide on methods for assessing the acceptability of flaws in fusion welded structures” (incorporating Amendment 1), BSI, 1999. n.d

[106] Zhu XKK, Jang SKK, Chen YFF. A Modification of J-Q Theory and Its Applications. Int J Fract 2001; 111:47–52.

[107] Anderson TL, Dodds RH, Wolfenden A, Anderson TL, Dodds RH. Specimen Size Requirements for Fracture Toughness Testing in the Transition Region. J Test Eval 1991; 19:123–34.

[108] Mostafavi, M., Pavier, M. J. and Smith, D. J. (2009) Unified Measure of Constraint, ESIA10: Manchester, UK n.d.

[109] Mostafavi M, Smith DJ, Pavier MJ. Reduction of measured toughness due to out-of-plane constraint in ductile fracture of aluminium alloy specimens. Fatigue Fract Eng Mater Struct 2010; 33.

[110] Shlyannikov VN, Boychenko N V., Tumanov A V., Fernández-Canteli A. The elastic and plastic constraint parameters for three-dimensional problems. Eng Fract Mech 2014.

[111] Mu MY, Wang GZ, Tu ST, Xuan FZ. Three-dimensional analyses of in-plane and out-of-plane crack-tip constraint characterization for fracture specimens. Fatigue Fract Eng Mater Struct 2016; 39:1461–76

[112] Seal CK, Sherry AH. Predicting the effect of constraint on cleavage and ductile fracture toughness using area contour toughness scaling. Eng Fract Mech 2017; 186:347–67.

[113] Xu JY, Wang GZ, Xuan FZ, Tu ST. Unified constraint parameter based on crack-tip opening displacement. Eng Fract Mech 2018; 200:175–88.

[114] Mu MY, Wang GZ, Xuan FZ, Tu ST. Unified correlation of in-plane and out-of-plane constraints with cleavage fracture toughness. Theor Appl Fract Mech 2015; 80:121–32.

[115] Yang J, Wang GZ, Xuan FZ, Tu ST. Unified correlation of in-plane and out-of-plane constraint with fracture resistance of a dissimilar metal welded joint. Eng Fract Mech 2014; 115:296–307.

[116] Mostafavi M, Smith DJ, Pavier MJ. Fracture of aluminium alloy 2024 under biaxial and triaxial loading. Eng Fract Mech 2011; 78.

[117] Wilson CD, Mani P. Plastic J-integral calculations using the load separation method for the center cracked tension specimen. Eng Fract Mech 2002; 69:887–98.

[118] Barhli SM, Mostafavi M, Cinar AF, Hollis D, Marrow TJ. J-Integral Calculation by Finite Element Processing of Measured Full-Field Surface Displacements. Exp Mech 2017; 57.

[119] 2019., Barhli SM. OUR-OMA

[120] arhli, S. M. (2017). Advanced quantitative analysis of crack fields, observed by 2D and 3D image correlation, volume correlation and diffraction mapping (PhD thesis). University of Oxford. n.d.

[121] 2000, Kovesi P. Phase congruency: A low-level image invariant. Psychol Res Forsch; 64:136–48.

[122] Barhli SM. Advanced quantitative analysis of crack fields, observed by 2D and 3D image correlation, volume correlation and diffraction mapping. University of Oxford., 2017.

[123] ABAQUS/Standard User's Manual, Version 6.9. / Smith, Michael. Providence, RI : Simulia, 2009. n.d.

[124] Simpson CA, Tonge S, Cinar A, Reinhard C, Marrow TJ, Mostafavi M. Validating 3D two-parameter fracture mechanics for structural integrity assessments. Procedia Struct Integr 2018; 13:965–70.

[125] Vo NT, Atwood RC, Drakopoulos M. Superior techniques for eliminating ring artifacts in X-ray micro-tomography. Opt Express 2018; 26:28396–412.

[126] owd BA, Campbell GH, Marr RB, Nagarkar V V, Tipnis S V, Axe L, et al. Developments in synchrotron x-ray computed microtomography at the National Synchrotron Light Source. Proc.SPIE, vol. 3772, 1999.

[127] Ruggieri C, Panontin TL, Dodds RH. Numerical modeling of ductile crack growth in 3-D using computational cell elements. Int J Fract 1996; 82:67–95.

[128] Zhao LG, Tong J, Byrne J. Stress intensity factor K and the elastic T-stress for corner cracks. Int J Fract 2001; 109:209–25.

[129] 1968, Hutchinson JW. Singular behaviour at the end of a tensile crack in a hardening material. J Mech Phys Solids; 16:13–31.

[130] Mostafavi M, Collins DM, Cai B, Bradley R, Atwood RC, Reinhard C, et al. Yield behavior beneath hardness indentations in ductile metals, measured by three-dimensional computed X-ray tomography and digital volume correlation. Acta Mater 2015; 82.

[131] Barhli SM, Mostafavi M, Cinar AF, Hollis D, Marrow TJ. J-Integral Calculation by Finite Element Processing of Measured Full-Field Surface Displacements. Exp Mech 2017; 57.

[132] Barhli, S. M. (2017). Advanced quantitative analysis of crack fields, observed by 2D and 3D image correlation, volume correlation and diffraction mapping (PhD thesis). University of Oxford. n.d.

[133] 2000, Kovesi P. Phase congruency: A low-level image invariant. Psychol Res Forsch; 64:136–48.

[134] Mostafavi M, Collins DM, Cai B, Bradley R, Atwood RC, Reinhard C, et al. Yield behavior beneath hardness indentations in ductile metals, measured by three-dimensional computed X-ray tomography and digital volume correlation. Acta Mater 2015; 82.

[135] Mostafavi M, Smith DJ, Pavier MJ. Reduction of measured toughness due to out-of-plane constraint in ductile fracture of aluminium alloy specimens. Fatigue Fract Eng Mater Struct 2010;33.

[136] Yang J, Wang GZ, Xuan FZ, Tu ST. Unified characterization of in-plane and out-of-plane constraint based on crack-tip equivalent plastic strain. Fatigue Fract Eng Mater Struct 2012;36:504–14.

[137] Mu MY, Wang GZ, Xuan FZ, Tu ST. Unified correlation of in-plane and out-of-plane constraints with cleavage fracture toughness. Theor Appl Fract Mech 2015;80:121–32.

[138] Mostafavi M, Pavier MJ, Smith DJ. Unified Measure of Constraint. Eng. Struct. Integr. Adv., Manchester, UK: 2010.

[139] BS 7910: “Guide on methods for assessing the acceptability of flaws in fusion welded structures” (incorporating Amendment 1), BSI, 1999. n.d.

[140] etegón C, Hancock JW. Two-Parameter Characterization of Elastic-Plastic Crack-Tip Fields. Journal of Applied Mechanics 1991. doi:10.1115/1.2897135.

[141] doi:10.1016/0013-7944(95)00033-R., O’dowd NP. Applications of two parameter approaches in elastic-plastic fracture mechanics. Engineering Fracture Mechanics 1995.

[142] Hutchinson JW. Singular behaviour at the end of a tensile crack in a hardening material. Journal of the Mechanics and Physics of Solids 1968;16:13–31. doi:10.1016/0022-5096(68)90014-8.

[143] Zhang B, Guo W. Three-dimensional stress state around quarter-elliptical corner cracks in elastic plates subjected to uniform tension loading. Eng Fract Mech 2007.

[144] Zhao J, Guo W, She C, Meng B. Three dimensional K-Tzstress fields around the embedded center elliptical crack front in elastic plates. Acta Mechanica Sinica/Lixue

Xuebao 2006. doi:10.1007/s10409-006-0095-5.

[145] Zhao J. Three-parameter approach for elastic–plastic stress field of an embedded elliptical crack. Engineering Fracture Mechanics 2009;76:2429–244.

[146] Kavale SM, Kodancha KG, Ekabote N. Effect of Poisson's ratio on KI, T11 and T33 for SENB and CT specimen – A FE study. Procedia Structural Integrity 2019; doi:https://doi.org/10.1016/j.prostr.2019.05.072., 14:584–96.

[147] Clausmeyer H, Kussmaul K, Roos E. Influence of Stress State on the Failure Behavior of Cracked Components Made of Steel. Applied Mechanics Reviews 1991; doi:10.1115/1.3119495., 44:77–92.

[148] Yuh-Jin C, Poh-Sang L. On the use of constraint parameter A2 determined from displacement in predicting fracture event. Engineering Fracture Mechanics 1998; doi:https://doi.org/10.1016/S0013-7944(98)00078-2., 61:487–502.

[149] Dodds RH, Anderson TL, Kirk MT. A framework to correlate a/W ratio effects on elastic plastic fracture toughness. International Journal of Fracture 1991; 48:1–22.

[150] Mostafavi M, Smith DJ, Pavier MJ. Reduction of measured toughness due to out-of-plane constraint in ductile fracture of aluminium alloy specimens. Fatigue and Fracture of Engineering Materials and Structures 2010; doi:10.1111/j.1460-2695.2010.01483.x., 33.

[151] Yang J, Wang GZ, Xuan FZ, Tu ST. Unified correlation of in-plane and out-of-plane constraint with fracture resistance of a dissimilar metal welded joint. Engineering Fracture Mechanics 2014; doi:https://doi.org/10.1016/j.engfracmech.2013.11.01, 115:296–30

[152] Yang J, Wang GZ, Xuan FZ, Tu ST. Unified characterization of in-plane and out-of-plane constraint based on crack-tip equivalent plastic strain. Fatigue and Fracture of Engineering Materials and Structures 2012; 36:504–14.

[153] Wang YH, Wang GZ, Tu ST, Xuan FZ. Ductile fracture prediction based on J-integral and unified constraint parameters for cracked pipes. Eng Fract Mech 2019; 215:1–15.

[154] Tonge SM, Simpson CA, Reinhard C, Connolley T, Sherry AH, Marrow TJ, et al. Unifying the effects of in and out-of-plane constraint on the fracture of ductile materials. Journal of the Mechanics and Physics of Solids 2020; doi:https://doi.org/10, 141:103956.

[155] Brar NS, Joshi VS, Harris BW. Constitutive Model Constants for Al7075-T651 and Al7075-T6. Shock Compression of Condensed Matter 2009, vol. 1195, AA(University of Dayton Research Institute, University of Dayton, Dayton, OH 45469-0182), AB(Naval Surface War

[156] Wasylyk AP, Sherry AH. Size effects on fracture in uncontained plasticity conditions in 304(L) stainless steel. American Society of Mechanical Engineers, Pressure Vessels and Piping Division (Publication) PVP, vol. 7, 2011, p. 337–44. doi:10.1115/PVP2011-

[157] Yasufumi I, Tomokazu M. Effect of side grooves on the elastic-plastic stress state of fracture toughness specimens—three-dimensional finite element analysis. Engineering Fracture Mechanics 1982; doi:https://doi.org/10.1016/0013-7944(82)90019-4., 16:659–68.

[158] Zhao J, Guo W, She C. Three-parameter approach for elastic–plastic fracture of the semi-elliptical surface crack under tension. International Journal of Mechanical Sciences 2008; doi:https://doi.org/10.1016/j.ijmecsci.2008.04.006, 50:1168–82.

[159] James MA, Newman JC. The effect of crack tunneling on crack growth: experiments and CTOA analyses. Engineering Fracture Mechanics 2003; doi:https://doi.org/10.1016/S0013-7944(02)00131-5., 70:457–68.

[160] Moran B, Shih CF. Crack tip and associated domain integrals from momentum and energy balance. Engineering Fracture Mechanics 1987; doi:https://doi.org/10.1016/0013-7944(87)90155-X, 27:615–42.

[161] Rice JR, Rosengren GF. Plane strain deformation near a crack tip in a power-law hardening material. J Mech Phys Solids 1968; 16:1–12.